AD NUMBER

AD871155

LIMITATION CHANGES

TO:

Approved for public release; distribution is unlimited.

FROM:

**Distribution authorized to U.S. Gov't. agencies and their contractors;
Administrative/Operational Use; FEB 1970. Other requests shall be referred to Army Aviation Materiel Labs., Fort Eustis, VA.**

AUTHORITY

USAAMRL ltr 23 Jun 1971

USAAVLABS TECHNICAL REPORT 69-97

INVESTIGATION TO DETERMINE THE FEASIBILITY OF DETECTING IMPENDING METAL FATIGUE FAILURE THROUGH USE OF AN INDUCTIVE SENSING DEVICE

By

George G. Moross

February 1970

U. S. ARMY AVIATION MATERIEL LABORATORIES
FORT EUSTIS, VIRGINIA

CONTRACT DAAJ02-68-C-0005
MECHANICAL TECHNOLOGY INCORPORATED
LATHAM, NEW YORK

Disclaimers

The findings in this report are not to be construed as an official Department of the Army position unless so designated by other authorized documents.

When Government drawings, specifications, or other data are used for any purpose other than in connection with a definitely related Government procurement operation, the United States Government thereby incurs no responsibility nor any obligation whatsoever; and the fact that the Government may have formulated, furnished, or in any way supplied the said drawings, specifications, or other data is not to be regarded by implication or otherwise as in any manner licensing the holder or any other person or corporation, or conveying any rights or permission, to manufacture, use, or sell any patented invention that may in any way be related thereto.

Disposition Instructions

Destroy this report when no longer needed. Do not return it to the originator.

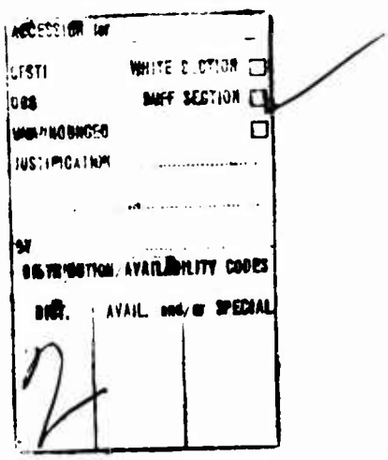

DEPARTMENT OF THE ARMY
HEADQUARTERS US ARMY AVIATION MATERIEL LABORATORIES
FORT EUSTIS, VIRGINIA 23604

The effort reported herein is a part of a program to develop concepts of aircraft maintenance, inspection, and diagnostic equipment suitable for field application. The report presents the results of the evaluation of an inductive sensing device as a candidate concept for detecting impending fatigue failure in metallic materials utilized in the production of Army aircraft.

This Command concurs with the findings of the contractor.

Task 1F162203A43405
Contract DAAJ02-68-C-0005
USAAVLABS Technical Report 69-97
February 1970

INVESTIGATION TO DETERMINE THE FEASIBILITY OF DETECTING IMPENDING METAL FATIGUE FAILURE THROUGH USE OF AN INDUCTIVE SENSING DEVICE

Final Report

by

George G. Moross

Prepared by

Mechanical Technology Incorporated
Latham, New York

for

U.S. ARMY AVIATION MATERIEL LABORATORIES
FORT EUSTIS, VIRGINIA

BLANK PAGE

ABSTRACT

This program is concerned with the evaluation and development of a sensing system to detect surface and near-surface flaws in material, specifically to detect early fatigue damage. The system shows great promise in that a signal is detected at a significant time before failure, and the amplitude of the signal increases with further damage. Samples have been fatigue-cycled up to 5×10^6 cycles, and signals have been observed as early as 38% of fatigue life, average results showing signals between 70 and 80%. These studies have been performed using aluminum, steel, and Inconel, and the results show essentially the same sensitivity of these materials. Intensive metallographic and microanalytic studies have been performed in order to define the particular phenomenon responsible for the signal. Microcracks have definitely proved to be responsible for the signal, and thus the sensitivity of the system has been evaluated.

TABLE OF CONTENTS

LIST OF ILLUSTRATIONS

SECTION 1

INTRODUCTION

1.1 GENERAL

Much effort has been applied in recent years to the prevention of failure in operating systems. Failure in mechanical systems is directly attributable, in many cases, to metal fatigue, a result of repetitive loading of the structure. In order to prevent failures arising from fatigue damage in structures, it is necessary to inspect these structures for evidence of fatigue damage and to repair or replace them as may be required. The process of inspection for fatigue damage has been the subject of intensive investigation. With the advent of larger and more sophisticated mechanical systems, where failure may become catastrophic, great emphasis has been placed on the development of reliable, nondestrictive inspection methods for detecting fatigue damage and impending failure.

Methods have been devised that take advantage of many physical phenomena: penetration of tracers into discontinuities in surfaces (penetrant techniques), location of inhomogeneities and discontinuities in bulk material (ultrasonic techniques), and variations in electrical, magnetic, or electromagnetic characteristics of materials, to name a few. All of these methods have met with some success in laboratory use; however, not all of these methods may be efficiently applied under conditions normally encountered in the field or repair shop. Demands on the availability and reliability of modern aircraft provide strong incentives for accurate and early detection of impending failures of critical parts and components. This is particularly true of those parts that are prone to fatigue failure, since they normally operate for extended periods before failing without warning and often catastrophically. Early detection will prevent this and will provide a rational criterion for maintenance. It is to this problem, the investigation to determine the feasibility of detecting impending fatigue failure in metals by use of an inductive detection system, that the present effort has been directed.

1.2 PURPOSE OF INVESTIGATION

The objective of this program was to evaluate an inductive detection system for its abilities to detect fatigue damage. Fatigue-prone components include elements of the airframe, power trains, and engines. Such elements as wing spars, gears, compressor and turbine blades and disks, struts, shafts, and bearings are good examples. Consequently, certain classes of materials are involved; namely, nonferrous alloys (such as aluminum, magnesium, and titanium), heat-treatable steels (52100, A286, and 4340), stainless steel (316 and 410), and high-temperature alloys (chrome-nickel, M151, and cobalt-base alloys). Thus, the evaluation of the system has included a series of identical tests using three different materials in order to replicate, as closely as possible, the range of

materials commonly encountered. As preliminary experiments had indicated and testing has shown (as will be seen in the results), the inductive system is able to detect fatigue damage at an early stage in all three materials with approximately equivalent signal amplitudes.

In addition to the requirement that the inspection system be capable of fatigue-damage detection among many materials, other questions must be taken into consideration during the feasibility study; for example, reliability of results across many samples (both false-positive and false-negative), correlation (if possible) of signal characteristics with size of damaged area, smallest size of flaw or crack seen, and effect of environmental factors. Ultimately, the question to be answered relates to the probability of successful development of a field-portable instrument that will simply and reliably determine the extent, if any, of fatigue damage.

1.3 THEORY OF OPERATION

The inductive sensing system used in the performance of this work consists of a probe, oscillator, bridge circuit and detector. The probe consists of a "U" shaped core constructed of soft iron wire wound on one leg. This "U" is arranged such that the probe is axially symmetric about the wound leg. A second equivalent core-coil combination is placed behind the first one to provide temperature compensation. These two coils are then connected in a half-bridge configuration into the A.C. bridge circuit. The signal from the bridge is fed to a synchronous detector and filter whose output is a D.C. signal corresponding to bridge unbalance. The probe is positioned so that the sample material forms the flux path between the legs of the "U". The bridge is initially balanced, and the probe is then scanned over the sample. Since the system is a reluctance device, length of flux path causes a bridge unbalance wa well as a change in the effective permeability. For this reason the standoff distance must be maintained at a constant value, which was done in our work by placing shim material between the probe and the sample. The remaining reason for bridge unbalance then relates to the local characteristics of the material being examined. As the probe is scanned along a surface a relatively constant output signal is obtained until a flaw appears within the sensitive area of the probe. At that point the bridge becomes unbalanced, this being shown as a change in the D.C. output signal.

The recorder traces presented here are the changes in D.C. output as the probe is scanned along the sample.

1.4 SCOPE OF INVESTIGATION

This program has encompasses approximately a one-and-one-half-man-year effort, performed primarily at Mechanical Technology Incorporated, and has included both fatigue testing and microanalytic work.

Vibratory beam fatigue tests were conducted on six samples at each of three stress levels. Samples were fabricated of 6061-T6 aluminum, 9310

steel, and Inconel X. The samples were periodically scanned and examined; the results will be presented.

Roll tests were conducted on a total of 12 samples at different stress levels. These samples were fabricated of 8620-H steel. The samples were periodically scanned and examined. The results of this examination will be presented.

Vibratory beam tests were run on four specially prepared samples of each of the three materials. Inductive scans and acetate replicas were taken on both sides periodically during the tests. The replicas were shadowed and examined by electron microscopy. The scans and photographs are presented in Section 3.

Vibratory beam tests were run on four specially prepared samples of each of the three materials; however, the tests were terminated at the first appearance of a signal from the inductive sensing system. These samples were subsequently sectioned, mounted, and examined by scanning electron microscopy. The photographs and scans are presented in Section 3.

One sample of each material of task 4 was examined using an electron microprobe, providing a point-by-point elemental analysis of the area of interest. These photographs also appear in Section 3.

SECTION 2

EXPERIMENTAL METHODS

2.1 MATERIALS AND SAMPLE PREPARATION

All of the work performed under this contract was concerned with four materials (6061-T6 Aluminum, 9310 Steel, Inconel X, 8620-H Steel). Three of these materials were selected for their frequency of application in helicopter and other airframe construction; the fourth material is one commonly used for gears.

The samples, as shown in Figures 1a, 1b, and 1c, were fabricated from these materials. Figures 1a and 1b were used for vibratory beam testing, and Figure 1c was used for geared-roller testing. Since the motivation for the fatigue testing was to produce fatigue damage (i.e., cracking) in a controlled fashion, a 1/4-inch by 1/2-inch by 5-inch sample, with stress-raiser, was used. At the beginning of testing, the configuration shown in Figure 1a was run, and the inductive probe was scanned along the radius. The radius, which was intended to force the location of the fatigue crack, was not small enough. For this reason, a number of runs resulted in a fatigue failure initiating outside the scanned area. This suggested a change in sample configuration to the one shown in Figure 1b, wherein a simple notched beam provides a sufficient stress-raiser for reliable results. The samples for Section 1.4 (1) were run, as machined, with no special surface preparation; samples of the same configuration for Section 1.4 (3), Section 1.4 (4), and Section 1.4 (5) were electropolished after fabrication, providing a smooth, polished surface to insure clarity of acetate replicas and scanning electron micrographs of high quality.

The roll test samples were fabricated of 8620-H steel and subsequently hardened and ground to a 1.000-inch roll diameter. No special precautions were taken to present a polished surface.

2.2 TEST SETUP

2.2.1 Vibratory Beam Machines

A photograph of the vibratory beam fatigue machine is shown in Figure 2. Two of these machines were used in order to facilitate the running of the tests, since the tests required constant monitoring. The dial gage was used during initial setup to measure deflection and to insure a totally reversing stress. An optical sensor was used to measure the actual motion at speed. The difference between the two measurements, which amounted to .002 inch, was then taken into consideration. Therefore, the deflections quoted in the data are actual deflections under dynamic conditions. The machines, which run at a nominal speed of 3450 cycles per minute, were provided with a speed control which allows a small variation in cycle rate to avoid damaging resonances. The total number of cycles was recorded electronically.

The sample was firmly clamped in the vise, the upper rod was clamped to the sample, and the system was adjusted to provide the desired positive and negative deflection. The sample was scanned (and replicated for task (3) of Section 1.4), and the test was started. During the initial phases of testing, many inductive scans were taken prior to the first acquisition of a signal; however, with experience, the number of readings prior to signal could be reduced without losing any information. After the first appearance of the signal, readings were taken periodically until failure occurred, which we have defined as fracture.

2.2.2 Geared-Roller Test Machine

A photograph of the geared-roller test machine is shown in Figure 3. This machine provides a practical means of studying many of the problems associated with contact pressures which involve rolling or rolling combined with sliding such as occurs on gears, bearings, and cams. The test rig consists of two test rollers mounted on parallel horizontal shafts, as shown schematically in Figure 4. The upper shaft is secured in a frame, which is hinged at one end to the base; the base holds the lower shaft. This forms a "nutcracker" type of mechanism. The 3-inch-center distance between the shafts is maintained by the rollers. The shafts themselves are supported on roller bearings.

Load is applied to the free end of the upper frame through a lever arrangement, which is actuated by a pneumatic roto-chamber. Loads from 66 to 8000 pounds can be applied to the rollers. The actual load is determined with a calibrated, strain-gaged load rod and is monitored during the test by a pressure gage. The lower shaft is coupled to a 10-horsepower motor. The upper shaft is driven by the lower shaft through a set of phasing gears. These phasing gears can be changed to provide various percentages of relative slip between the roll surfaces, thus simulating the degree of slip that is normally encountered in gears.

A photograph of the sample is shown as Figure 5. The area of rolling contact is the 1.00-inch-diameter section in the center of the sample. A 5.00-inch-diameter crowned roller on the upper shaft bears against the sample, producing an extremely high Hertzian stress. Loads were selected to provide varying times to failure.

An inductive scan was taken prior to the test and, subsequently, during the test until failure occurred, which was defined as a significant pit in the surface.

2.3 MICROANALYTIC TECHNIQUES

Four methods of microanalysis were applied in order to determine the sensitivity and applicability of the inductive detection system. In an attempt to correlate the results of our examination with other methods, a number of attempts were made to examine a signal-bearing sample with Zyglo, a fluorescent-dye penetrant; see Figure 6. Figures 6c and 6d are photographs of two Inconel X specimens. Figures 6e and 6f show the results of

an inductive scan, and Figures 6a and 6b show heavily filtered photographs of the Zyglo test. Figure 6b shows no indication of dye penetration, while Figure 6a shows two dots (plus one dust particle) in the area where the crack would be expected.

Since this was the only one of several such investigations that showed any evidence at all of Zyglo penetration, it is shown here. This technique obviously did not provide the required correlation between signal and visible damage.

A number of preliminary tests were run at the beginning of the program while test parameters were being finalized. In these investigations, samples were cycled until a signal appeared; at that point, the surface was polished and/or etched and examined under a microscope. These investigations showed no perceptible cracks while showing evidence of working of the surface. These tests also were destructive in that it was necessary to polish and etch the samples in order to see surface flaws clearly at high magnifications. For this reason, a significant effort was expended later in the program to replicate specimen surfaces and to examine these replicas with standard high-magnification techniques.

2.3.1 Electron Microscopy

The specially prepared specimens (electropolished) were scanned as in the other tasks of the program; however, in addition to the scanning, they were replicated using the following technique. A specially fabricated, .005-inch-thick acetate replicating tape was cut to approximate size, and one surface was saturated with pure acetone. The acetate film softened, and the soft surface was pressed against the specimen. The film was allowed to dry in place; when it was peeled off, it contained a topographic negative of the specimen surface. The replica was then mounted and placed in a vacuum chamber, where a thin layer of chromium was deposited on it. A heavier layer of carbon followed. At this point, the replica was removed from the chamber and was sectioned into approximate, 3-millimeter circles. The acetate film was dissolved away in acetone, leaving 3-millimeter-diameter topographic positive of the original sample, which was then examined by electron microscopy.

This method provided a nondestructive, noninvasive technique for high-magnification examination of the specimen surface. Replicas were taken at intervals during the testing and provided high-quality visual evidence of the progress of fatigue damage.

2.3.2 Scanning Electron Microscopy

The specially prepared samples (electropolished) were run as in the rest of the program; however, at the first appearance of a signal, the run was terminated and the sample was sectioned in order to fit it into the specimen chamber of the scanning electron microscope.

Scanning electron microscopy (SEM) enables the analyst to

examine directly the surface of interest without the need for the replication process (as described in 2.3.1) required for transmission electron microscopy. Probably the most striking advantage of SEM is the extremely large depth of focus, which ranges up to 300 times that available by optical microscopy, thereby generating a "three-dimensional" effect in the photographs. The magnification in SEM is generated without the use of lenses as used in conventional electron microscopy; i.e., the size of the scan and thus the magnification of the image are controlled by the deflection of the electron beam. The electron beam impinges upon the sample and causes both emission of secondary electrons and backscattered electrons. These are detected, amplified, and displayed on a Cathode Ray Tube, from which the photographs are taken.

2.3.3 Electron Microprobe Analysis

As an exploratory effort, one sample of each of the three materials from the specially prepared group was examined by an electron microprobe.

The electron microprobe generates a focused beam of electrons which is accelerated through a field of 5-50 KV. This beam is scanned in a raster across the surface of the sample, and a number of analysis methods are available. The sample may be imaged by measuring and amplifying the current through the specimen due to the beam (specimen current mode), thus generating a picture of surface conductivity. The mode of operation that is of most interest to the present work in the spectrometer. In this mode the X-rays emitted by the sample under electron bombardment are examined by X-ray spectrometers, which will detect emissions from various elements present. A point-by-point elemental analysis is performed, generating images taken in different elements. The photographs, which show concentrations of contaminants near the fatigue crack, are shown in Section 3.

SECTION 3

RESULTS

3.1 PRELIMINARY EXPERIMENTATION

In preparation for the high-cycle fatigue tests to be run as the main body of testing, a few preliminary, low-cycle fatigue tests were performed using readily available cold-rolled steel for the sample material.

One sample was prepared from the above material using the configuration shown in Figure 7. Dimension a is nominally .375-inch, b is .750-inch, c is .090-inch, and d is .037-inch. The top face of the sample was prepared by polishing to provide a smooth, flat surface for scanning with the inductive probe. The notch was cut with an abrasive wheel before polishing.

The history of the sample from original condition to failure (which occurred at 11 cycles) is recorded in Figure 8. Figure 8a shows a scan along the length of the sample (perpendicular to the notch), taken along the top surface. The arrow, as in the other traces, indicates the approximate location of the notch. This arrow is necessary since the scan is performed manually, and the spacing of signals is not perfectly uniform.

Figure 8b shows the effect of one cycle upon the probe signal. One cycle consists of bending the two ends of the sample (see Figure 7) up to a total angle of 10 degrees and subsequently bending the ends back down to maintain flatness of the top surface. Figure 8 shows a definite growth of the signal over the notch.

Figure 8d shows the size of the signal after three fatigue cycles. Visual examination of the top surface showed no discernible cracks. Microscopic examination showed distressed metal but no long, continuous cracks.

Figure 8e shows the signal after four cycles of the specimen. A crack was not visible to the unaided eye.

Figures 8f and 8g show essentially the same signal as Figure 8e. The specimen failed during the eleventh cycle. The width of the signals, as mentioned above, is a function of the speed with which the probe is scanned over the sample. Since the probe is scanned by hand, the width may vary.

For another preliminary run, a sample was cut from cold-rolled steel to the following dimensions: a, .315-inch; b, .750-inch; c, .050-inch; and d, .036-inch. The top surface was polished as before.

Figure 9a shows a scan along the length of the sample before any fatigue cycling took place. Again, there is a slight signal over the region of the notch.

Figure 9b, after one cycle, shows a definite increase of a signal. For this sample, the cycle included bending the two ends of the sample up to a 5-degree-total angle (half of the angle used previously). Figure 9c shows the signal after the specimen had been subjected to three cycles. At this point, the test was stopped and a Tally-Surf measurement was taken. This measurement is shown in Figure 9d.

The points m and n in Figure 9d show the approximate locations of the edges of the notch. The rolloff to the left of m apparently shows a deviation from flatness on the order of .0002 inch. Most important, however, is the smoothness of the trace above the notch, proving that flawed material above the notch was neither protruding above nor indented below the surface, thereby causing an erroneous signal.

To further investigate the condition of the material above the notch, the sample was lapped and etched for metallographic examination.

Figure 10a shows a top view of the sample. At this point it has been subjected to three cycles, the inductive trace of which is shown in Figure 9c. The notched area is faintly visible in Figure 10a, due undoubtedly to the worked metal at the top surface. No cracks are seen here nor at the root of the notch in Figure 10b. Figure 10c shows a photomicrograph of the notches area at 100-power magnification, and there are no cracks visible. The lines seen are the coarse polishing marks, which can be seen also in Figure 10a.

Figure 10d shows the notched area after a polishing operation which consisted of grinding with 280-, 320-, and 600-grit silicon-carbide paper, followed by a fine polish using 3μ and 0.5μ powdered alumina. Approximately .005-inch of material was removed in the polishing operation. Figure 10e shows a photomicrograph of the same area over the notch after etching with a 2% Nital solution. A normal ferritic structure, consisting of ferrite (white regions) and perality (dark regions), is visible. Figure 10f shows the same area at a higher magnification. Figure 10g shows a top view of the sample after polishing and etching.

At this point, the surface was lightly polished and the sample was subjected to one more cycle. Figure 10h shows the area above the notch, and Figure 10i shows the area away from the notch. The mottling of the surface above the notch indicates that the material had been worked. Figures 10 j through 10m show the notched area and unnotched area at 100-power and 300-power magnification after a 2% Nital etch. The two areas show essentially the same structure with a slightly preferential attack by the etchant on the worked surface.

Figure 10n shows the inductive scan of the surface after the polishing operation and after the one additional cycle, but prior to etching. The signal is unmistakable.

3.2 VIBRATORY BEAM TESTS

3.2.1 6061-T6 Aluminum

Eighteen samples were fabricated, prepared (as described previously), and tested using the methods outlined in Section 2.2.1. Deflections for the three stress levels were set at $\pm$ .040, $\pm$ .050, and $\pm$ .055 inch. The cycles to failure averaged 1.4×10^6, $.7 \times 10^6$, and $.43 \times 10^6$, respectively. The bar graph shown in Figure 11 presents the results of all 18 aluminum samples. The top of the black portion of a bar indicates the number of cycles at which a signal appeared. The top of the clear portion indicates the number of cycles at which failure occurred. The ordinate is calibrated in number of cycles, while the abscissa shows test number. The number at each bar indicates the percentage of life at which the signal appeared.

Because scanning was performed periodically during the test, the crack had developed considerably by the time the first scan was taken. This implies that the signal could have been observed at an earlier period had a reading been taken then and that a lower percentage would have been indicated. A correction has not been applied; thus, the asterisk indicates that the given percentage figure is conservative.

The average percentage for the $\pm$ .040-inch deflection is 76.7% (with three asterisks); for the $\pm$ .050-inch, 74.5% (three asterisks); and for the $\pm$ .055-inch, 64.0% (two asterisks). The average percentage across all 18 samples is 71.7%, which, when taking the conservative treatment of data into account, would indicate a figure of below 70% of time to failure at which the signal appeared. The earliest signal appeared at 37% of life (sample 14), while the latest indication of 91% showed a very large signal amplitude at that point; hence, it is reasonable to assume that acquisition of signal should have been much earlier.

The full tapes for sample 17 ($\pm$ .055-inch deflection) are presented as being a representative run (Figures 12a through 12p). Figures 12a and 12b show a scan prior to testing. Figure 12e (front, 240,000 cycles) shows an extremely small amplitude signal which is marginal; however, based on our experience, it shows the proper configuration. We have not called this a firm signal for purposes of calculating the percentage of life; however, the reading happened to be taken at the most propitious time. In Figure 12g, taken 60,000 cycles later, the signal on the front had grown considerably. At 462,000 cycles (Figure 12k) the signal had grown and a crack had become visible. At this point, the back of the sample had been deformed; by 540,000 cycles, a crack had developed in the back of the sample as well. The sample broke at 562,000 cycles.

The full tapes for sample 6 are also presented (Figures 13a through 13l, $\pm$ .050-inch deflection). Test of this sample shows a characteristic that was seen a number of times during the program. Figures 13a and 13b show pretest readings; Figures 13c and 13d show a large signal

on the front and a smaller signal on the back, indicating cracks on both sides. The signal grew in amplitude in an alternate fashion between front and back until at 760,000 cycles the front surface was badly deformed around the crack, as in the back, while the crack signal was extremely large. Two thousand cycles later, the sample failed.

It was mentioned earlier that the signal in Figure 12e was marginal but of the correct configuration, based on an experience factor. It can be seen in Figures 12e, 12g, and 12i that the signal consists of a downward peak surrounded by two peaks in the opposite direction. Signal amplitudes were measured from the base-line; however, the two satellite peaks still generated considerable interest. These satellite peaks were consistently seen on the aluminum samples and to a much lesser degree on the Inconel. On the steel they were not seen at all. It was suspected that the satellite peaks were due to worked, extruded material around the crack because of the higher ductilities of aluminum and Inconel. This hypothesis was confirmed after the scanning electron micrographs were examined. Both the aluminum and Inconel samples show torn, extruded material at the edges of the crack, while the micrographs of the steel do not show this.

Figure 14 shows the growth of the signal with life for all 18 aluminum samples. The curves show the increase in signal amplitude (in scale divisions) as the ordinate and the number of cycles as the abscissa. Samples 1-6 were run at $\pm$ .050-inch deflection, 7-12 were run at $\pm$ .040-inch deflection, and 13-18 were run at $\pm$ .055-inch deflection. It is evident that signal amplitude correlates well with fatigue life history. Sample 2 obviously needed more readings.

3.2.2 Inconel X

Eighteen samples were fabricated, prepared, and run as described previously. Deflections for the three levels were set at $\pm$ .090 inch, $\pm$ .100 inch and $\pm$ .130 inch. The cycles to failure averaged 1.4×10^6, $.94 \times 10^6$, and $.33 \times 10^6$, respectively. The bar graph shown in Figure 15 presents the results of all 18 Inconel samples. The legend for the graph has been presented in Section 3.2.1.

The average percentage for the $\pm$ .090-inch deflection is 83.0% (one asterisk); for the $\pm$ .100-inch deflection, 78.8%; and for the $\pm$ .130-inch deflection, 77.7%. The overall average percentage of life at time of signal is 79.6%. The earliest signal appeared at 67% of life (sample 32), while the latest indication of 93% showed a very large amplitude signal at that point, indicating that the percentage figure could have been lower.

It is significant to note that, while the test results for aluminum show a wide variation in life for a given deflection along with a fairly wide variation in percentage of life at the time of signal, the Inconel demonstrates a much tighter clustering of lives for a particular deflection and a relatively small variation in life at the time of signal.

Figure 16 shows the growth of signal with life for all 18 Inconel X samples. As for the aluminum samples, the signal amplitude correlates well with fatigue life history.

The full tapes for sample 26 (± .100-inch deflection) are presented as being a representative run (Figures 17a through 17l). Figures 17a and 17b show a scan prior to testing. Figure 17c shows a small but definite signal on the front. The signal increased in amplitude until 1,128,000 cycles (Figure 17i), when the crack became visible; it further increased until at 1,184,000 cycles the sample failed.

Figures 18a through 18j show a full run of tapes for sample 35 (± .130-inch deflection). Again, an extremely small but unmistakable signal appeared (Figure 18c) and increased in amplitude until at 6,000 cycles after Figure 18i when the sample failed.

3.2.3 9310 Steel

Eighteen samples were fabricated, prepared, and run as described previously.

Deflections for the three stress levels were set at ± .070 inch, ± .080 inch and ± .085 inch. The cycles to failure averaged 1.24×10^6, $.46 \times 10^6$, and $.32 \times 10^6$, respectively. The bar graph shown in Figure 19 presents the results of all eighteen, 9310-steel samples. The legend for the graph has been presented in Section 3.2.1.

The average percentage for the ± .070-inch deflection is 90.0% (two asterisks); for the ± .075-inch deflection, 76.2% (one asterisk); and for the ± .085-inch deflection, 78.3% (three asterisks). The overall average percentage of life at the time of the signal is 81.5%. The earliest signal appeared at 58%, while the latest indication of 98% showed a very large amplitude signal at that point, indicating that the percentage figure could have been lower; actually, all tests that show a percentage figure greater than 90 are marked with an asterisk.

Figure 20 shows the growth of the signal with life for all eighteen, 9310-steel samples. As for the aluminum and Inconel samples, the signal amplitude correlates well with the fatigue-life history.

The full tapes for sample 37 (± .070-inch deflection) are presented in Figures 21a through 21v. The signal appears in Figure 21c at 900,000 cycles and clearly shows a steady increase in amplitude until failure, which occurred at 1,032,000 cycles.

The full tapes for sample 51 (± .075-inch deflection) are presented in Figures 22a through 22p. The signal appears at 350,000 cycles (Figure 22c) and increases until at 410,000 cycles (Figure 22j) a signal appears on the back. Both signals increase until the sample fails at 456,000 cycles.

3.3 ROLL TESTS

Twelve samples were prepared from 8620-H steel for the roll tests. The samples were heat-treated to a hardness of RC-63 with a case depth of .073 inch. In order to produce surface-fatigue damage, the samples were run in contact with a crowned roller with a maximum Hertz compressive stress of up to 450. According to published S/N curves and MTI experience with this type of procedure, failure, as evidenced by the formation of a characteristic pit, should occur between 2×10^5 and 5×10^6 cycles. The fatigue lives for the roll tests fall within the range of 4.3×10^5 to 7.8×10^6 cycles. The fatigue lives for the roll tests fall within the range of 4.3×10^5 to 7.8×10^6 cycles. Some difficulty was encountered in the selection of particular stress levels to produce failure at a given number of cycles; however, this difficulty is in good agreement with published S/N data for these tests and is not surprising. Since the motivation for fatigue testing was to initiate fatigue damage for evaluation of the inductive sensor system, the uncertainty of actual S/N data was of little consequence.

The tapes from two sample runs are presented in Figures 23 and 24. Figure 23 shows tapes from the roll test for sample 10. The baseline remained quite smooth and regular through 12 readings to 585,000 cycles. At 596,000 cycles, a change occurred in the character of the noise from the machine; the scan was taken. Visual examination disclosed a small pit, which has been defined as evidence of failure.

Figure 24 shows the tapes from sample 9. Again, the baseline was smooth until the reading at 532,000 cycles, at which point a small, repeated (due to the shaft rotation) signal appeared. Approximately 3,000 cycles later, a large pit developed in the sample. A photograph of a sample showing a typical large pit of the characteristic triangular shape is shown as Figure 25.

Sample 9 was subsequently sectioned, mounted, and polished for metallographic examination. Photographs of this sample are presented as Figure 26. The cracks seen in Figures 26a and 26b are characteristic of rolling contact fatigue damage, in that the cracks propagate essentially parallel to the surface.

From the results presented here, it is believed that the use of the inductive detection system is not of significant value in the detection of rolling contact fatigue damage as produced in these experiments. This is probably true because of the difference in manner and direction of crack propagation in the sample. Where early detection was possible on beam specimens as the cracks propagated normal to the surface, very late detection was evident on the roll specimens as the cracks propagated parallel to the surface. It appears that the parallel propagation is the factor responsible for the inability to detect early damage.

3.4 RESULTS OF MICROANALYTIC STUDIES

3.4.1 Scanning Electron Microscopy

An example of two complete runs of fatigue tests run to signal, on aluminum samples; and scanning electron microscopy of the scanned area is presented here.

The inductive sensor scans of aluminum sample 5 are presented as Figure 27. Readings were taken at pretest, at 400,000 cycles, and at 600,000 cycles; a signal appeared at 800,000 cycles on the back surface. The sample was then run further to 915,000 cycles to generate a sizable crack. It should be noted that at 800,000 cycles, the signal shows a depression with a small "pip" in the center. At 900,000 cycles, the signal shows two large depressions, one on each side of the central signal. It is significant that this type of signal has been observed throughout the program as being characteristic of an incipient failure on an aluminum sample. A question has been raised as to the phenomenon responsible for this characteristic signal on aluminum. This can be answered by a study of Figures 28, 29, and 30. Figure 28 clearly shows a crack that turns into an induration on each side of an extrusion. Figure 29, taken closer to the center of the sample, shows an apparent tearing of material along the crack. The surface scratching, which is apparent but not serious in these scanning microscope pictures, is serious enough to obliterate detail in the electron microscope pictures. Figure 30 shows the leading end of the crack, 4.2 mm from the root of the notch. The photographs are labeled with a letter and one dimension. The letter indicates the distance from the root toward the center of the sample. Since the notch separation is 9.4 mm, Figure 30 is taken .5 mm from the center line of the specimen. From previous experiments, it has been determined that the area of sensitivity of the probe encompasses a width of approximately 4 mm (2. mm each side of center). Therefore, cracks shown in the photographs will be responsible for a signal indication if the dimension shown is greater than 2.7 mm. Figures 32, 33, 34, 35, and 36 are photomicrographs of sample 11 aluminum. The scan signals are shown as Figure 31. The last reading, 625,000 cycles (back), shows an extremely small "pip", which, experience has shown us, is the first indication of a valid flow signal. Figure 34 shows well-defined crack propagation; however, the position dimension shows that this was taken only 1.4 mm from the notch. Figure 35, taken .5 mm toward the center, shows much less damage, and the surface damage is seen to end at 2.1 mm in Figure 36. It is apparent that there is little damage beyond 2.1 mm, and the extremely small signal (most likely due to flux fringing at the edge of the probe, increasing the sensitive area) bears this out.

The inductive sensor scans of Inconel sample I17 are shown in Figure 37. As before, an extremely small signal at 1,100,000 cycles motivated termination of the test and preparation of the sample for scanning electron microscopy. Figure 38, 39, 40, and 41 show the damage at this point. Figure 38 shows gross damage at .73 mm from the root of the notch. Figures 39 and 40 show the crack at 1.5 and 2.28 mm from the

notch and, in addition, very clearly show the presence of slip parallel to the crack. Figure 41 shows the furthest easily observable propagation of the crack. Again, the presence of slip is evident parallel to the crack. Figure 42 shows the inductive scans of Inconel sample I10. A sizable signal at 800,000 cycles motivated termination of the test and preparation for scanning electron microscopy. Figures 43, 44, 45, and 46 are photomicrographs of the sample taken at 1.74 mm, 2.05 mm, 2.46 mm, and 3.03 mm, respectively, from the root of the notch. As before, these figures show a decrease in crack size with distance from the notch. The pock marks visible in these figures are most likely caused by the electropolishing procedure used in the initial preparation of the sample.

Figure 47 shows the inductive scans on steel sample S11. A sizable signal is apparent at 350,000 cycles. At this point the sample was prepared, and the photomicrographs shown in Figures 48, 49, 50, and 51 were taken. In general, the slip seen in the Inconel micrography is not evident, and the crack appears to be partially obscured by a white-appearing substance. This substance has been shown by electron microprobe analysis to be an oxide. As with the aluminum and Inconel samples, the photographs show a crack that decreases in size with distance from the root of the notch. It is significant to note that the crack has progressed further in the steel than in the other materials, which corroborates the later appearance of the signal in general for steel samples.

3.4.2 Electron Microscopy

The procedure for preparation of replicas for transmission electron microscopy was described in Section 2.3.1. As described in the procedure, after the replicas are shadowed, they are sectioned into 3-millimeter circles, which are placed on the microscope stage, where they are supported on grids. The replicas are actual three-dimensional topographic maps of the surface, and, as such, depressions such as cracks or pits tend to weaken the replica considerably (hence the grids). Since the coating thickness of the chromium is of the order of 100 Angstroms or so, the carbon is 3 or 4 times thicker than the chromium, the total thickness of the examined replica is of the order of 500 to 800 Angstroms. Therefore, it is not surprising that the replicas tend to separate at a crack. Since small sections of the replica, rather than the whole replica, are examined, it is virtually impossible to accurately locate a particular feature with respect to the original sample. The procedure for examination was to locate the edge of the crack, the tip also if possible, and to carefully examine and photograph features on the surface that may have been responsible for the inductive signals. In no case were features observed (other than cracks) that could give rise to a signal.

The aluminum samples were, in general, extremely soft in comparison with steel or Inconel. This extreme softness made the surface difficult to examine at high magnifications. Extra aluminum samples were tested, taking particular care not to disturb the surface; however, scratching was still evident. Figure 52 shows the surface of the sample in a relatively scratch-free area taken at 7500-power magnification. The

presence of slip is seen. A better photograph of slip near a crack is shown in Figure 53, taken of aluminum sample A12 at 9,000-power magnification, where the slip is clearly normal to the scratches. Figure 54 shows the opposite surface of aluminum sample A12, also at 9,000-power magnification. No distinct cracks are seen (the white lines are most probably separations of the replica); however, the pits from the electropolishing are very clearly presented.

Inconel has provided the most information from this examination, since the surface is quite free from scratches. Optical examination has shown slip to exist only near a crack; therefore, slip has provided a bench mark to corroborate proximity to a crack. Figure 55 shows an overview of the crack on Inconel sample I2 at 1,500,000 cycles. This photograph shows a jagged crack configuration and the presence of slip. Figure 56 shows the edge of the crack (right) and very clear slip bands at the center (Inconel sample I2, 1,100,00 cycles, 3,800-power magnification). Figure 57 shows an enlargement of the same area at 9,000-power magnification, where the slip bands are clearly visible. Figure 58 shows clear slip bands in the vicinity of a crack (upper left) with what appears to be a secondary crack (same replica and magnification). Figure 59 shows the tip of the primary crack (9,000-power magnification, Inconel sample I2, 1,100,000 cycles). It is important to note that there is no evidence of distressed metal in front of the crack, corroborating the conclusion of the examiner that no other features were seen.

Figures 60 and 61 clearly show the martensite-like structure on the surface of the steel samples. Figure 60 shows steel sample S1 at 3,000-power magnification, and Figure 61 shows steel sample S2 at 3,000-power magnification. Figure 62 shows a crack edge of steel sample S1 at 9,000-power magnification. The martensite-like structure is clearly visible; however, little or no slip is seen near the crack (as it was for Inconel and aluminum) because of the fineness of the micro-structure.

Figure 63 shows the tip of the main crack on steel sample S1, 750,000 cycles at 9,000-power magnification. Some structure is seen; however, features other than the crack, which could give rise to a signal, are not evident.

3.4.3 Electron Microprobe Analysis

The samples were inserted in the microprobe after washing with acetone to remove surface oil or grease and mounting in the specimen holder with silver paint as an adhesive.

Three types of studies were made of each sample:

(1) Specimen current image. In forming this image, a small area (100 x 130μ) of the sample is scanned by the microprobe beam, and the electron current absorbed by the sample at each point is used to modulate the intensity of a Cathode Ray beam scanning in synchronism

with the probe beam.

(2) X-ray image. In forming this image, again, a 100 x 130μ area of the sample is scanned by the probe beam. An X-ray spectrometer is focussed for a prominent characteristic line of one of the elements known or assumed to be in the sample. The signal from the flow proportional counter detector in the spectrometer is utilized to modulate the intensity of the CR scanning in synchronism with the microprobe beam.

(3) Step scan study. In this method, the microprobe beam is moved in 1μ steps along a straight line (at right angles to a crack) on the sample. One X-ray spectrometer is focussed for a characteristic line of one element suspected or known to be present in the sample. A second X-ray spectrometer is focussed for a characteristic line of another element suspected or known to be present. X-ray photons received by each spectrometer detector during a 50-second counting period at each step are recorded automatically on a paper tape. In general, the location of the crack across the line of scan can be determined from the position of a minimum or maximum in the number of counts due to one of the elements (e.g., in the case of the steel sample, the position of the crack coincided with a minimum in the number of counts due to Fe-K_α radiation and a maximum due to O-K_α radiation).

9310 Steel (Fig. 66)

(a) One O-K_α picture shows the presence of O along the crack.

(b) Other X-ray images (Ni-K_α, Cr-K_α, C$K_\alpha$images) give negative results.

(c) Step scan studies show an increase in O at the crack in agreement with observation (a). The amount of additional O is apparently less near the end of the crack than some distance back from the end. This may be a real effect or an artifact due to more of the O radiation being absorbed where the crack is narrower.

(d) Specimen current and X-ray images all show a lack of homogeneity in samples and the formation of ridges of disturbed alloy along both edges of the crack.

Aluminum (Fig. 64)

(a) The crack, in many regions at least, follows grain

boundaries.

(b) As is to be expected, the aluminum sample shows an oxide surface layer.

(c) X-ray images using O-K_α, Al-k_α, and Mg-K_α all show a deficiency of these elements along the crack itself, as is to be expected. There appeared to be no concentration of any of these elements along the edges of the crack. Aluminum differs from steel in this latter respect.

Inconel (Fig. 65)

(a) Sample current images suggest strong inhomogeneity of composition, which was not confirmed by the Ni, Cr, Fe, and Si X-ray images. The apparent inhomogeneity is probably due to different crystallographic orientations of the various grains or to the presence of slip.

(b) The crack follows grain boundaries in many cases.

(c) Displacements of material (slip) parallel to the direction of the crack are noted by observation of jogs in surface scratches crossing the cracks.

(d) At some points along the crack, entire grains appear to be displaced a few microns upward perpendicular to the surface of the sample.

Figures 67 and 68 show the results of step scans of the electron beam across the crack as described in 3.4.3 (3). The ordinate indicates the intensity of the K_α X-ray line of the element as measured for periods of one minute. The K_α lines of chromium and nickel show a decided decrease in intensity at the position of the crack (three runs each, Figure 67). Figure 68 (step scan on a steel sample) shows a significant peak in the oxygen K_α X-ray line, thus confirming the presence of corrosion as seen in the scanning electron microscope studies.

SECTION 4

CONCLUSION AND RECOMMENDATION

The results of the tests conducted for this program and reported in Section 3 clearly indicate that the use of an inductive detection system to detect impending fatigue failures in metals is extremely feasible. The roll test results point to the questionable value of such a detection system for detecting rolling contact fatigue; however, the vibratory-beam-test results clearly indicate that an inductive detection system is of significant value in detecting this type of metal fatigue. The etiology of signals has been investigated through use of modern microanalytic techniques as well as classical metallography, and the results of these investigations show that microcracks as well as larger cracks are responsible for these signals. The system, as used for this program, is a laboratory-type device; however, it can readily be packaged for field use without sacrifice of utility or sensitivity.

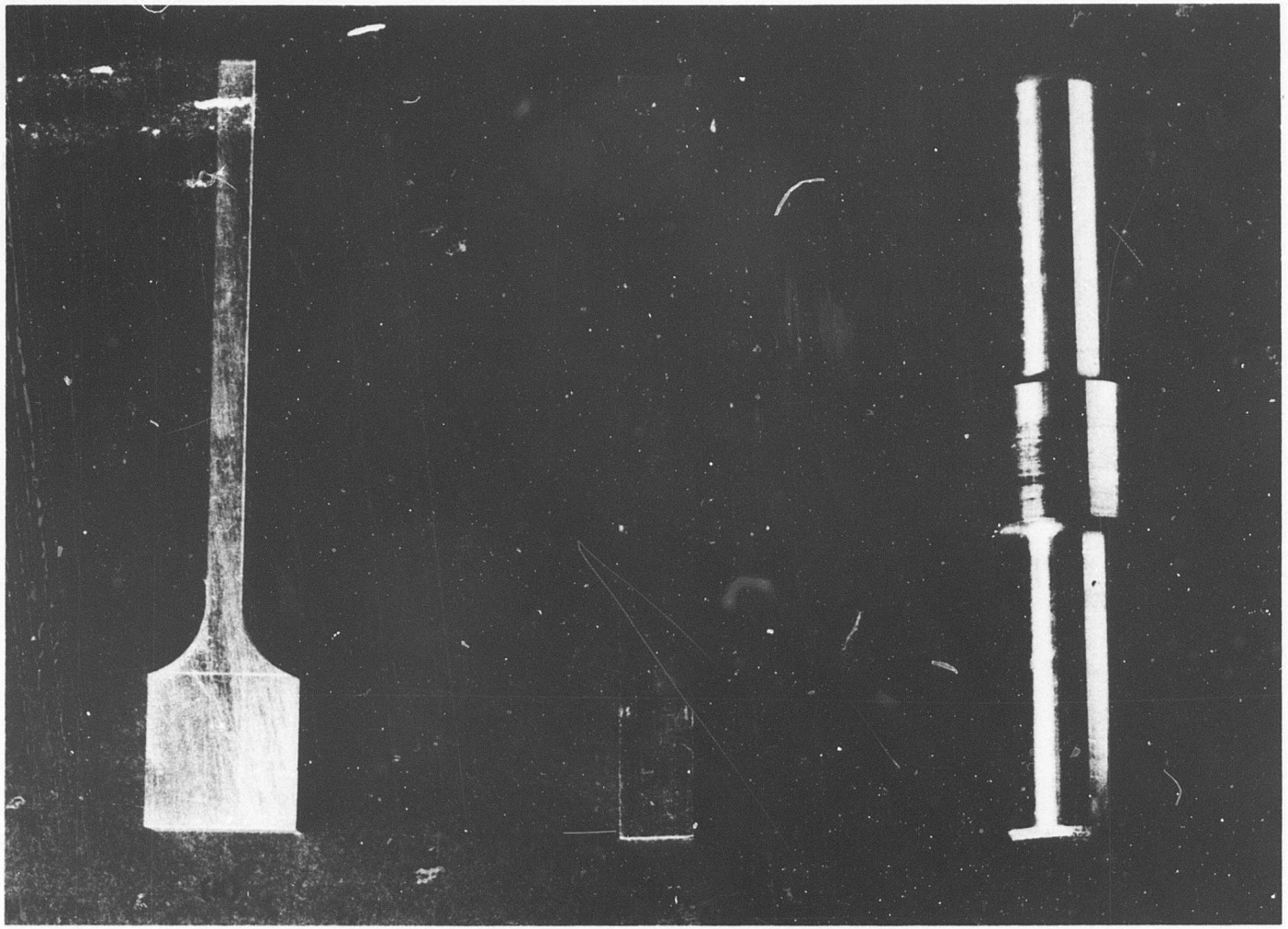

Figure 1. Test Samples.

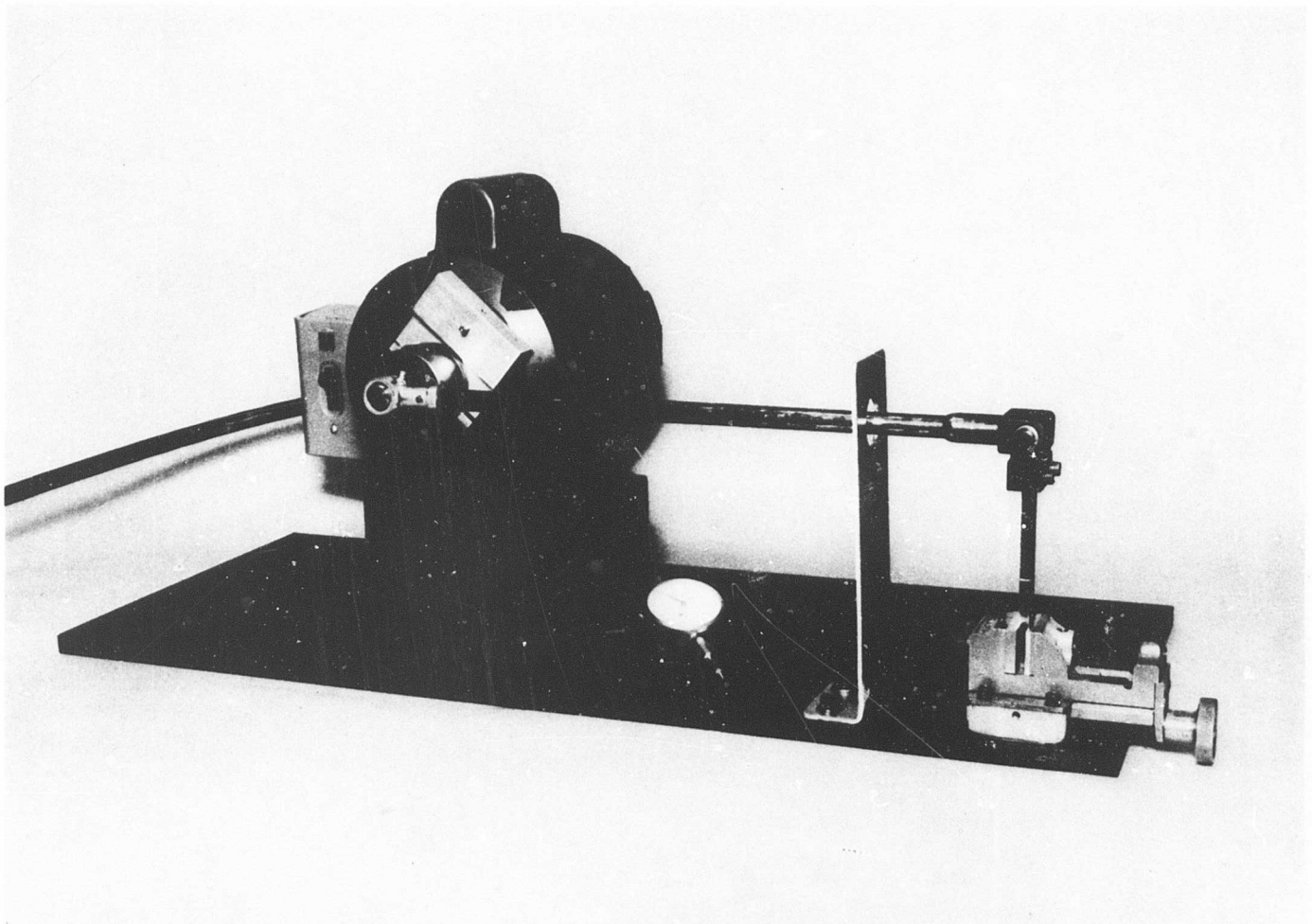

Figure 2. Vibratory Beam Fatigue Machine.

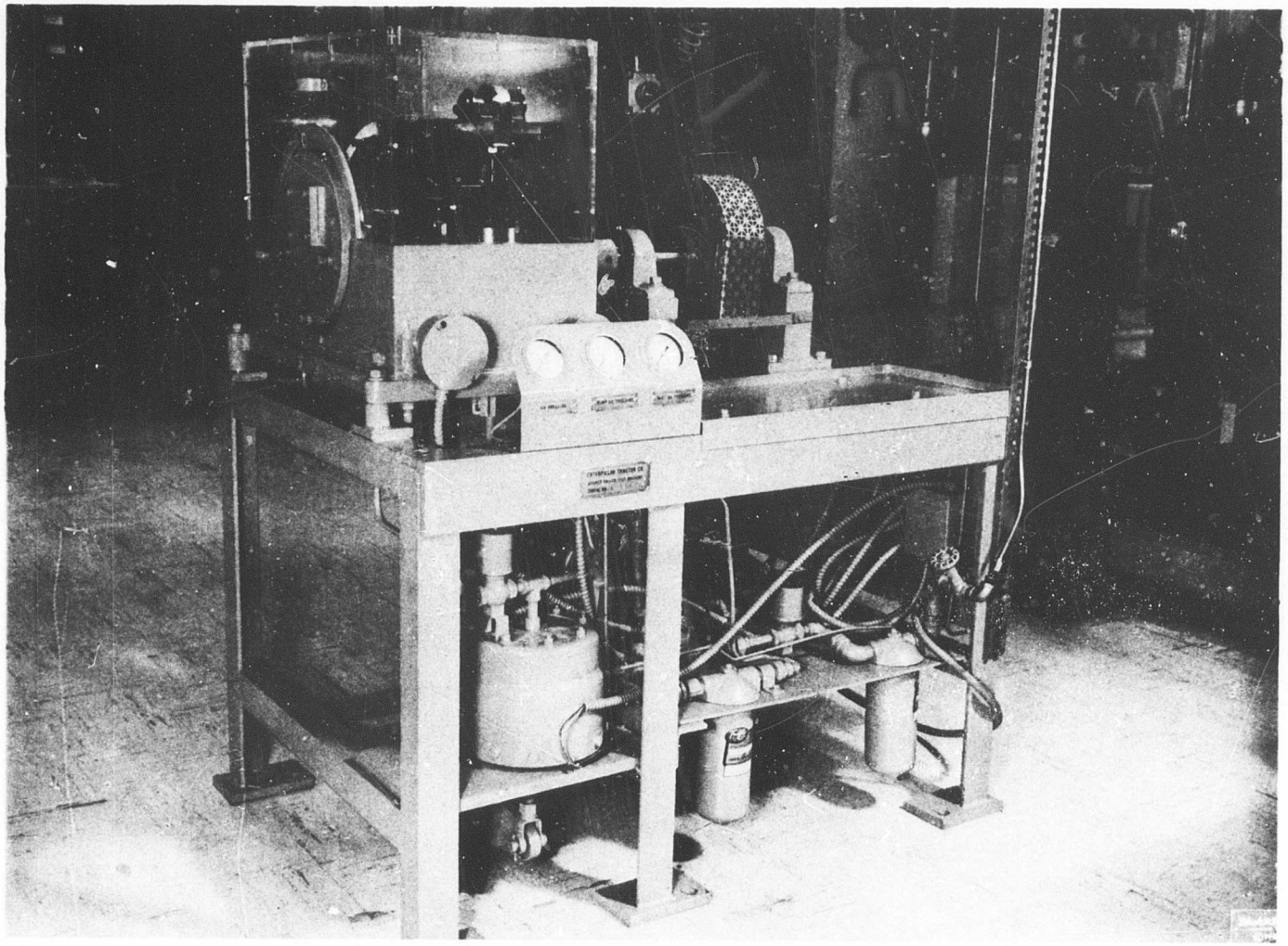

Figure 3. Geared-Roller Test Machine.

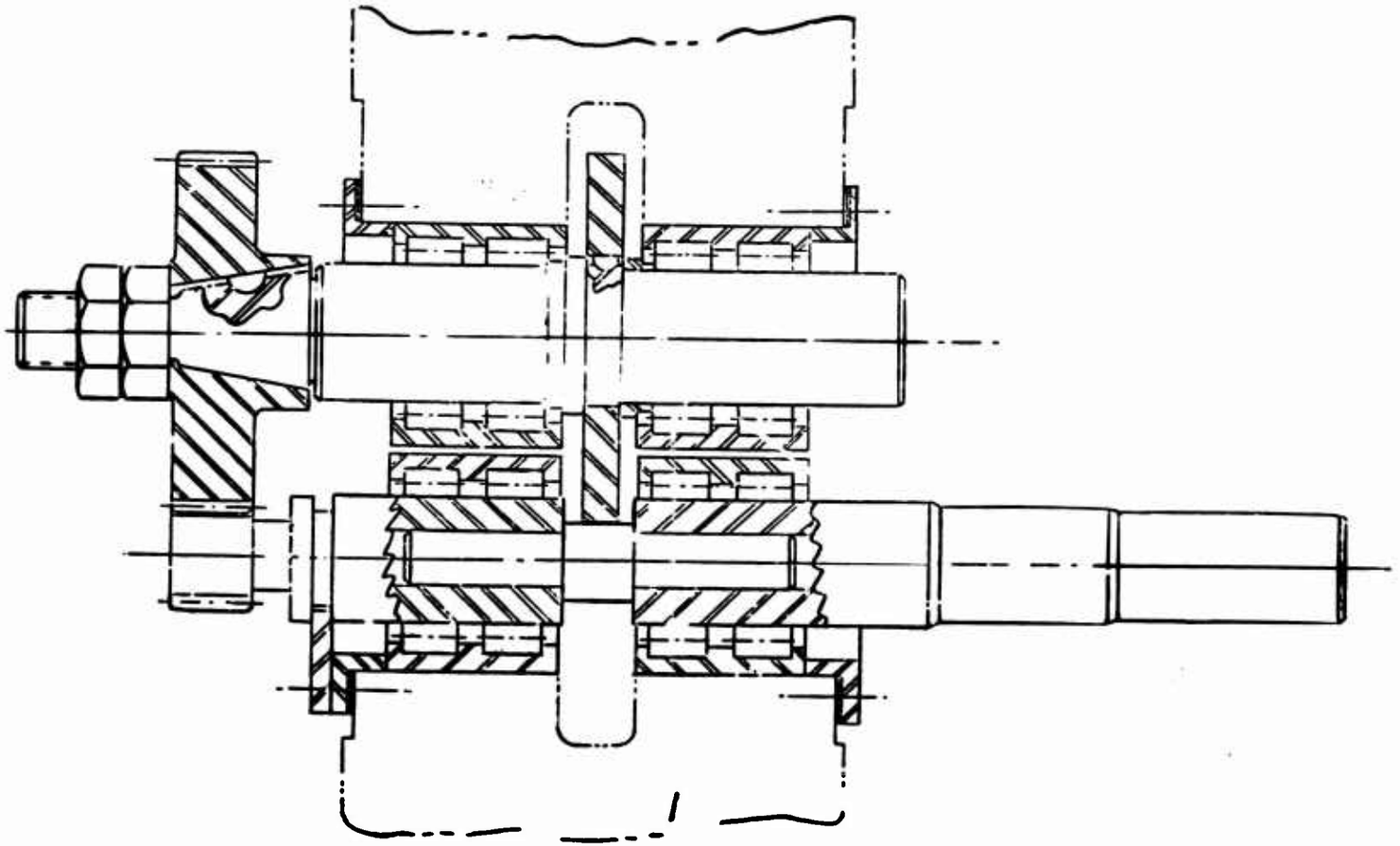

Figure 4. Schematic of Geared-Roller Test Machine.

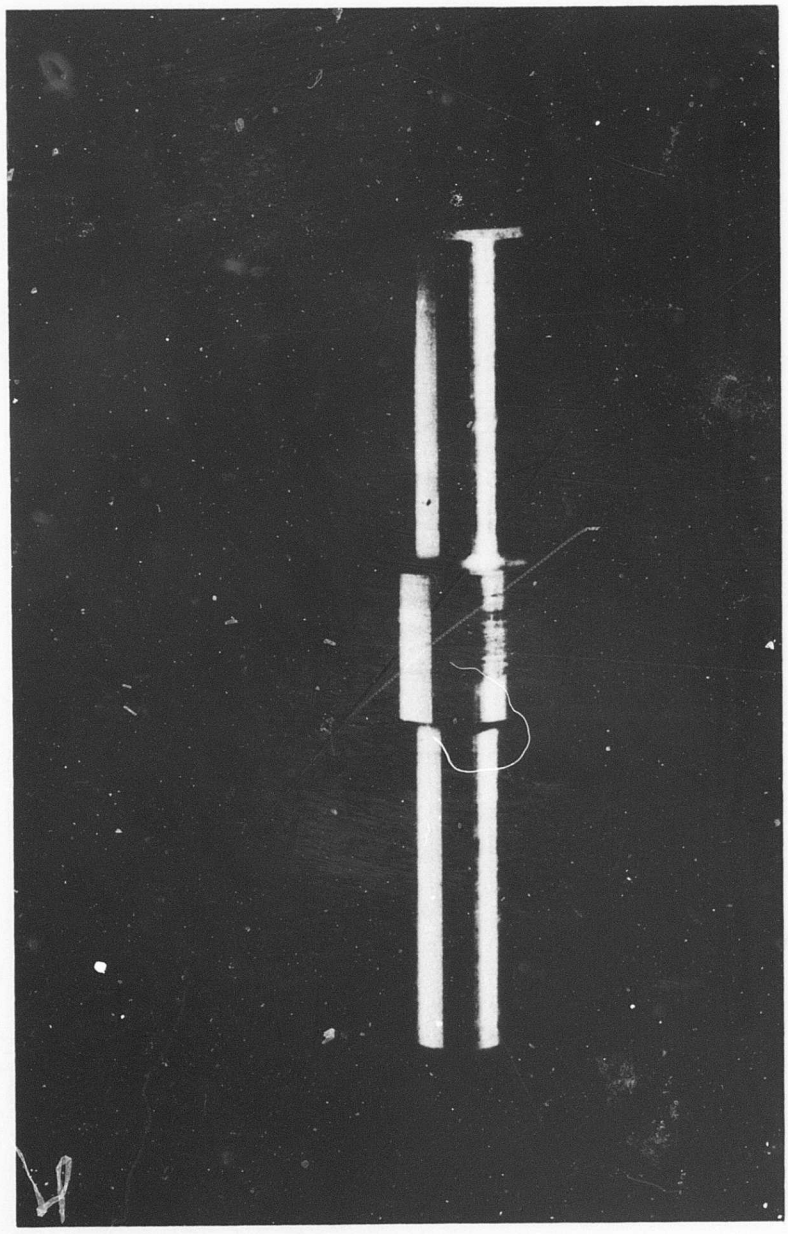

Figure 5. Roll Test Sample.

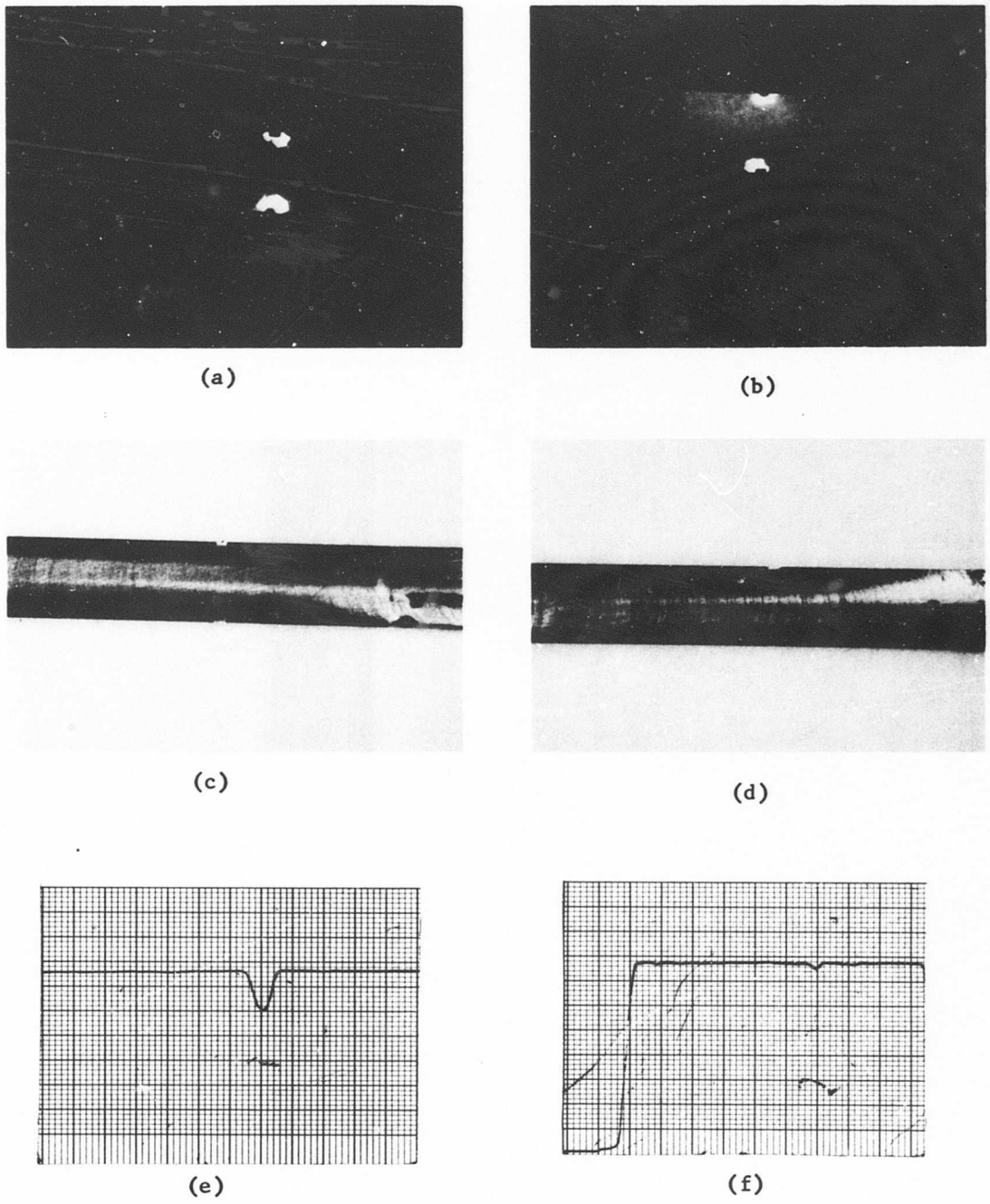

Figure 6. Comparison of Inductive Sensor With Dye Penetrant Technique.

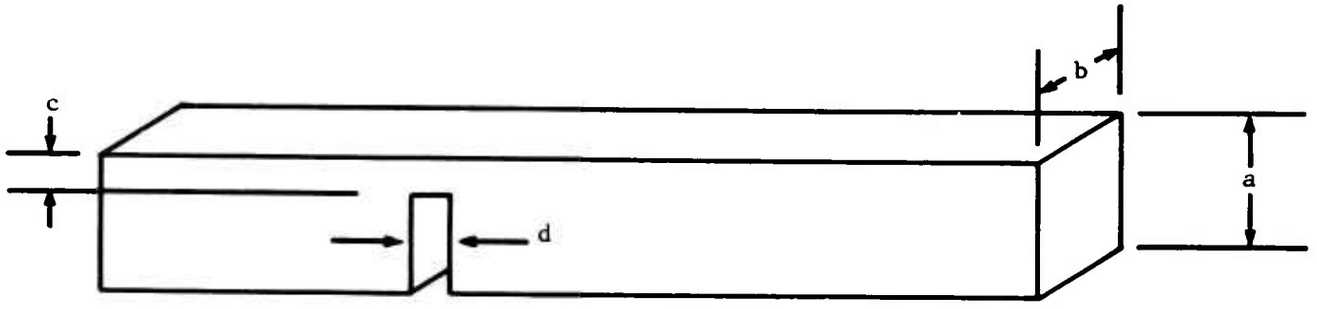

Figure 7. Sample for Preliminary Examination.

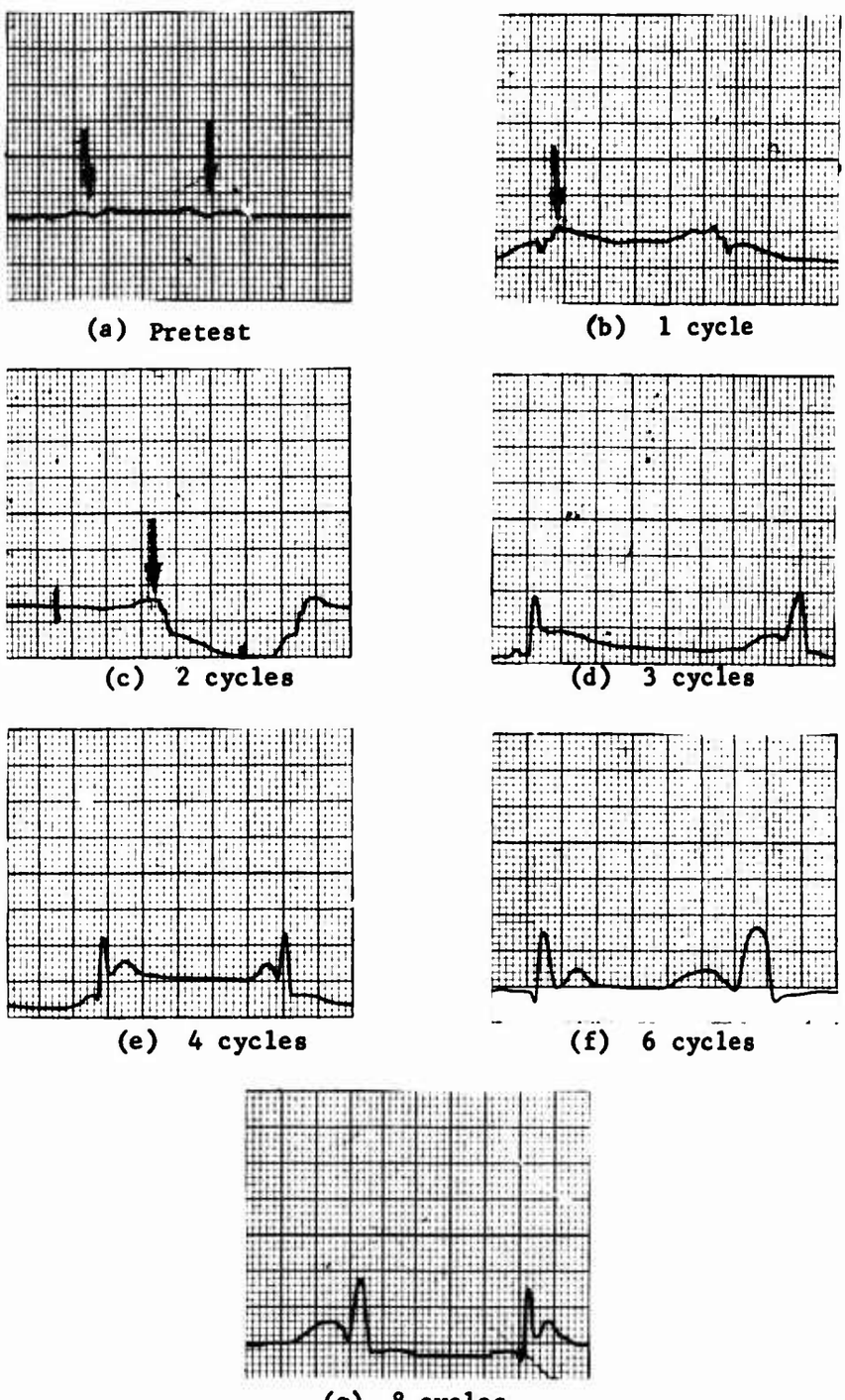

Figure 8. Preliminary Examination of Steel Sample.

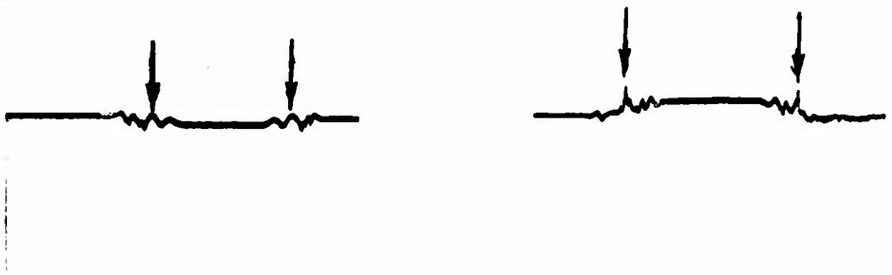

(a) (b)

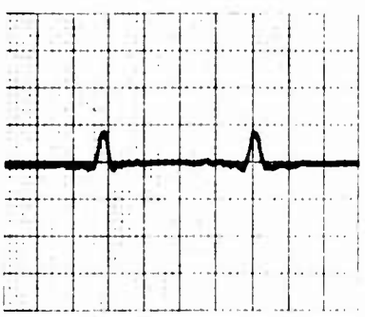

(c)

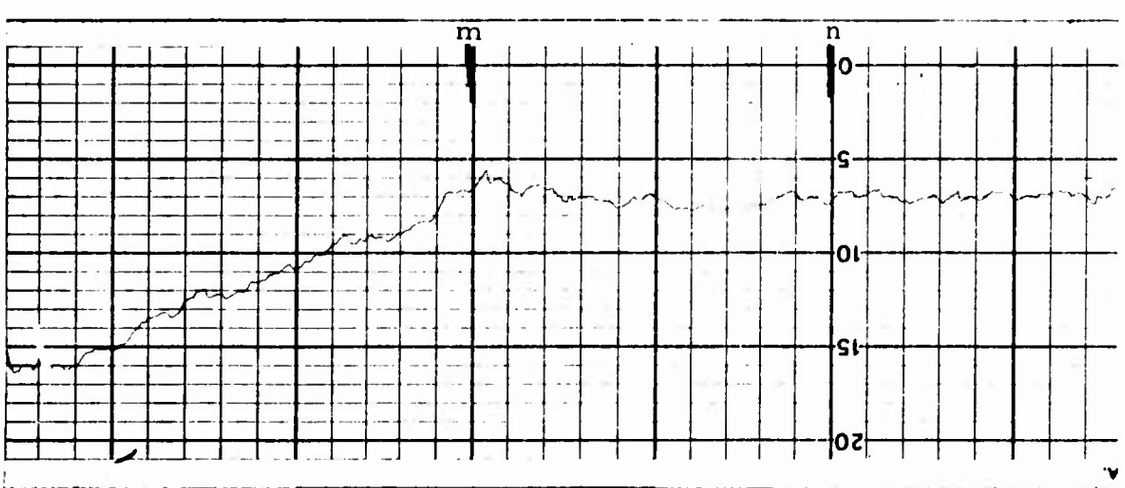

(d)

Figure 9. Preliminary Examination of Steel Sample.

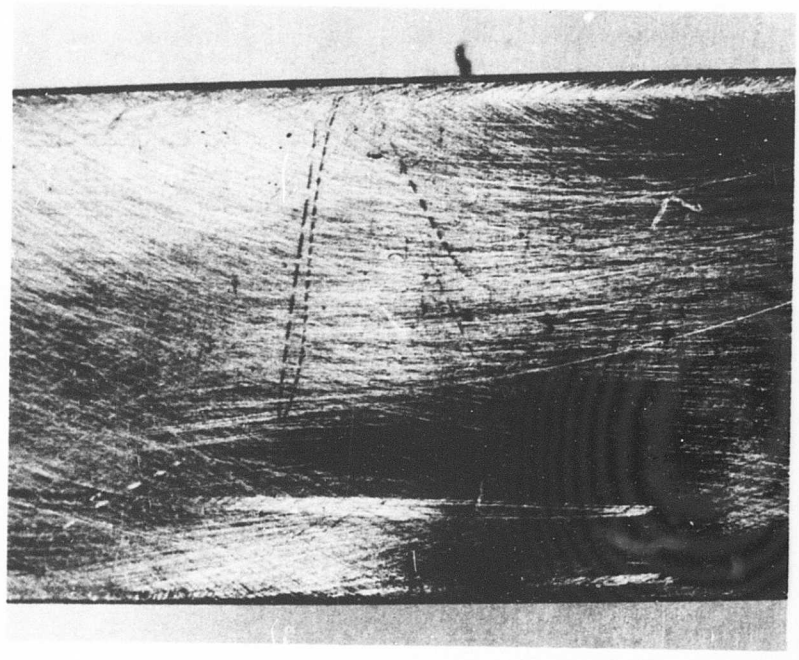

(a) X4 Mag, As Received

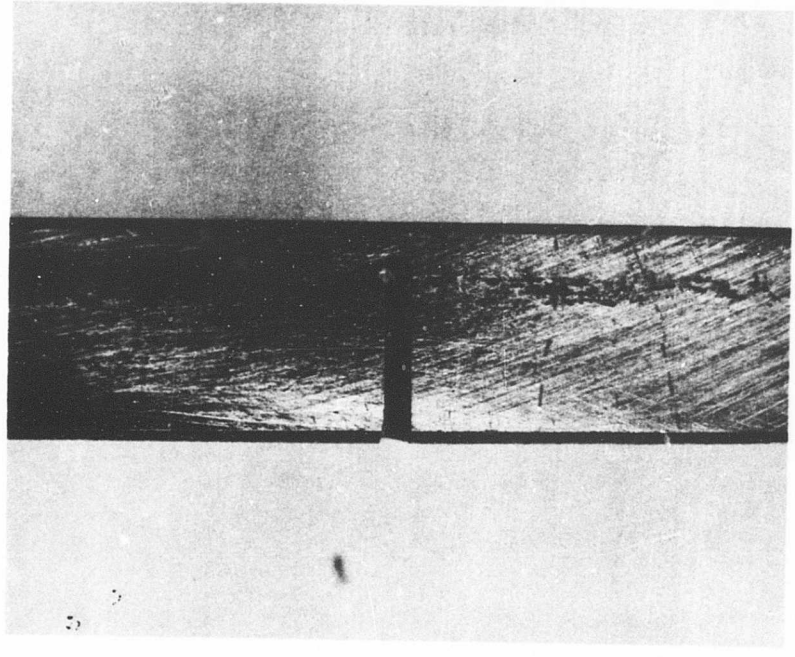

(b) X4 Mag, As Received

Figure 10. Preliminary Examination of Steel Sample.

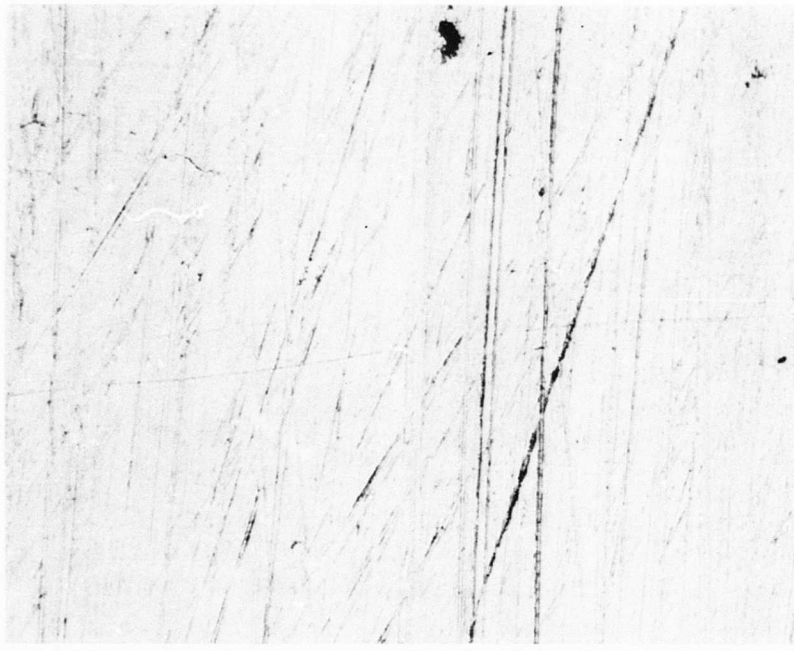

(c) X100 Mag, As Received

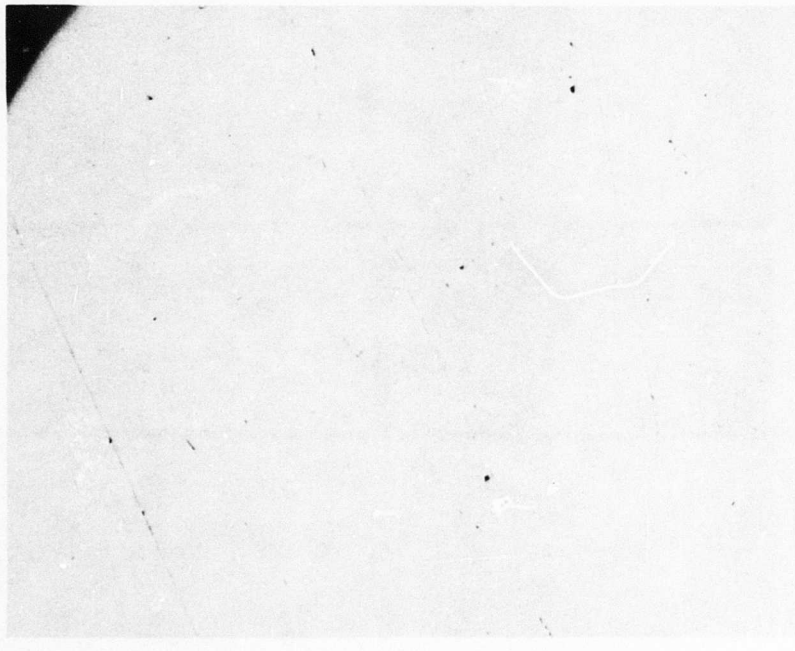

(d) X 100 Mag, Notched Area, After Polishing

Figure 10. (continued)

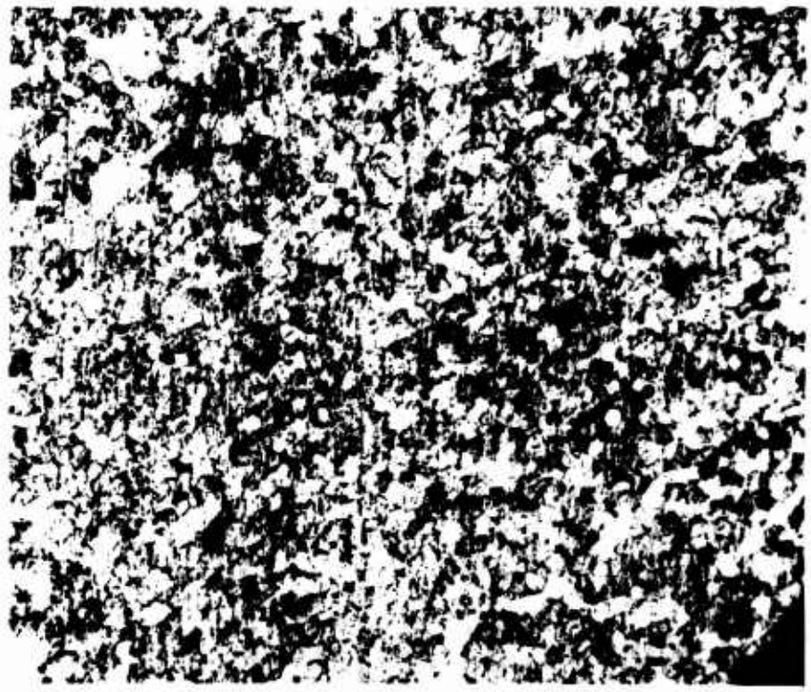

(e) X100 Mag, Notched Area, 2% Nital Etchant

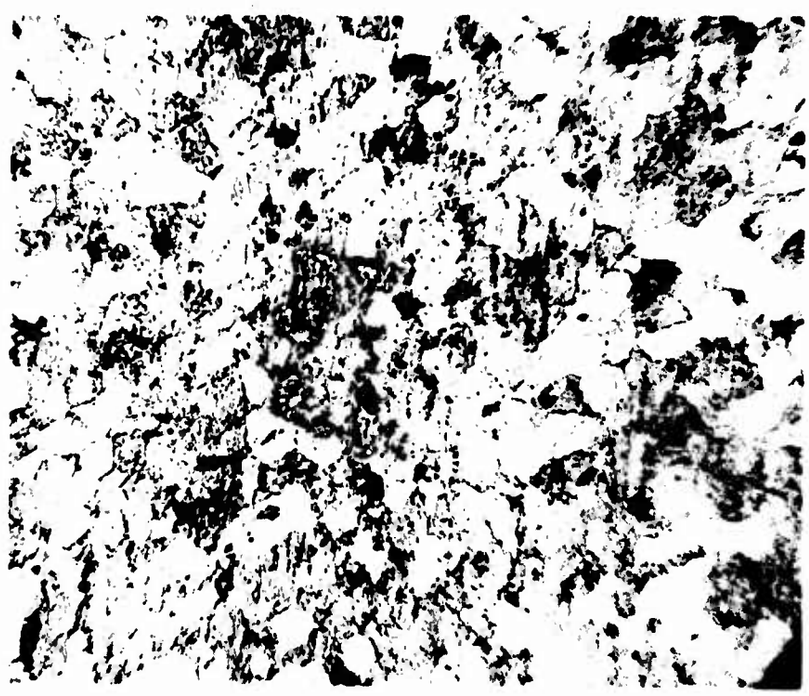

(f) X300 Mag, Notched Area, 2% Nital Etchant
Figure 10. (continued)

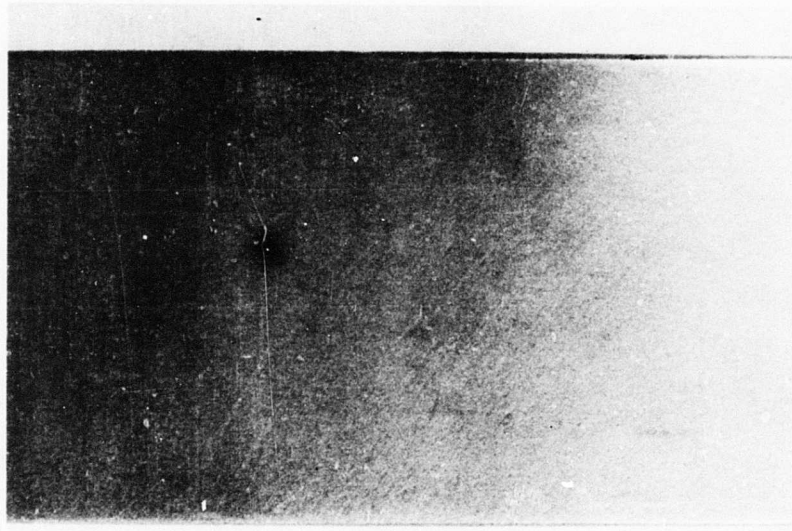

(g) X4 Mag, After Polishing and Etching,
2% Nital Etchant

Figure 10. (continued

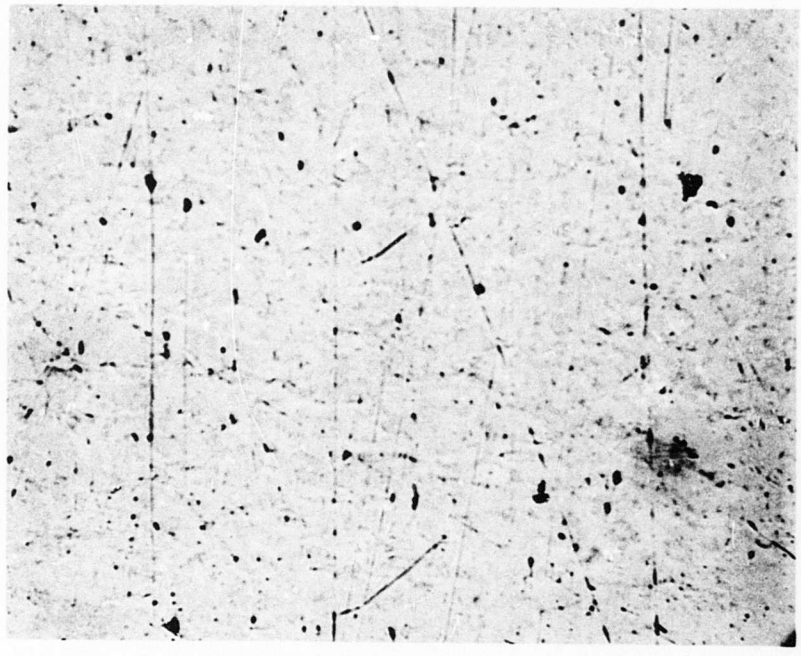

(h) X100 Unetched, Notched Area After Flexing 1 Cycle

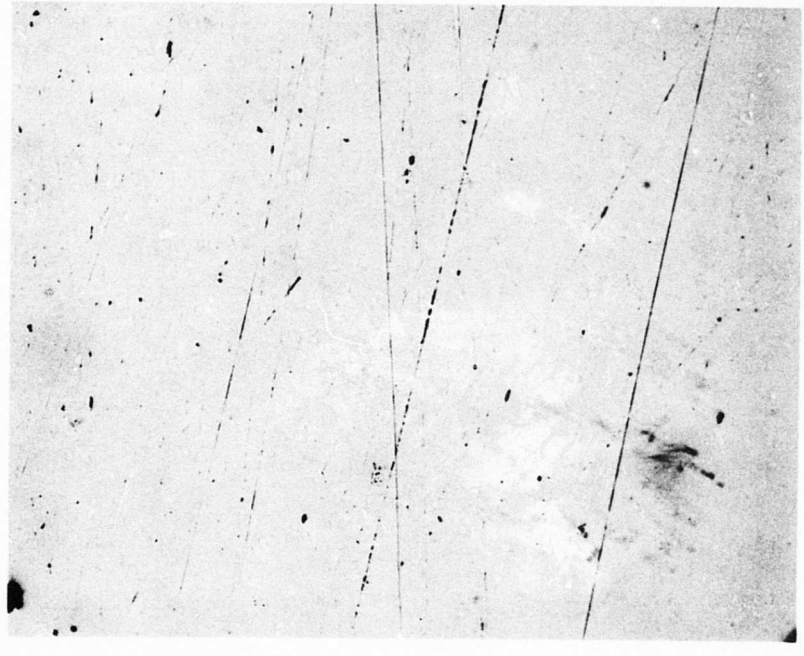

(i) X100 Unetched, Area Away From Notch After Flexing 1 Cycle

Figure 10. (continued)

(j) X100 Mag, Etched, Notched Area

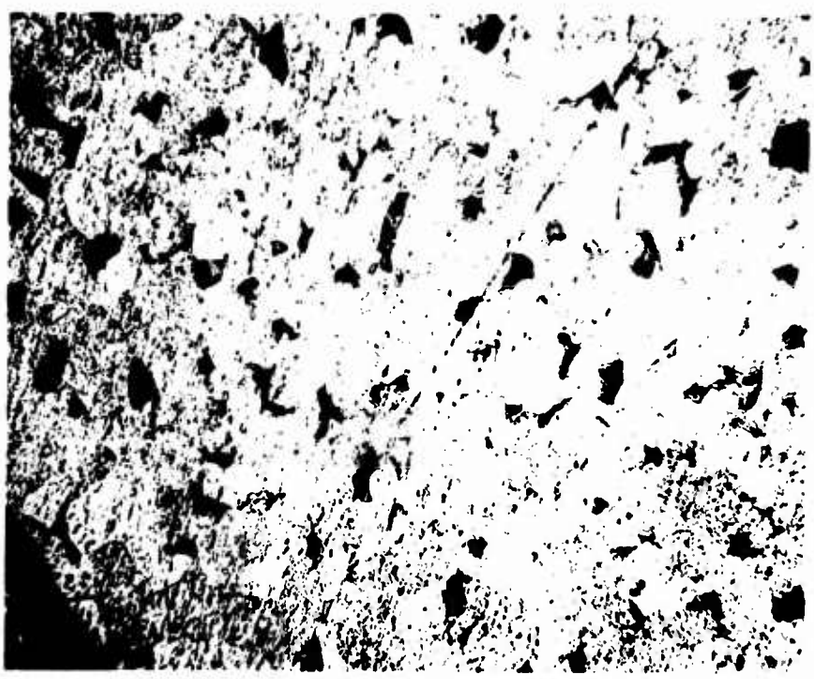

(k) X300 Mag, Etched, Notched Area

Figure 10. (continued)

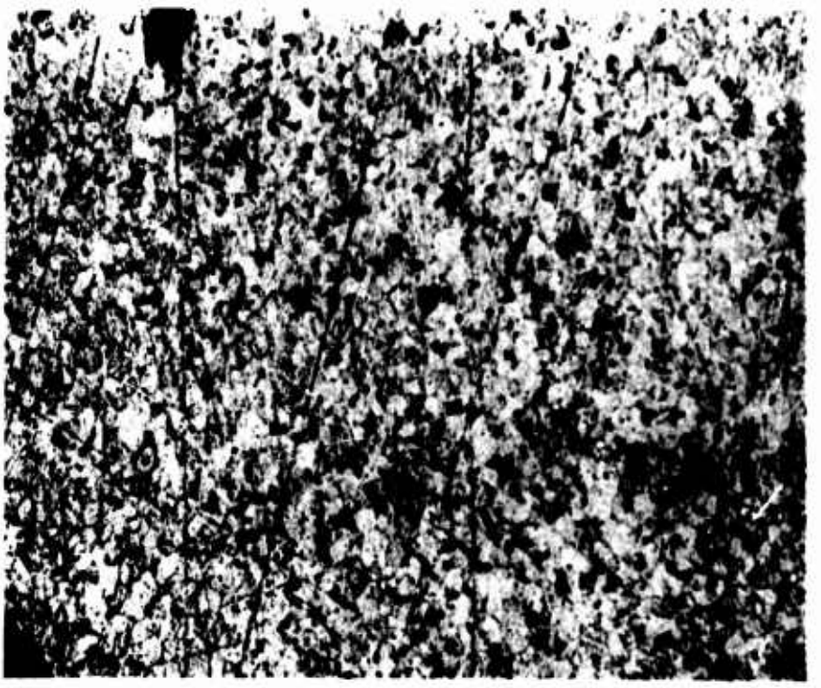

(l) X100 Mag, Etched, Area Away From Notch

(m) X300 Mag, Etched, Area Away From Notch

Figure 10. (continued)

(n) Inductive Scan, 1 Additional Cycle

Figure 10. (cont'd)

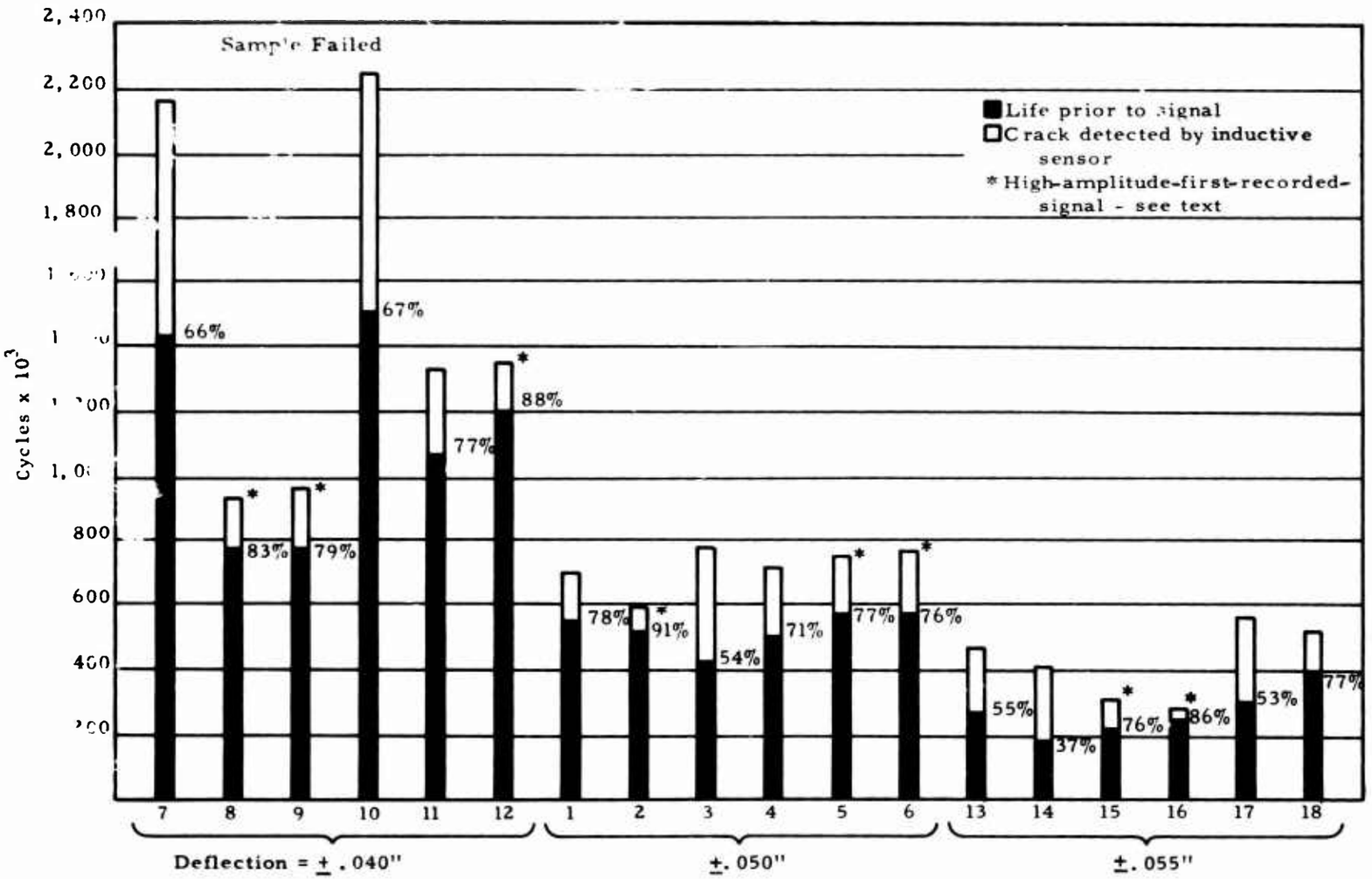

Figure 11. Graphical Presentation of Results, Aluminum.

Front

Back

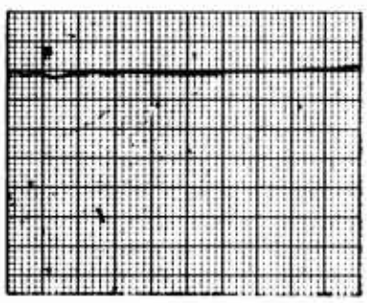

(a)

0

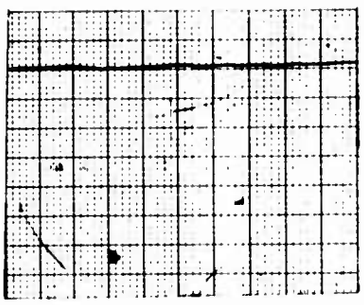

(b)

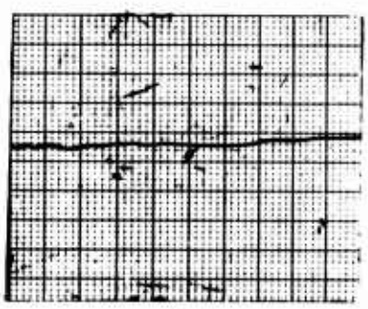

(c)

(d)

120,000 Bending Cycles

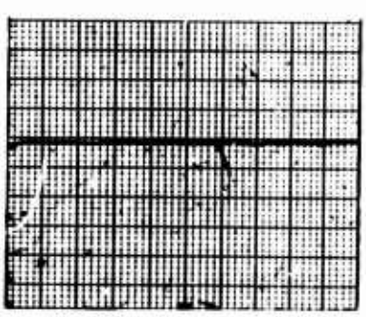

(e)

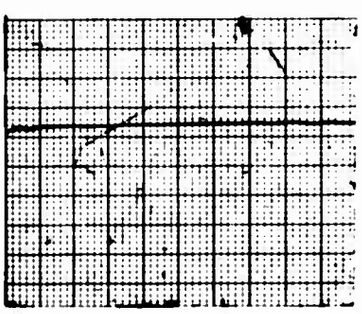

(f)

240,000

Figure 12. Aluminum Sample 17, ±.055" Deflection.

Front

Back

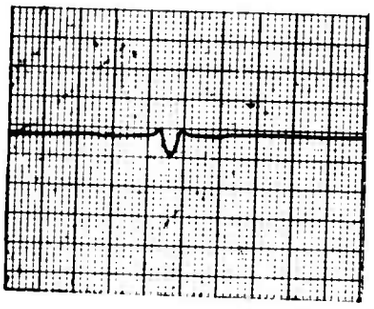

(g)

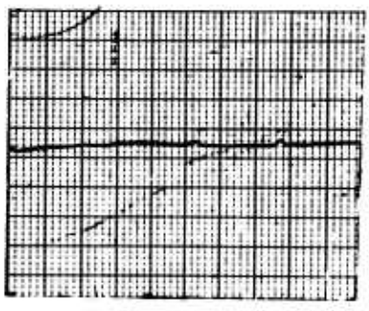

(h)

300,000 Bending Cycles

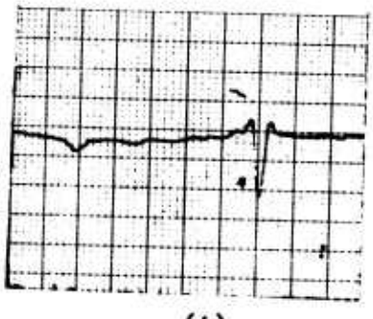

(i)

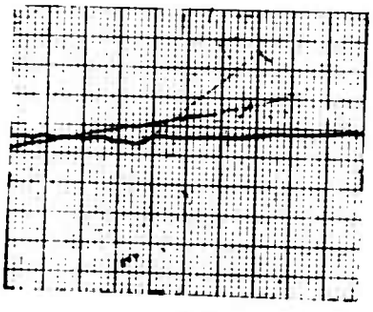

(j)

420,000

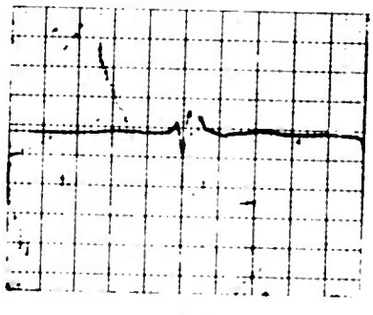

(k)

462,000

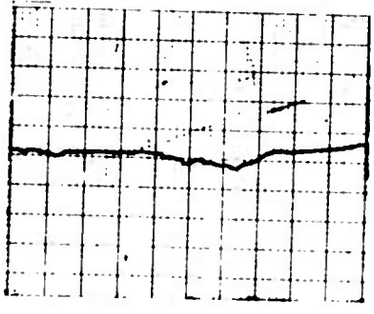

(l)

Figure 12. (continued)

Front

Back

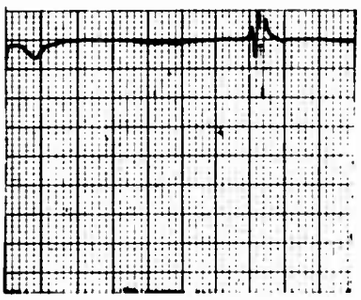

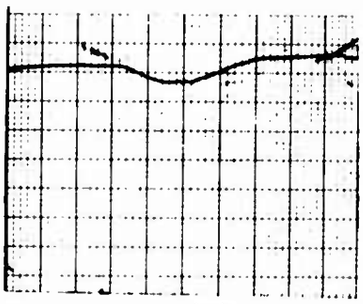

(m) 490,000 Bending Cycles (n)

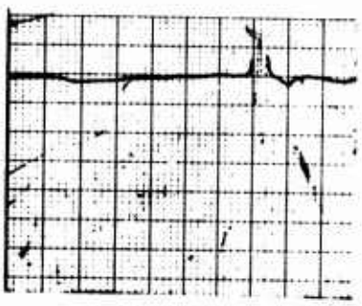

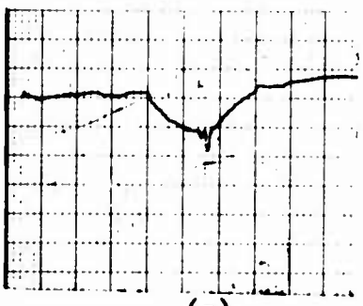

(o) 540,000 (p)

Sample failed at 526,000 cycles.

Figure 12. (continued)

Front

Back

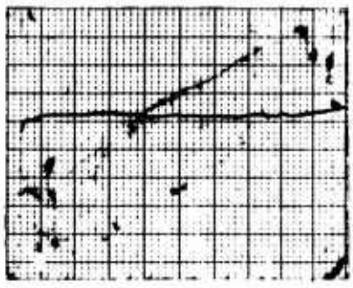

(a)

0

(b)

(c)

576,000 Bending Cycles

(d)

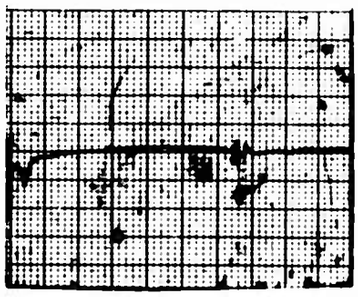

(e)

585,000

(f)

Figure 13. Aluminum Sample 6, ±.050" Deflection.

Front

Back

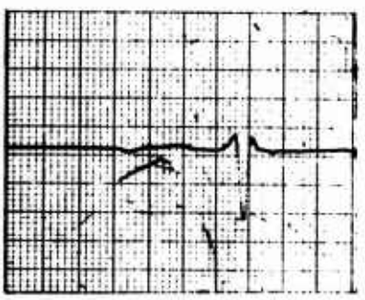

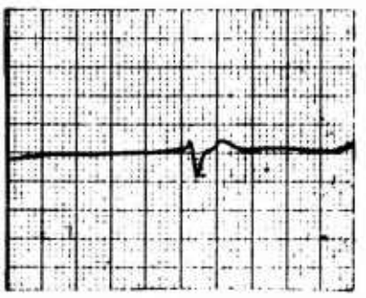

(g) 650,000 Bending Cycles (h)

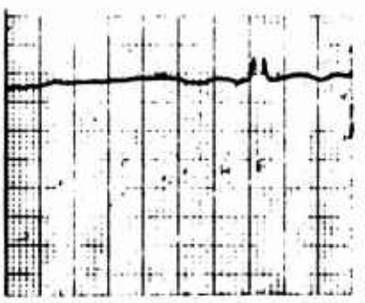

(i) Crack visible 730,000 (j)

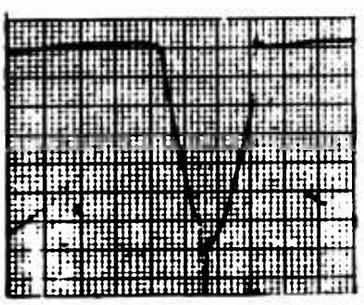

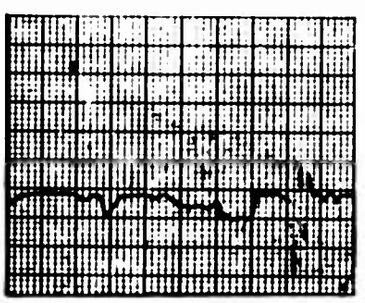

(k) 760,000 (l)

Sample failed at 762,800 cycles.

Figure 13. (continued)

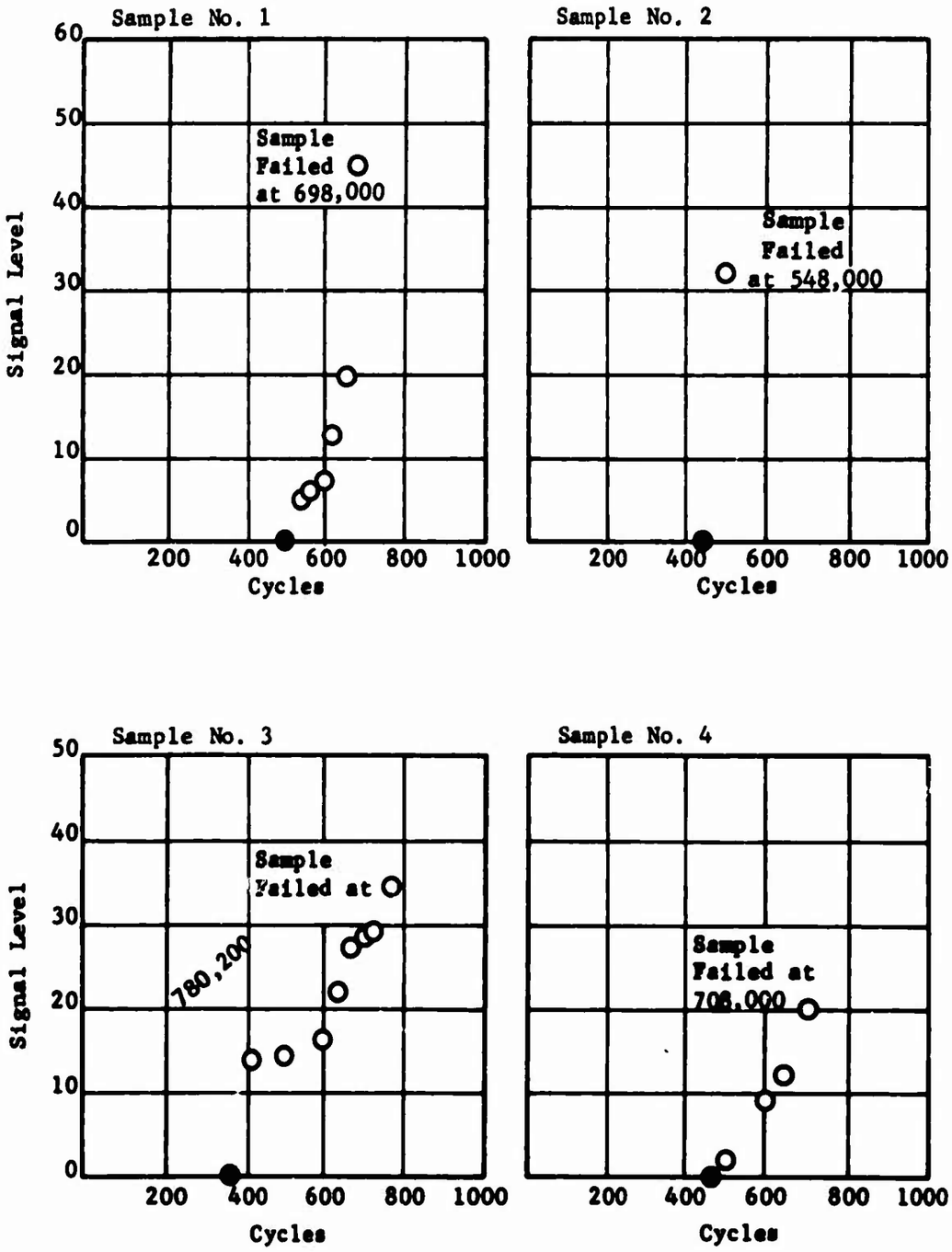

Figure 14. Output Signal vs. Number of Cycles, 6061-T6 Aluminum.

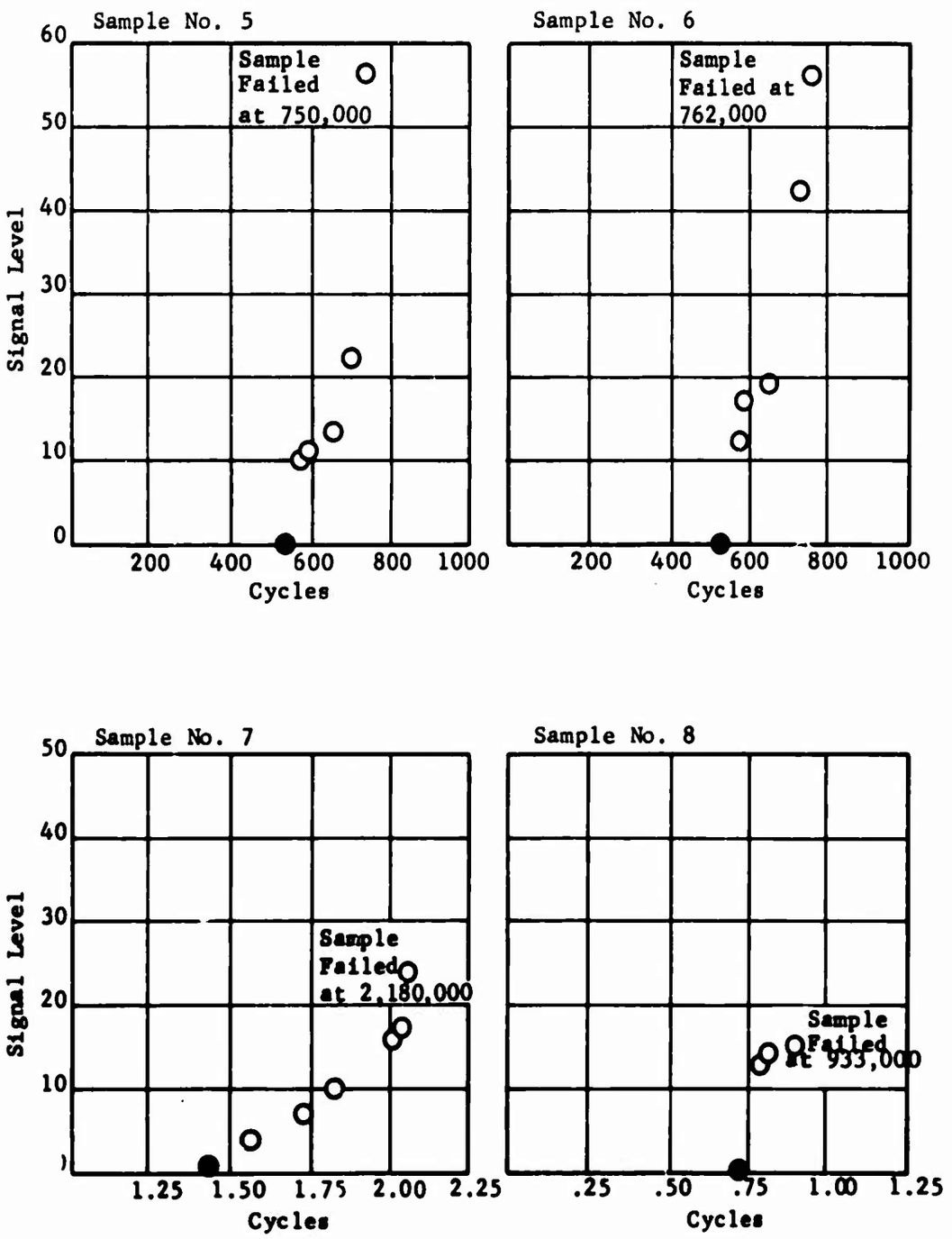

Figure 14. (continued)

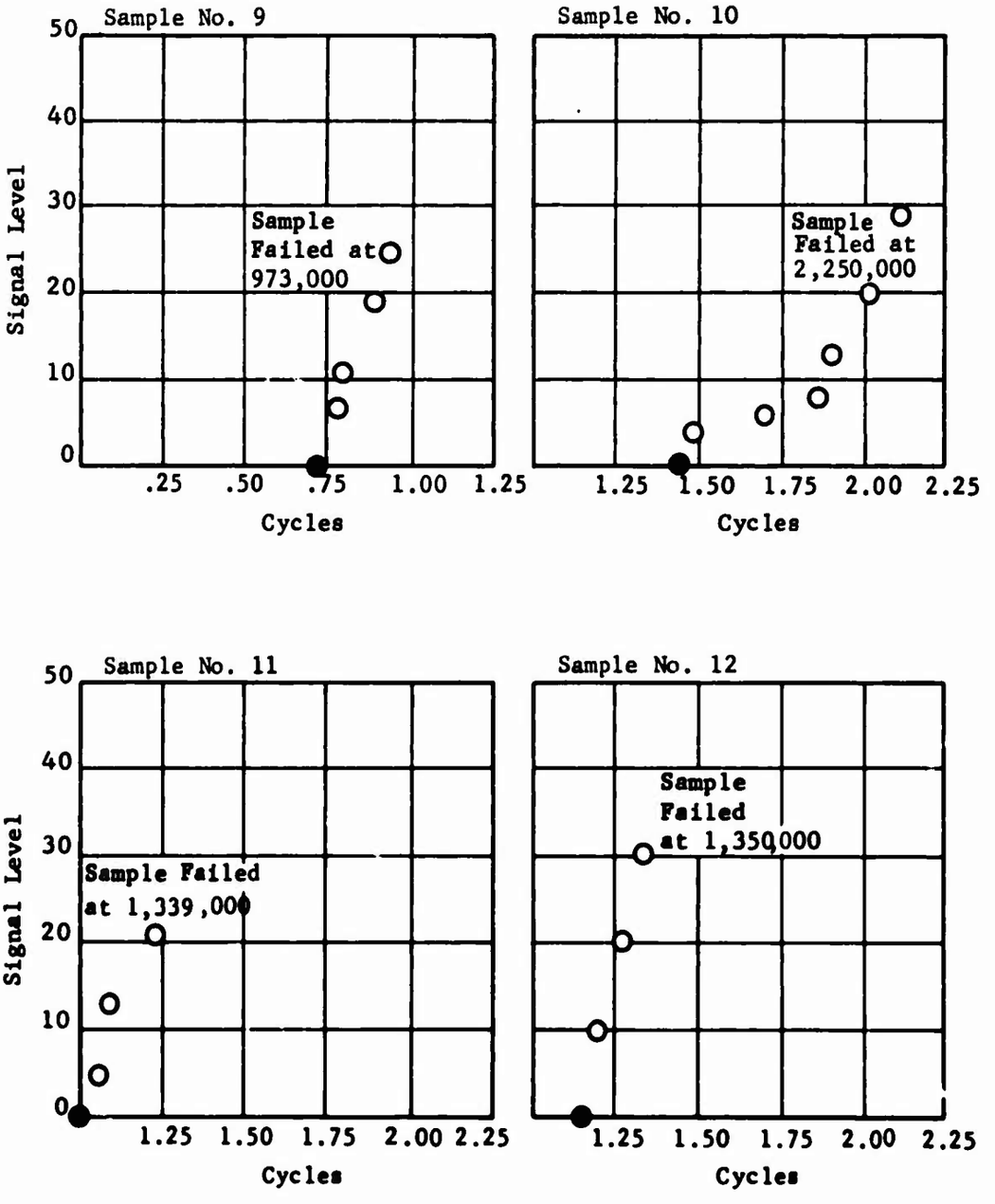

Figure 14. (continued)

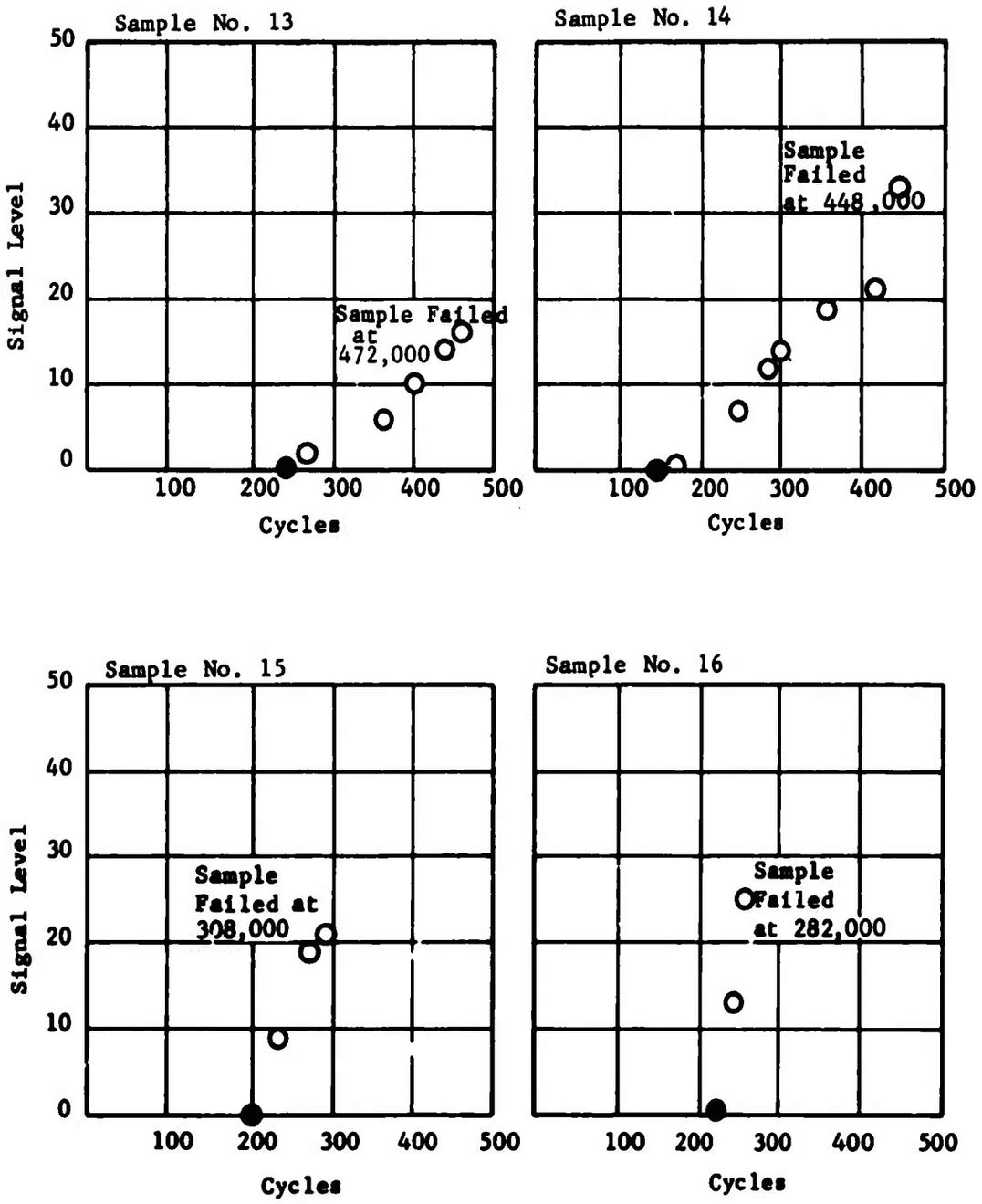

Figure 14. (continued

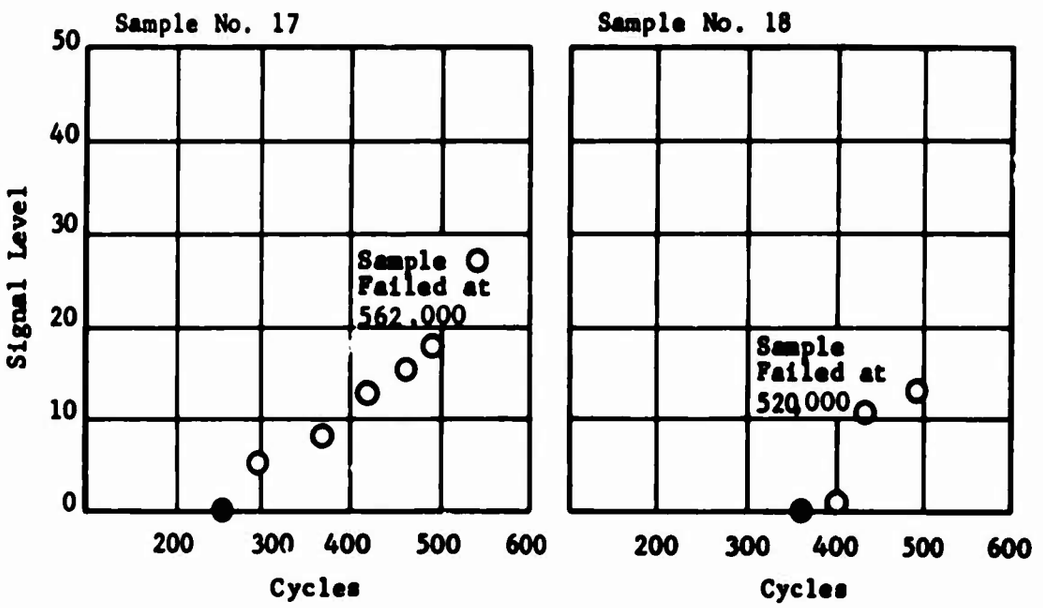

Figure 14. (continued)

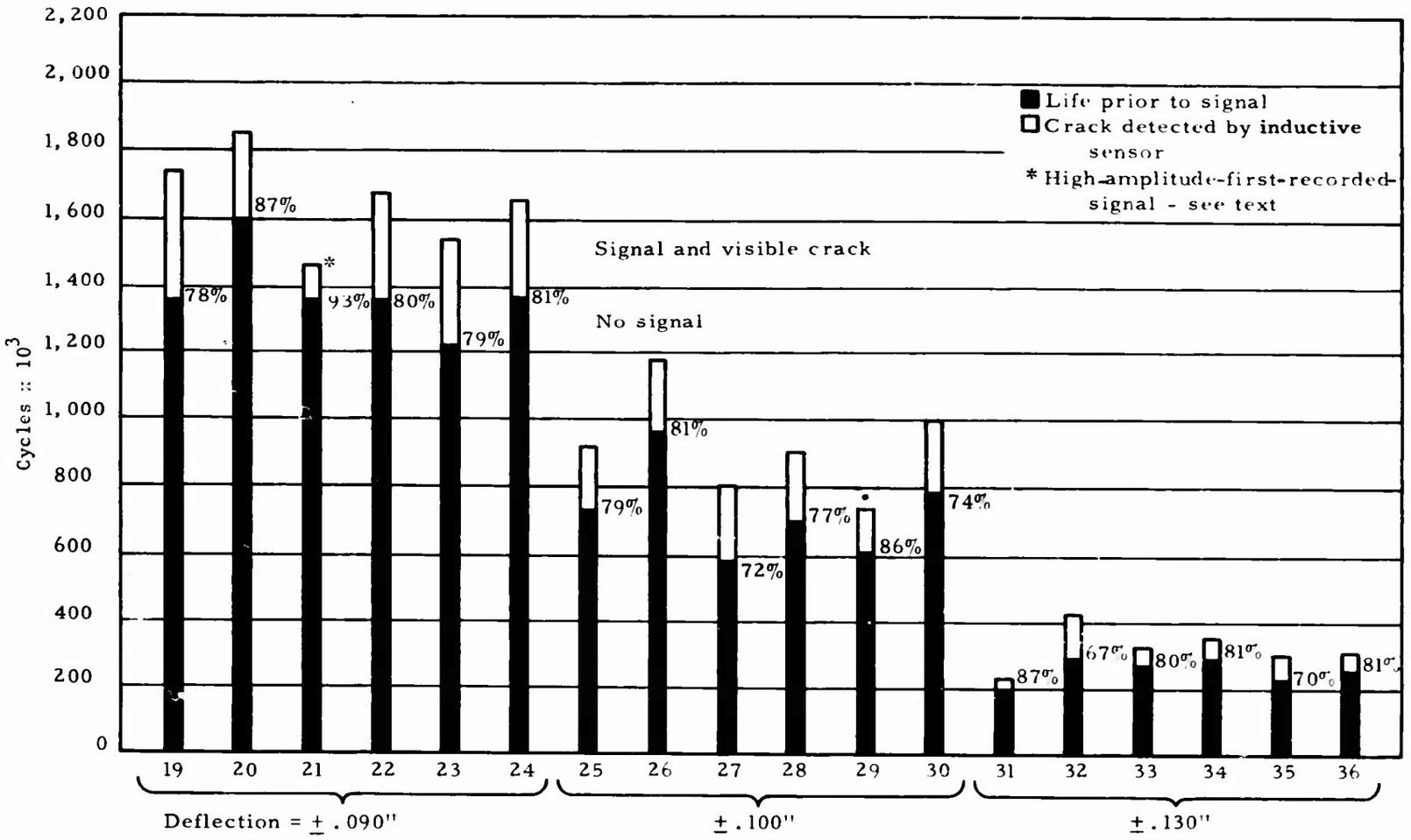

Figure 15. Graphical Presentation of Results, Inconel X.

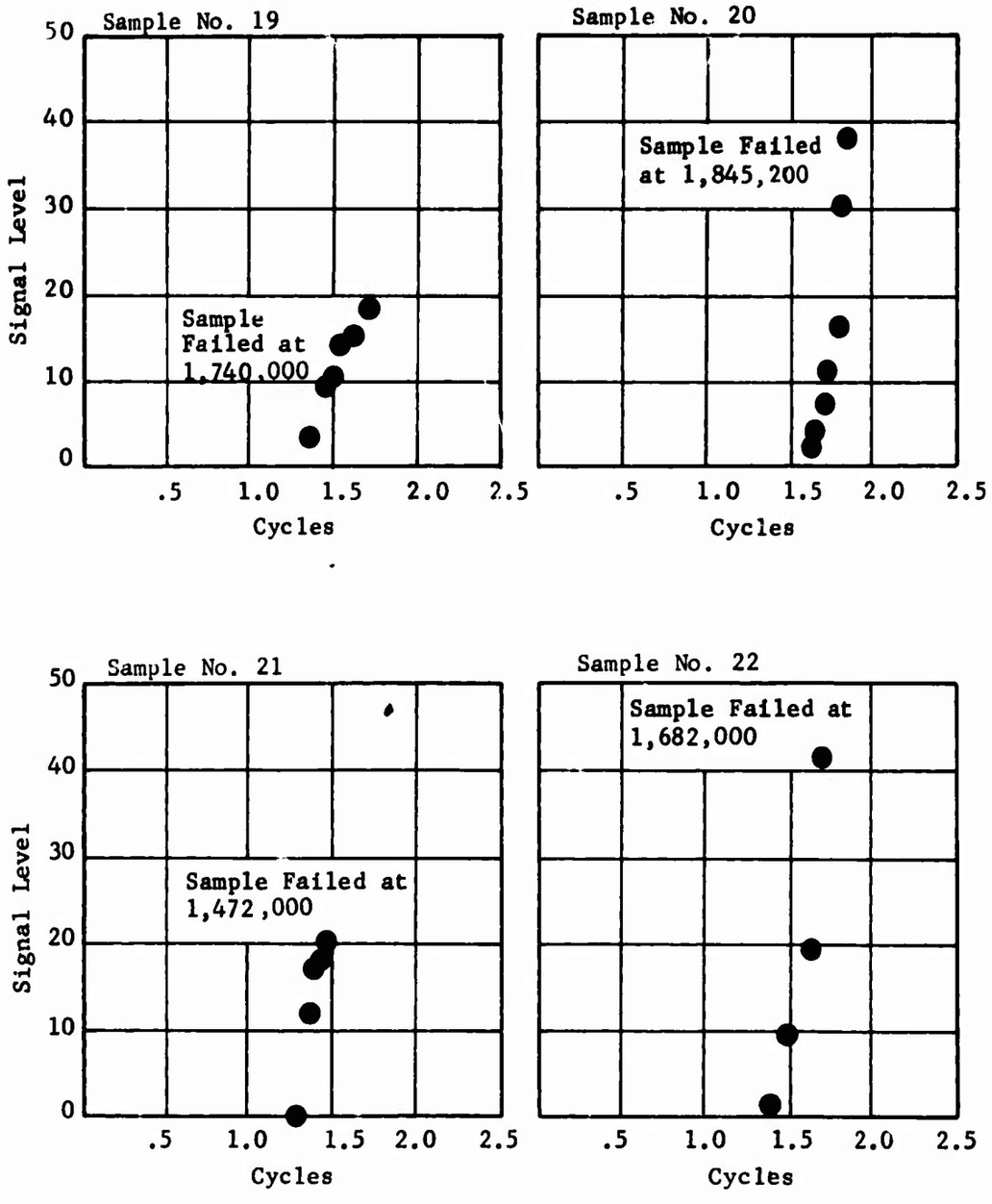

Figure 16. Output Signal vs. Number of Cycles, Inconel X.

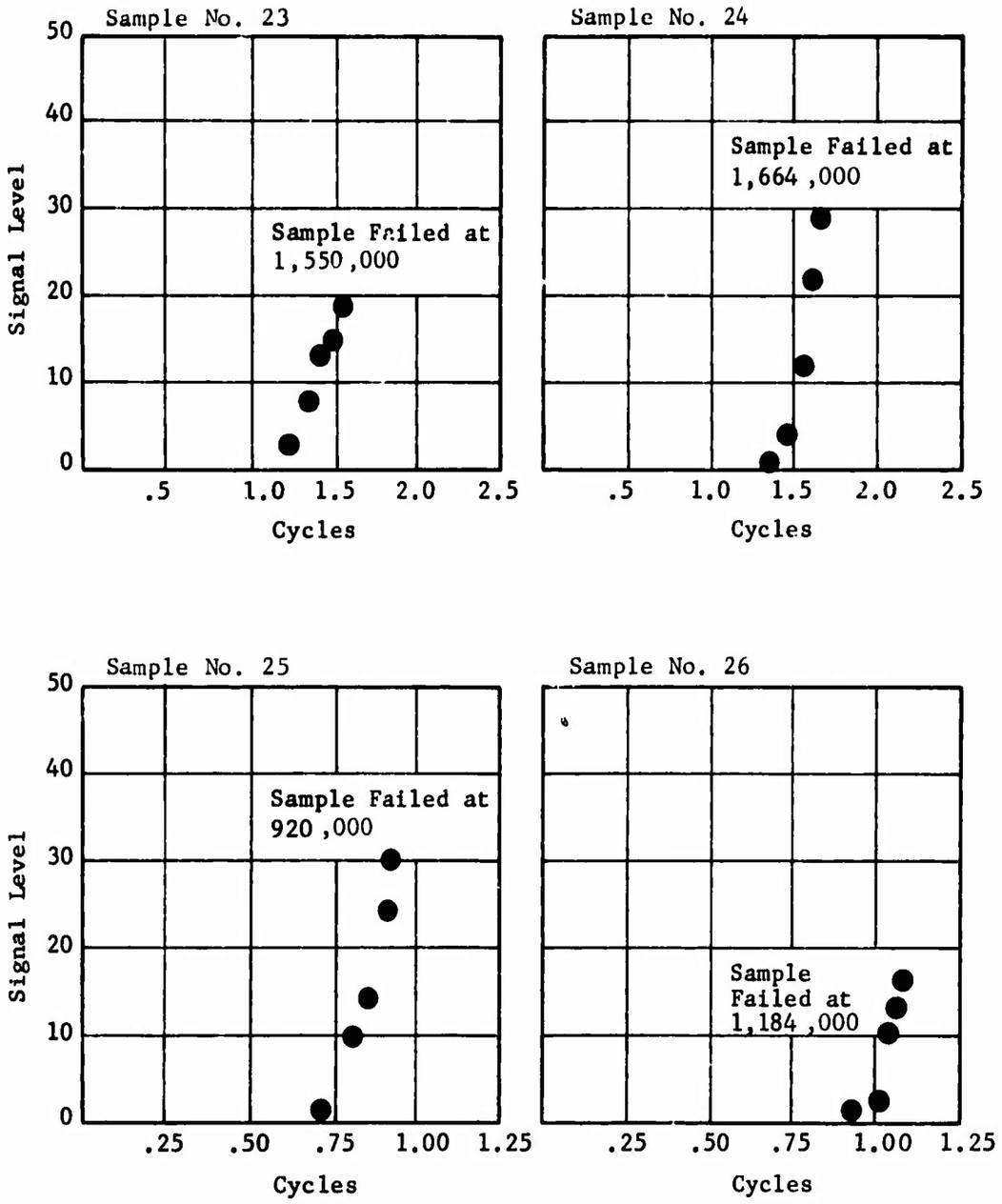

Figure 16. (continued)

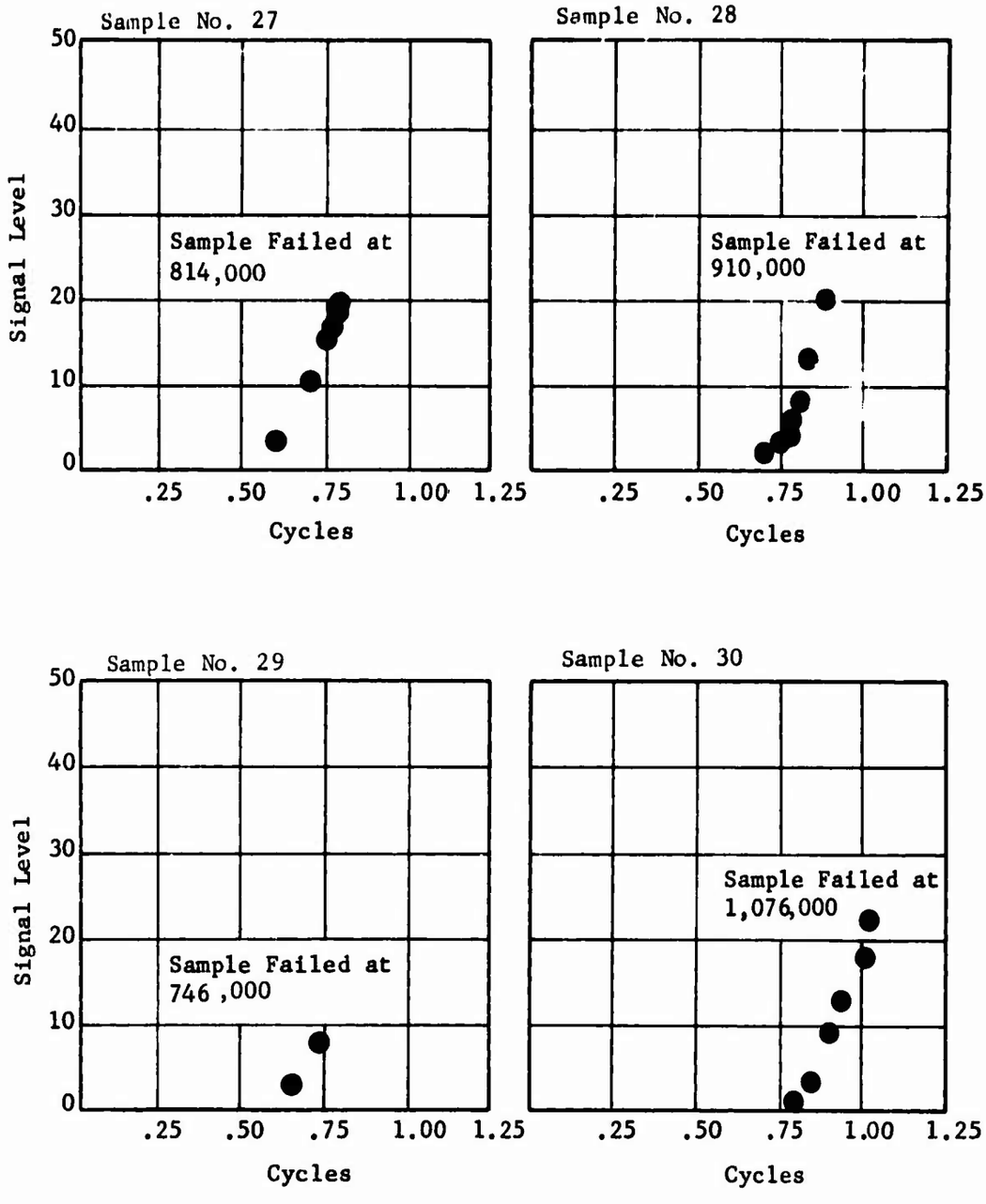

Figure 16. (continued)

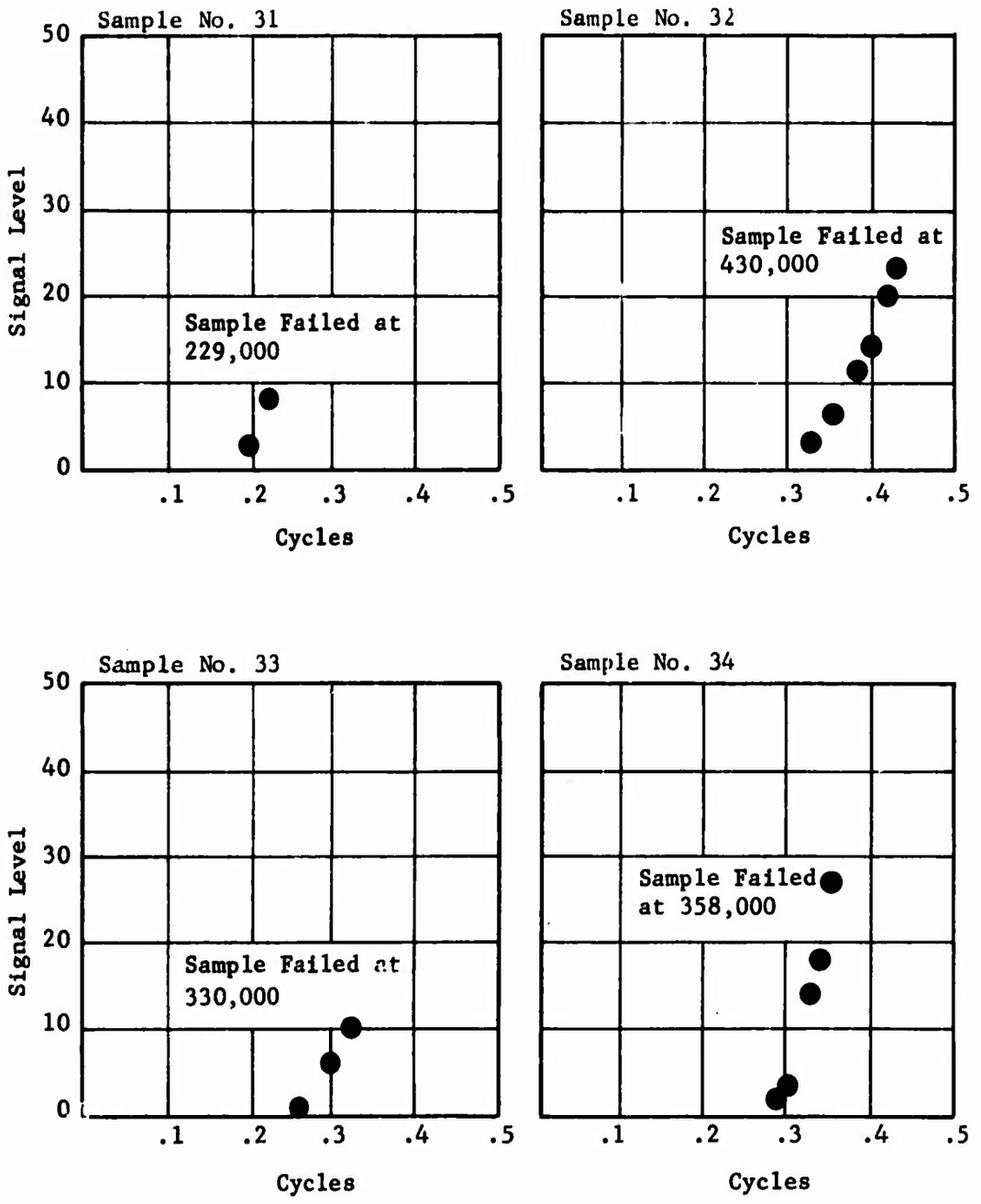

Figure 16. (continued)

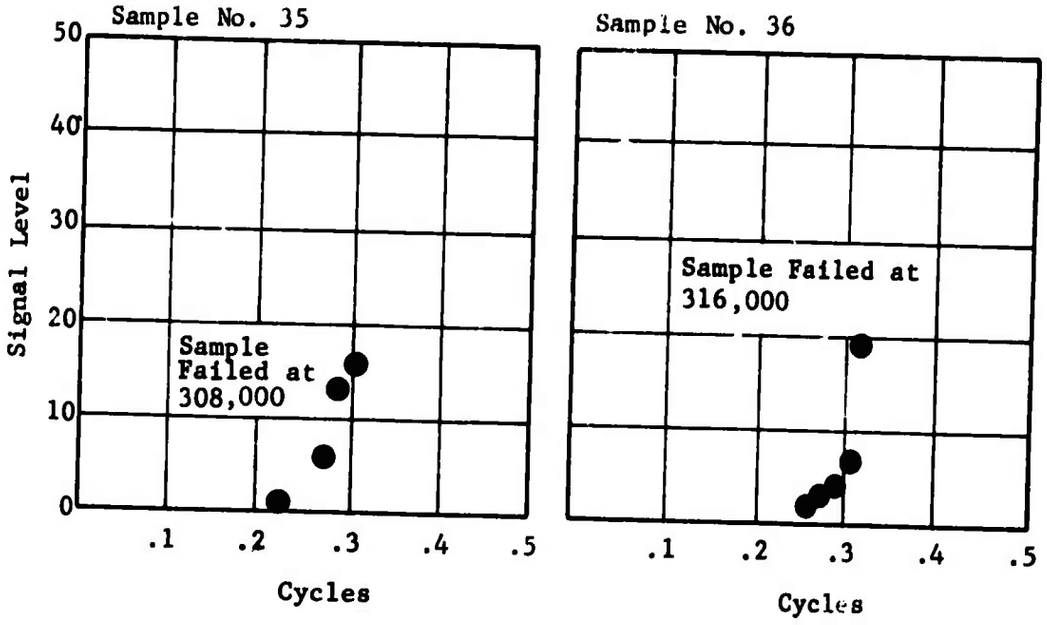

Figure 16. (continued)

Front

Back

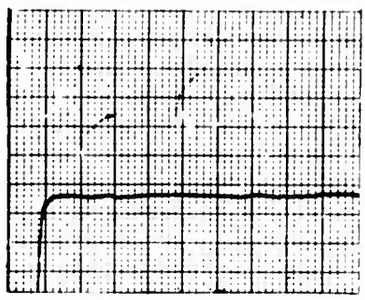

(a)

0

(b)

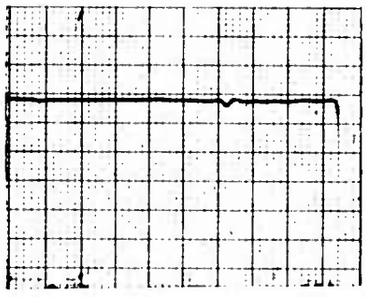

(c)

967,000 Bending Cycles

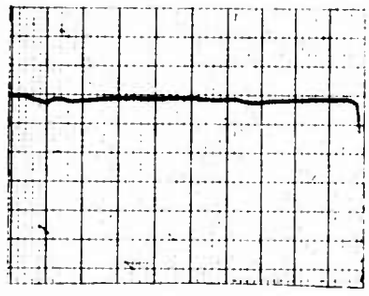

(d)

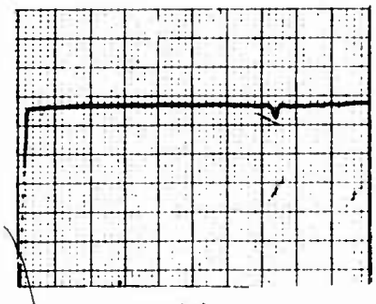

(e)

1,005,000

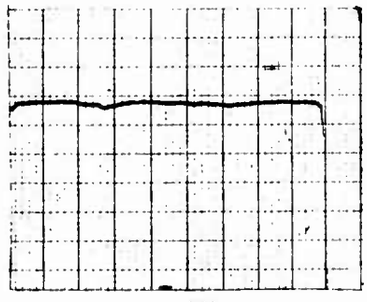

(f)

Figure 17. Inconel X Sample 26, ±.100" Deflection.

Front Back

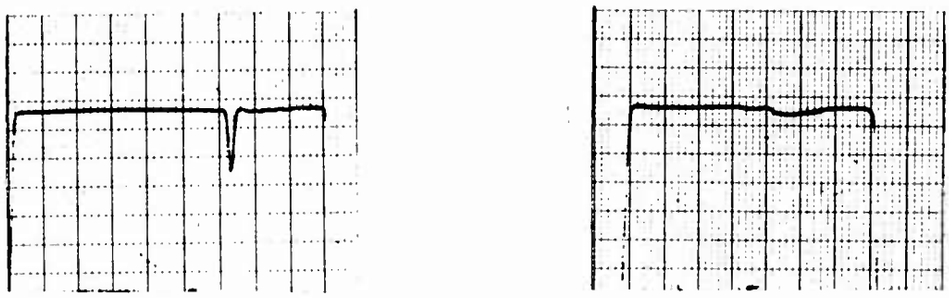

(g) 1,078,000 Bending Cycles (h)

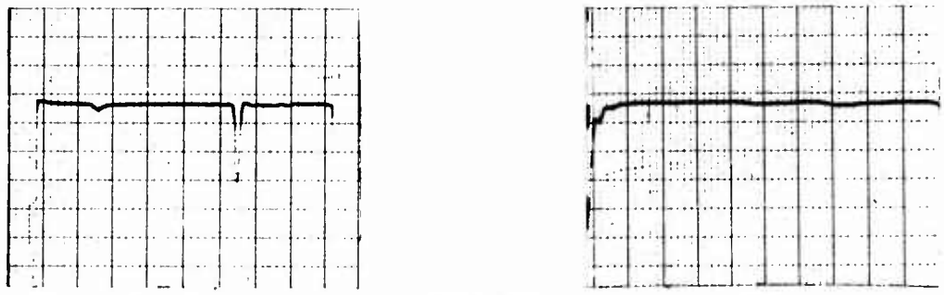

(i) Crack visible 1,128,000 (j)

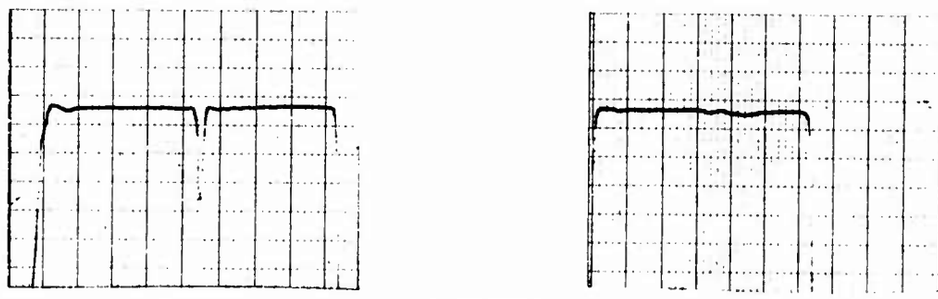

(k) 1,168,000 (l)

Sample failed at 1,184,000 cycles.

Figure 17. (continued)

Front

Back

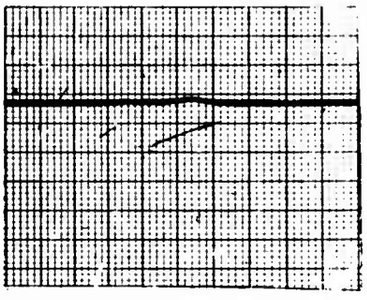

(a)

0

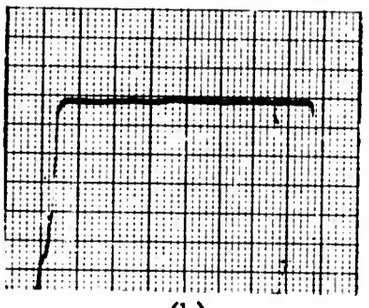

(b)

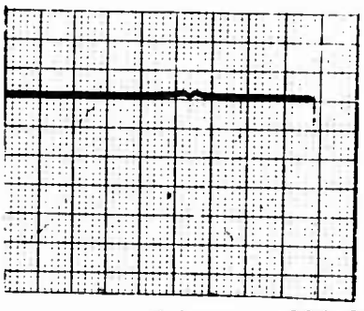

(c)

226,000 Bending Cycles

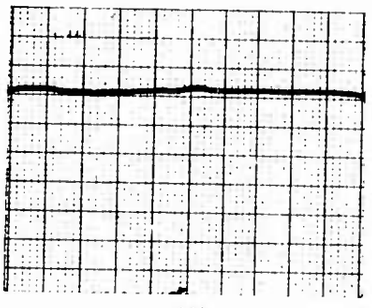

(d)

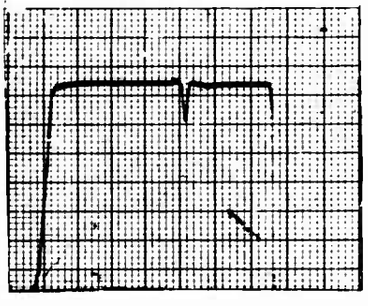

(e)

270,000

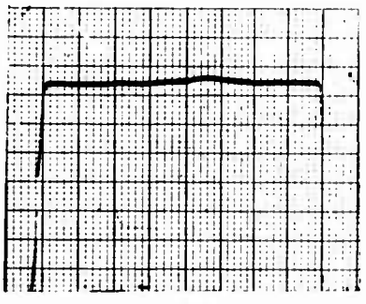

(f)

Figure 18. Inconel X Sample 35, ±.130" Deflection.

Front Back

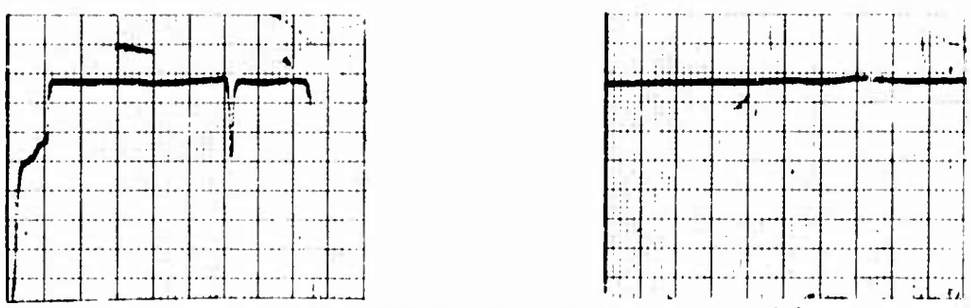

(g) 286,000 Bending Cycles (h)

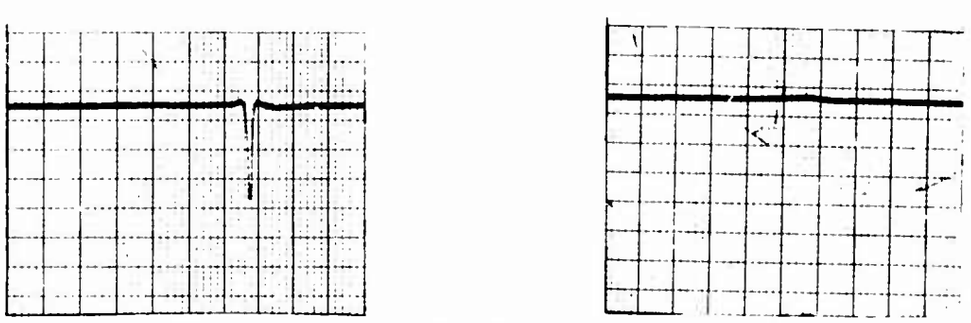

(i) 302,000 (j)

Sample failed at 308,000 cycles.

Figure 18. (continued)

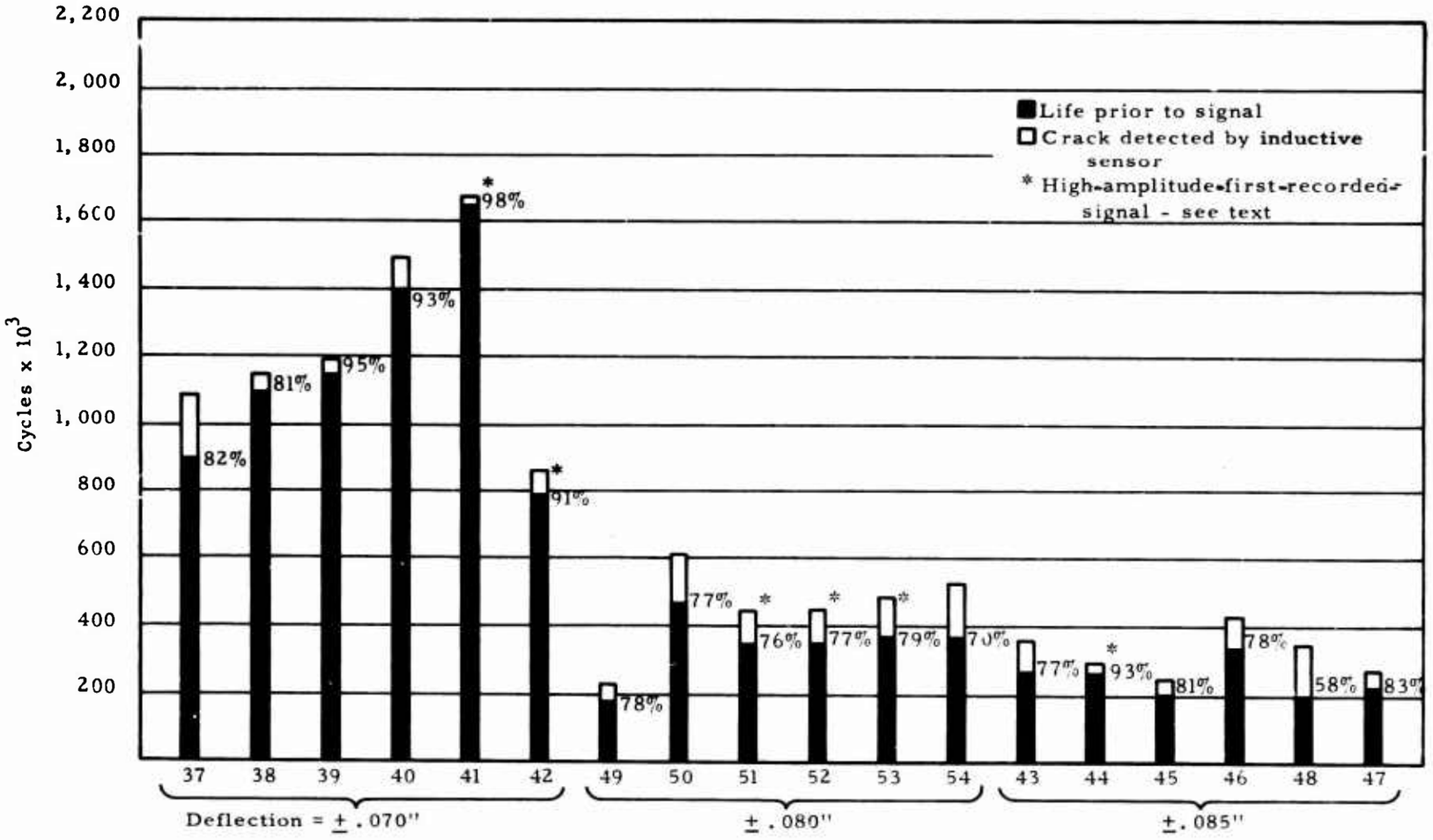

Figure 19. Graphical Presentation of Results, Steel.

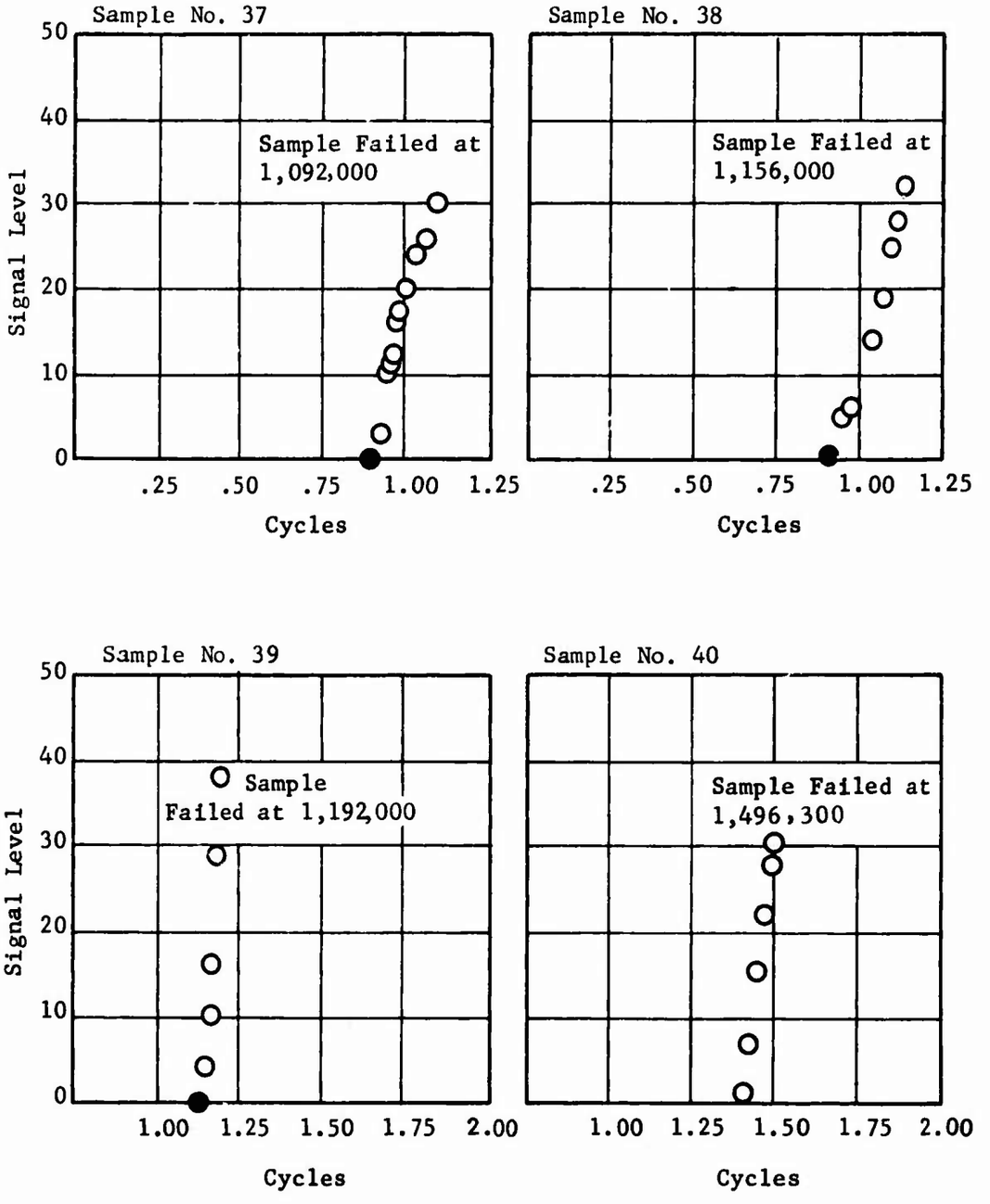

Figure 20. Output Signal vs. Number of Cycles, 9310 Steel.

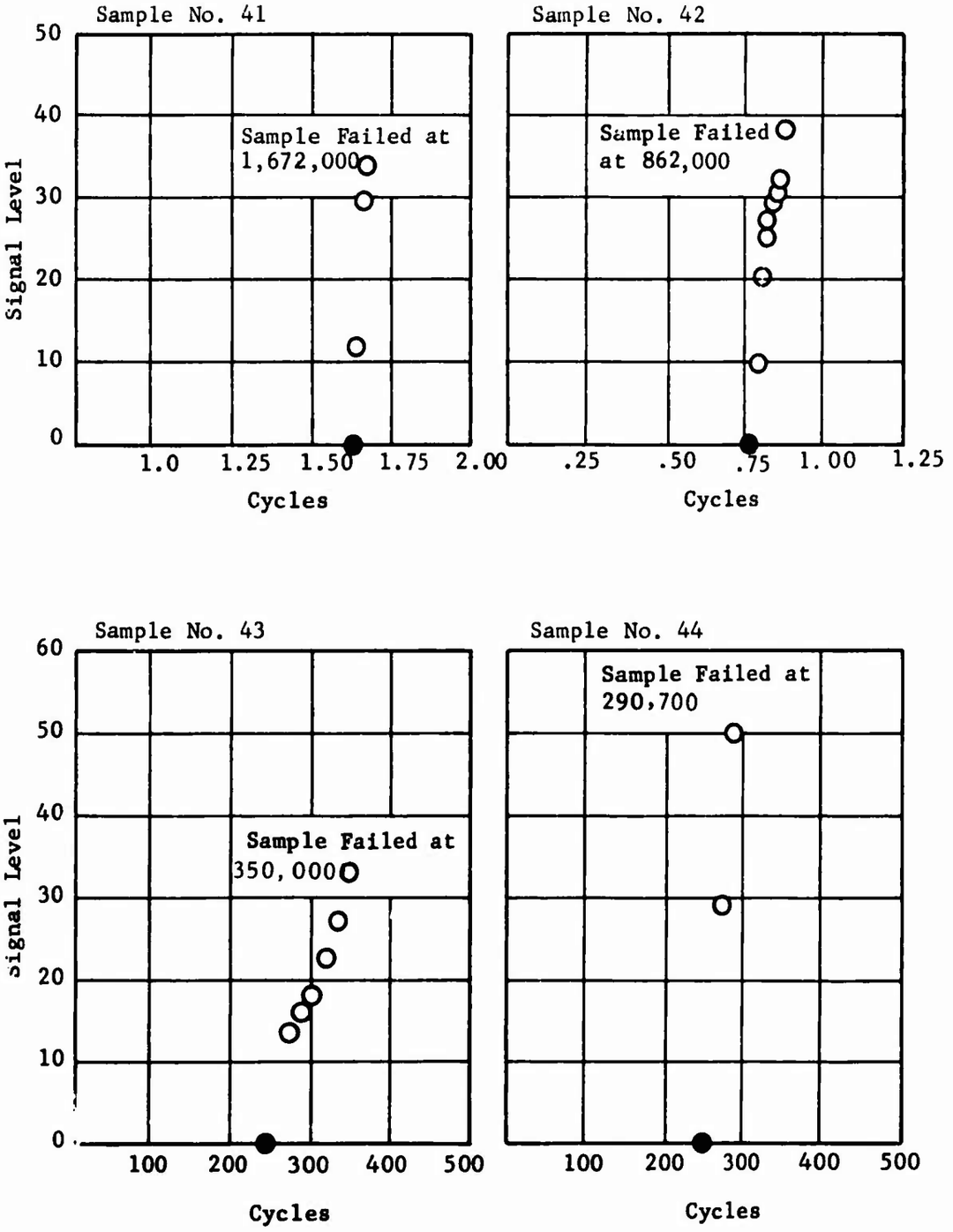

Figure 20. (continued)

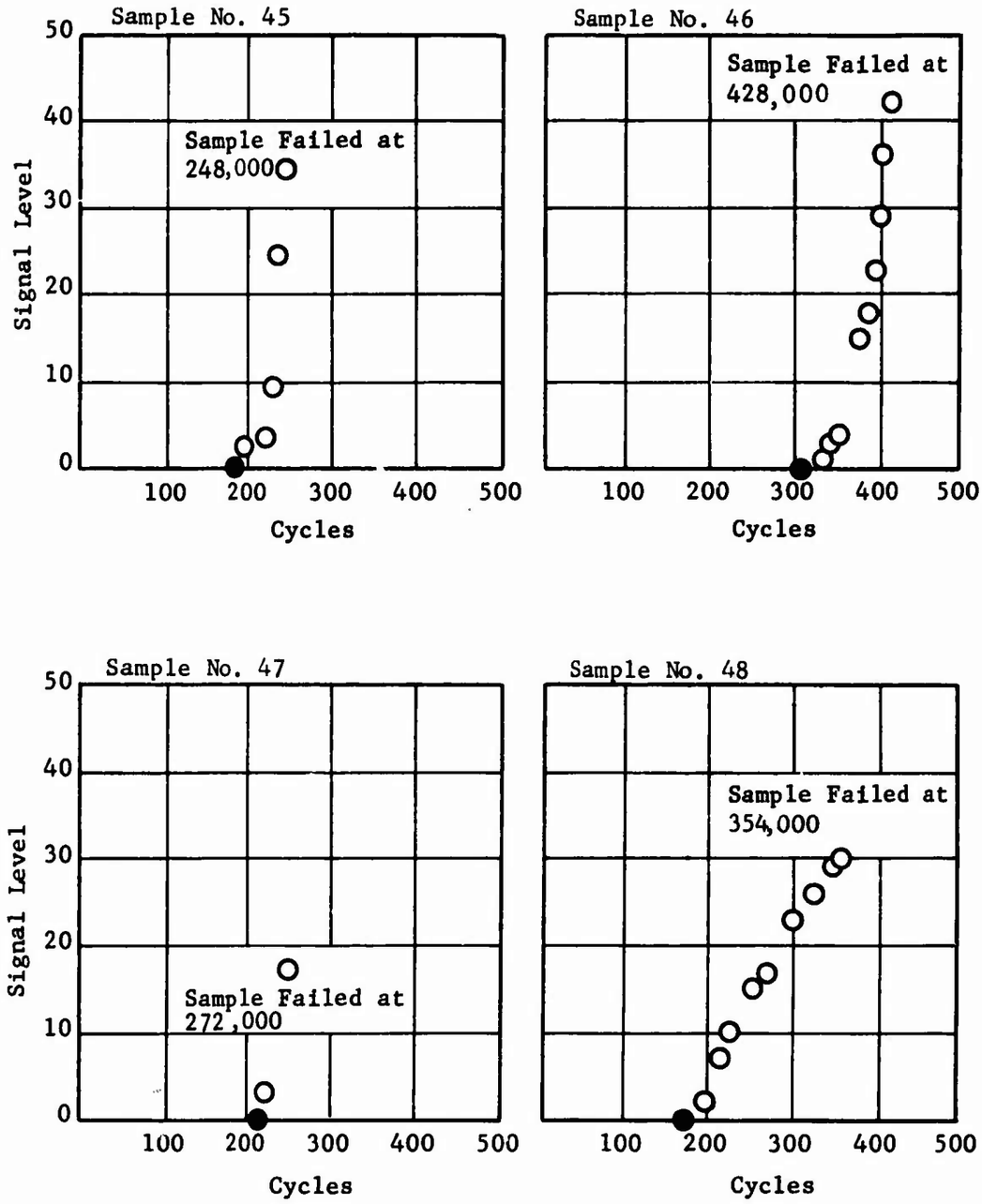

Figure 20. (continued)

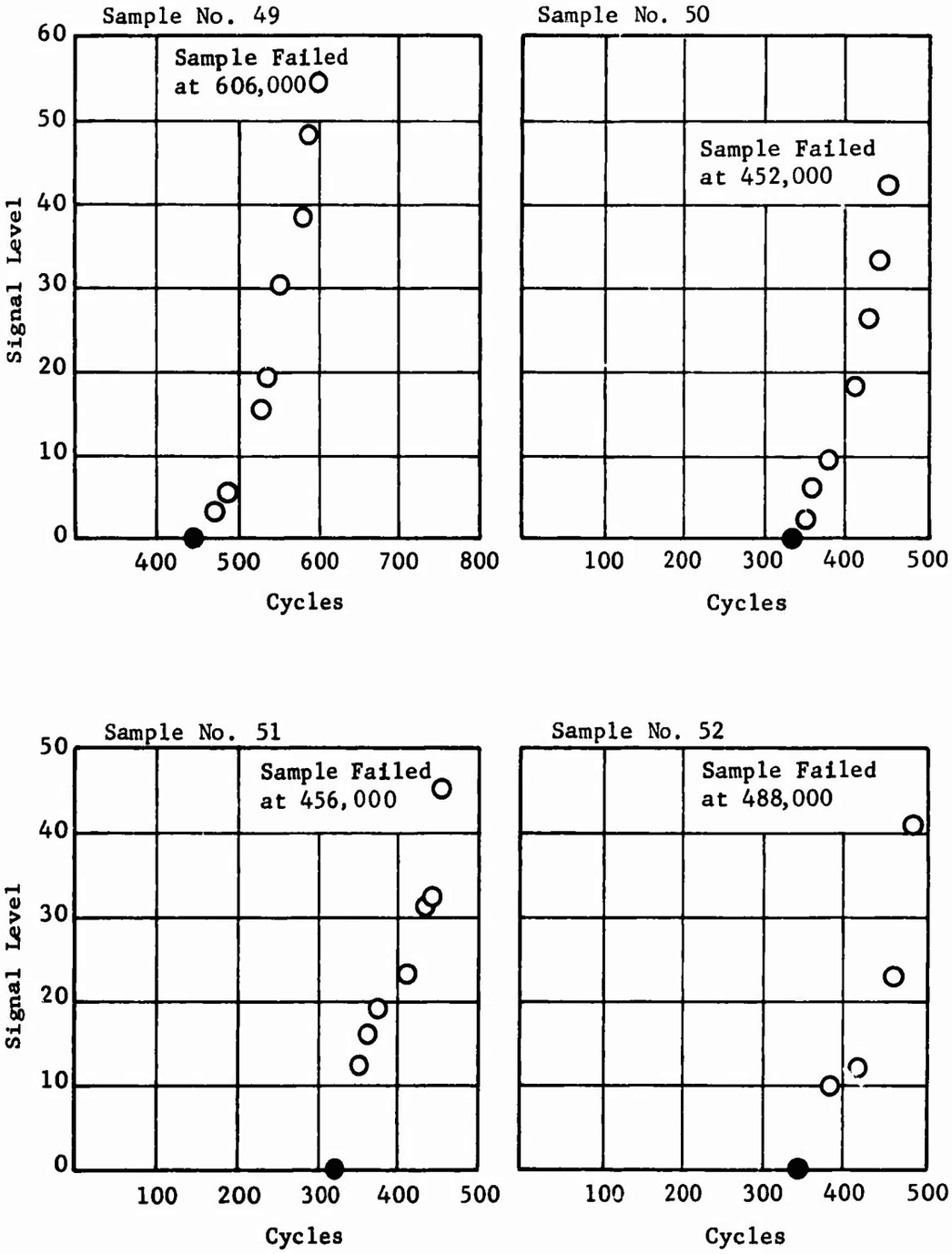

Figure 20. (continued)

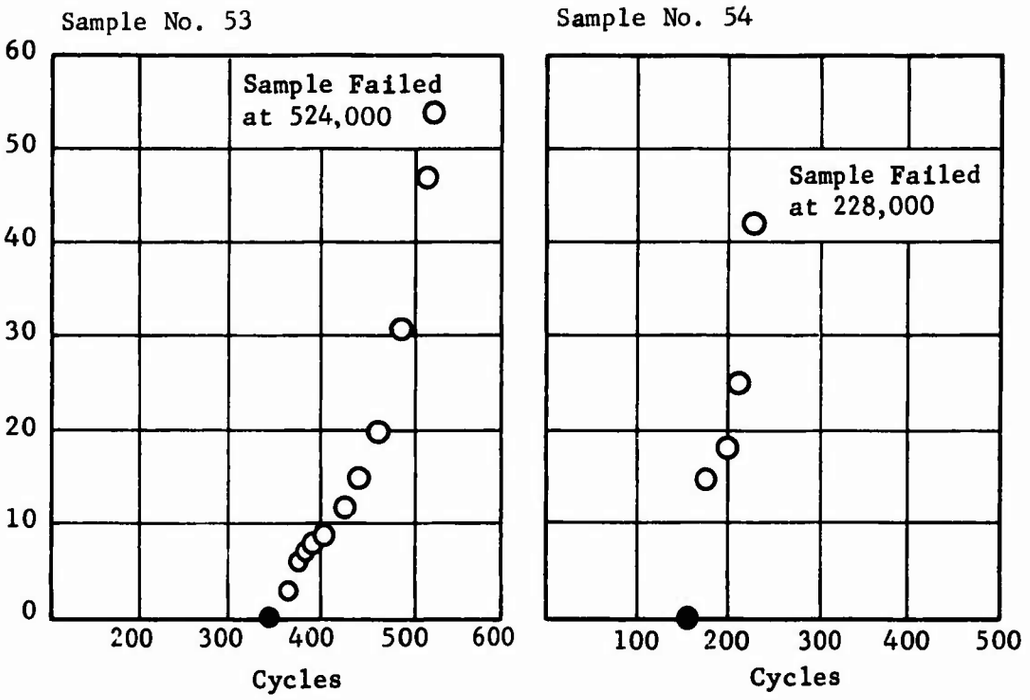

Figure 20. (continued)

Front Back

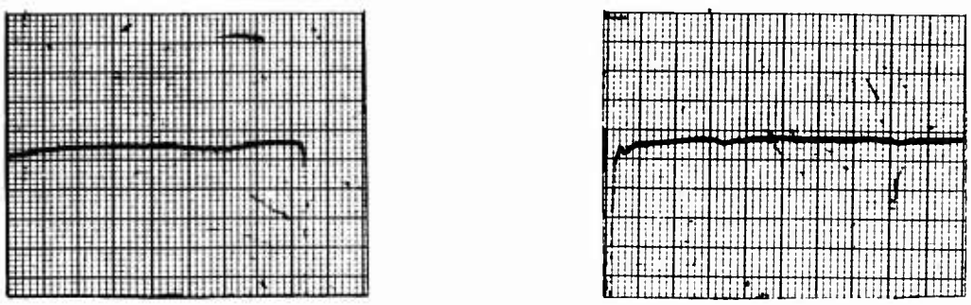

(a) 0 (b)

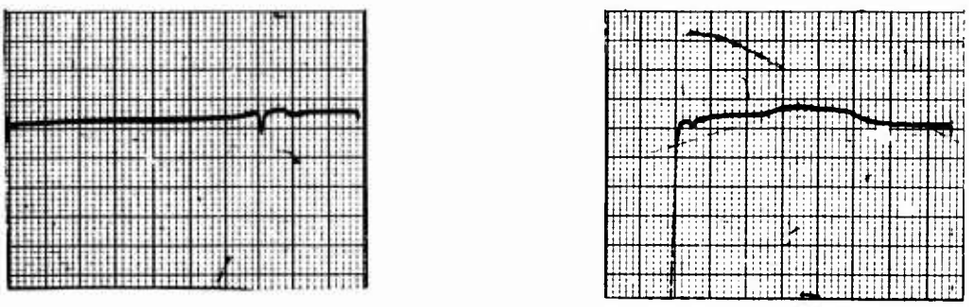

(c) 900,000 Bending Cycles (d)

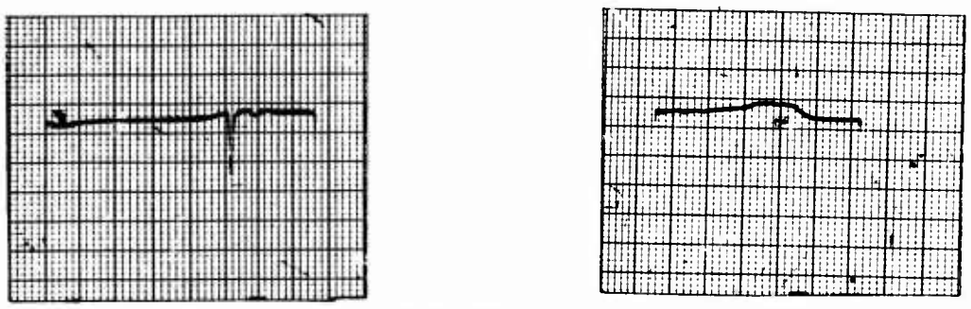

(e) 932,000 (f)

Figure 21. Steel Sample 37, ±.070" Deflection.

Front Back

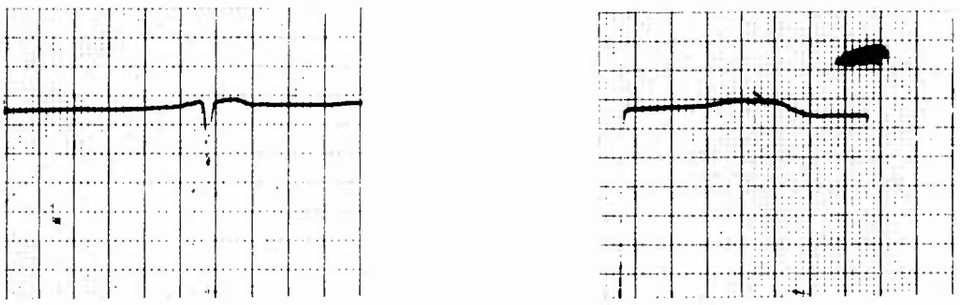

(g) 946,000 Bending Cycles (h)

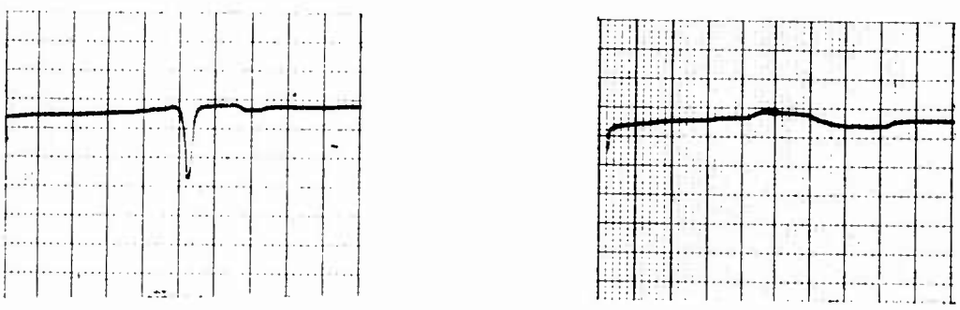

(i) 966,000 (j)

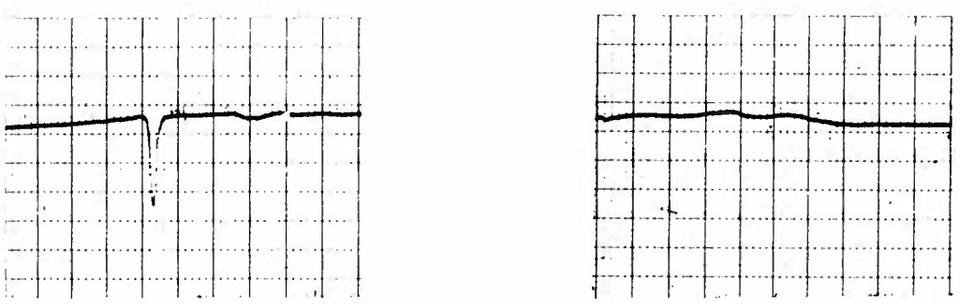

(k) Crack visible 970,000 (l)

Figure 21. (continued)

Front

Back

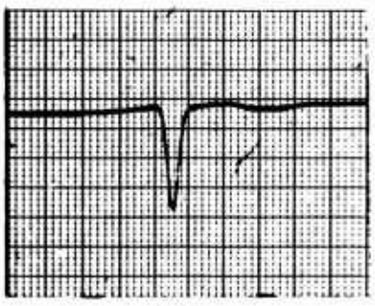

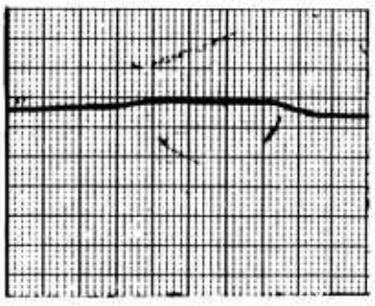

(m) 982,000 Bending Cycles (n)

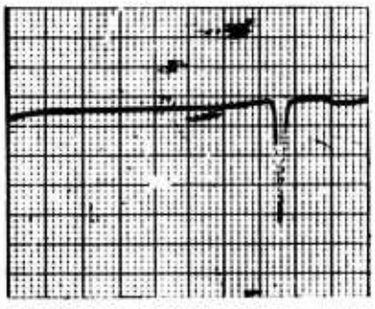

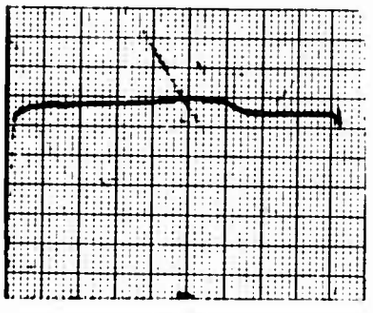

(o) 1,000,000 (p)

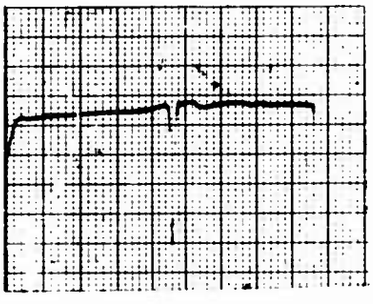

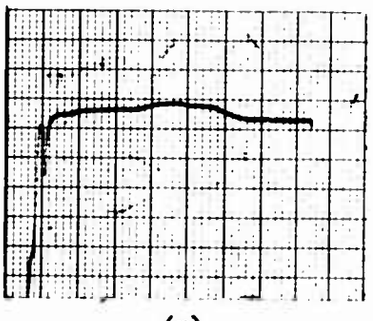

(q) 1,032,000 (r)

Figure 21. (continued)

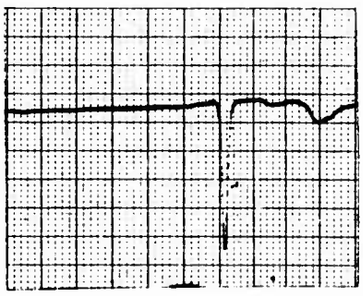

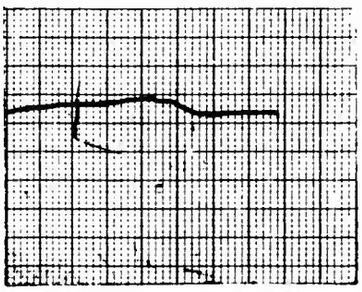

(s) 1,052,000 Bending Cycles (t)

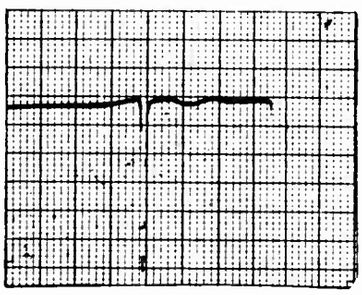

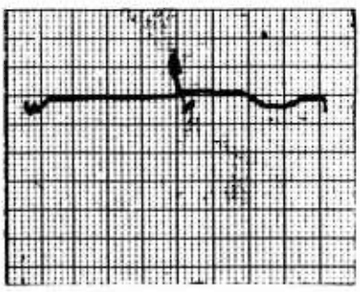

(u) 1,088,000 (v)

Sample failed at 1,032,000 cycles.

Figure 21. (continued)

Front

Back

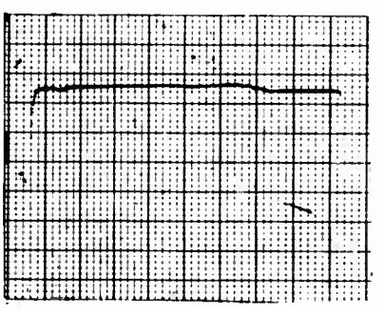

(a)

0

(b)

(c)

350,000 Bending Cycles

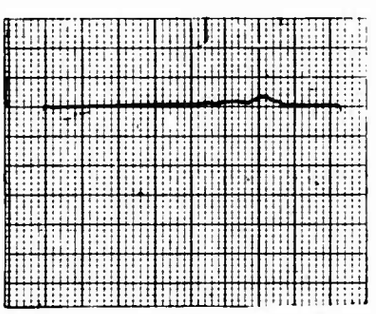

(d)

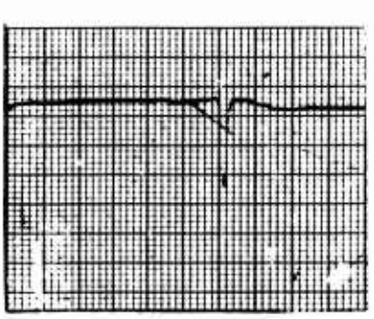

(e)

360,000

(f)

Figure 22. Steel Sample 51, ±.075" Deflection.

Front

Back

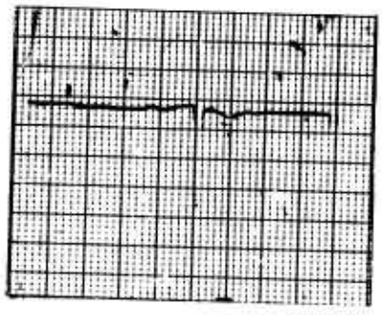

(g)

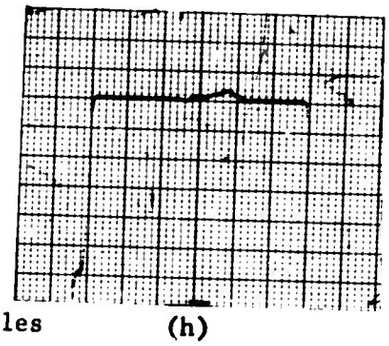

(h)

378,000 Bending Cycles

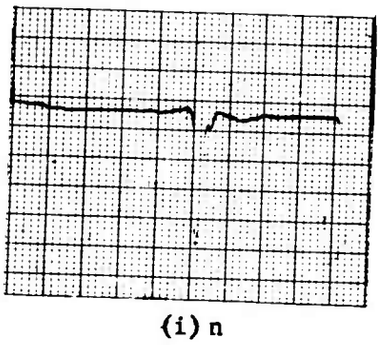

(i) n

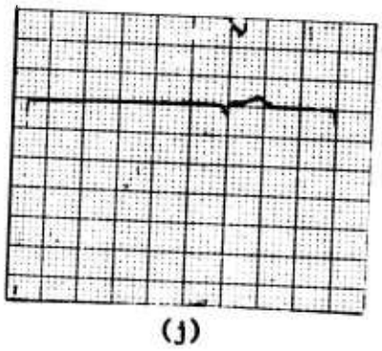

(j)

410,000

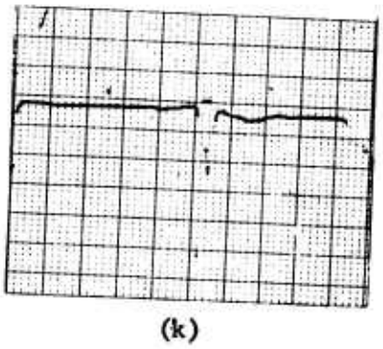

(k)

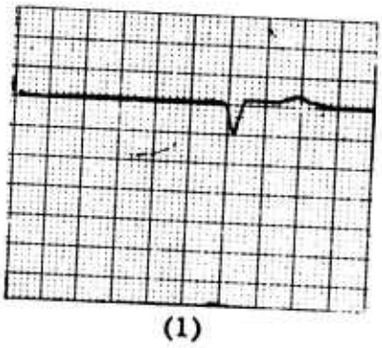

(l)

430,000

Figure 22. (continued)

Front Back

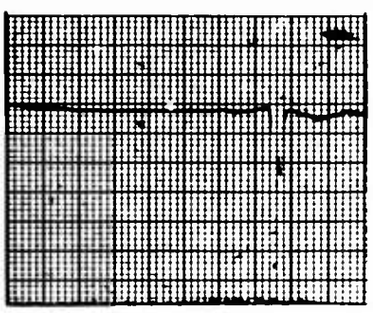

(m) 440,000 Bending Cycles (n)

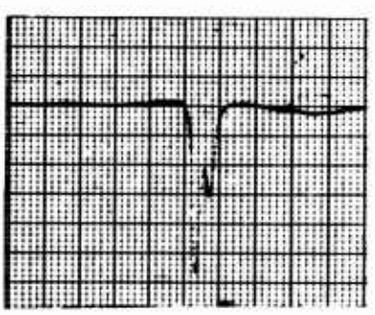

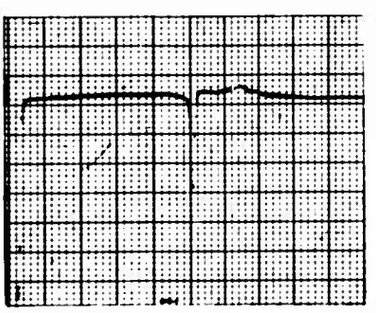

(o) Crack visible 450,000 (p)

Sample failed at 456,000 cycles.

Figure 22. (continued)

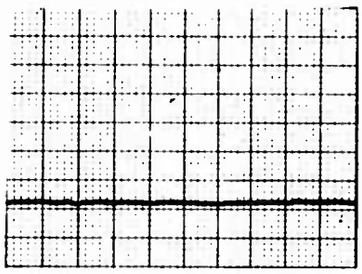

(a) 0

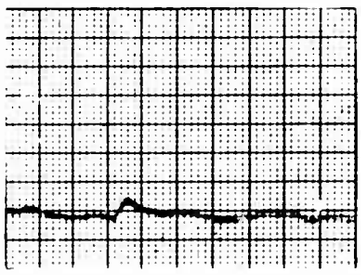

(b) 54,000 Bending Cycles

(c) 110,000

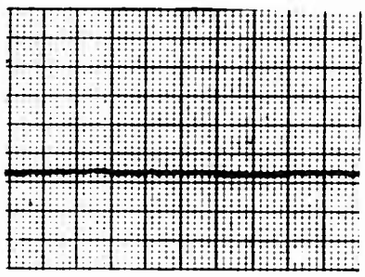

(d) 162,000

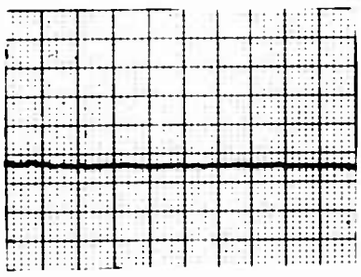

(e) 210,000

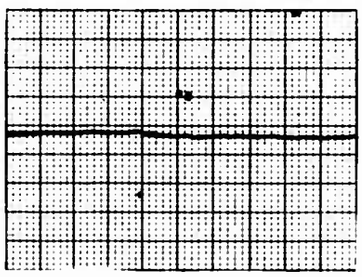

(f) 260,000

Figure 23. Roll Test, Steel Sample 10.

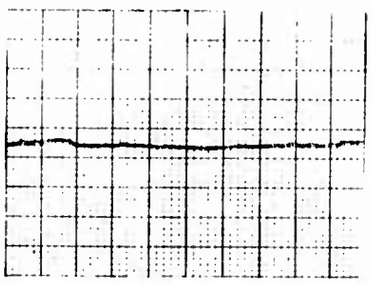

(g) 315,000 Bending Cycles

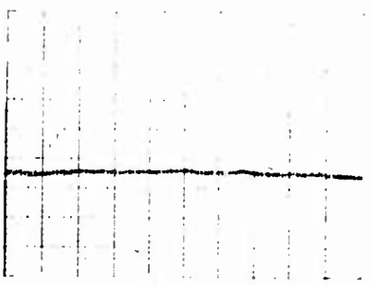

(h) 370,000

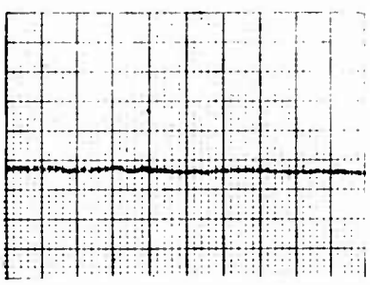

(i) 425,000

(j) 475,000

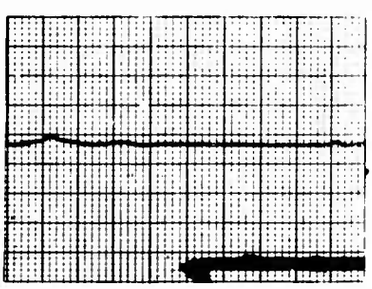

(k) 530,000

(l) 585,000

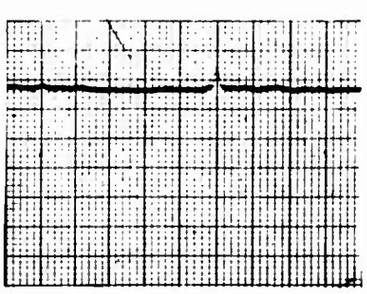

(m) 596,000

Figure 23. (continued)

(a) 0

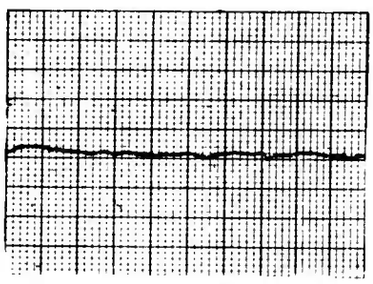

(b) 52,000 Bending Cycles

(c) 100,000

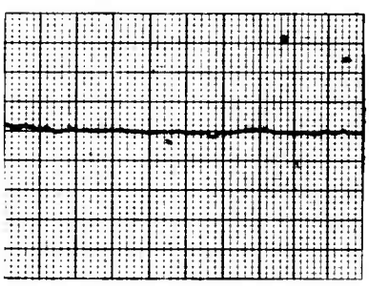

(d) 160,000

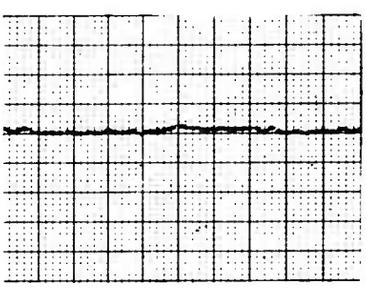

(e) 211,000

(f) 258,000

Figure 24. Roll Test, Steel Sample 9.

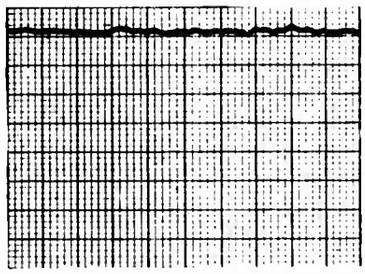

(g) 312,000 Bending Cycles

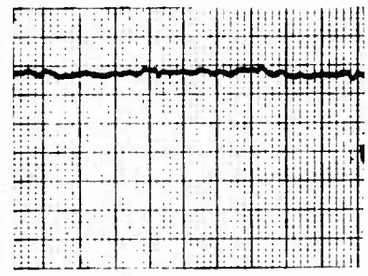

(h) 369,000

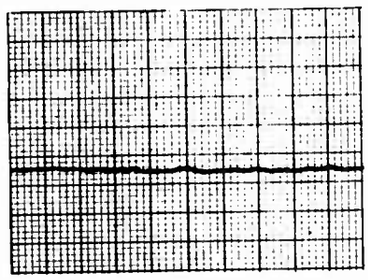

(i) 425,000

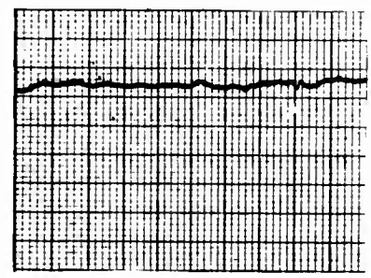

(j) 479,000

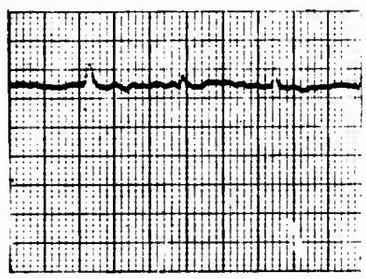

(k) 532,000

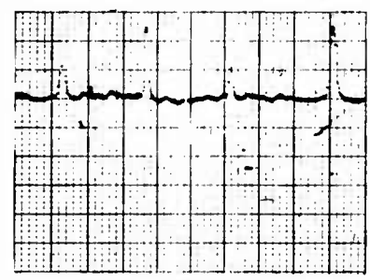

(l) 535,000

Figure 24. (continued)

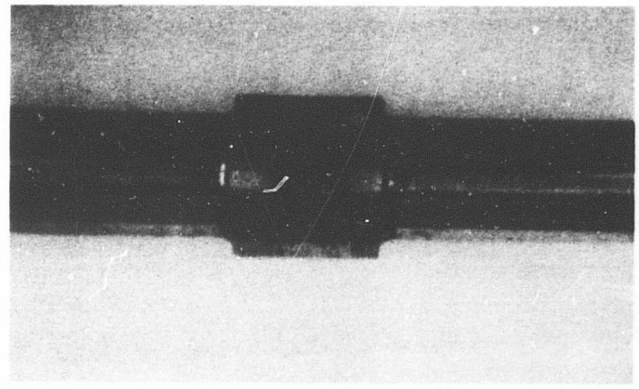

Figure 25. Typical Pit - Roll Fatigue Test.

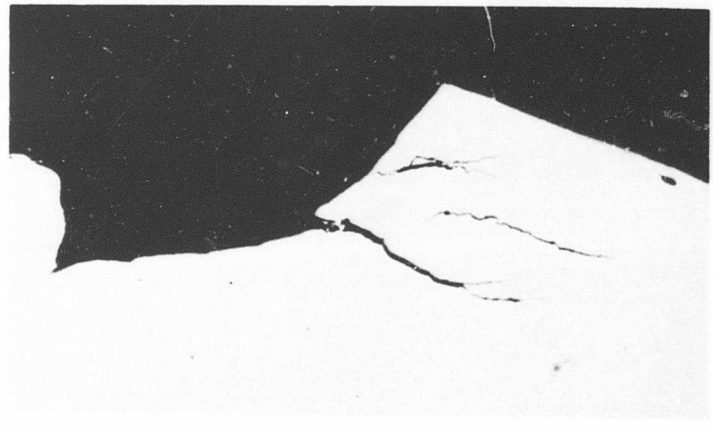

(a) X100

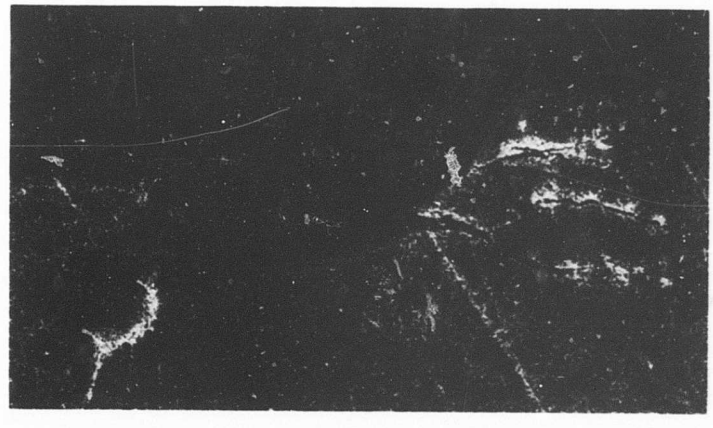

(b) Etched, X100

Figure 26. Section Through Edge of Pit.

Front

Back

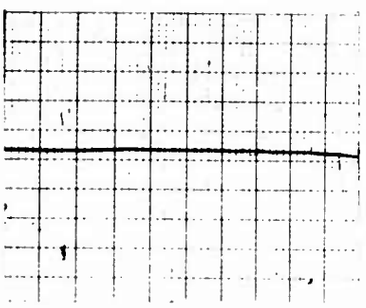

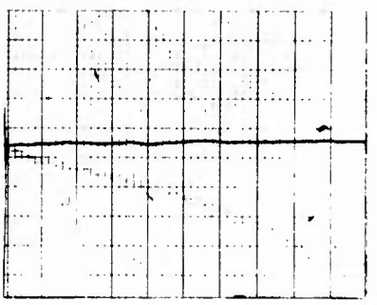

Pretest

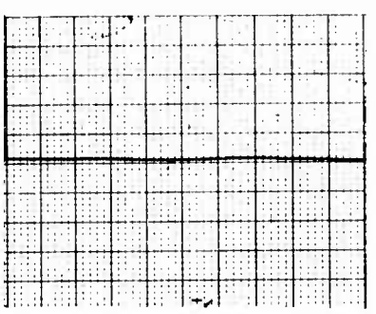

400,000 Bending Cycles

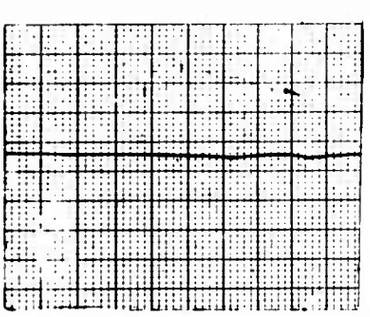

600,000

Figure 27. Aluminum Sample A5, ±.050" Deflection.

Front

Back

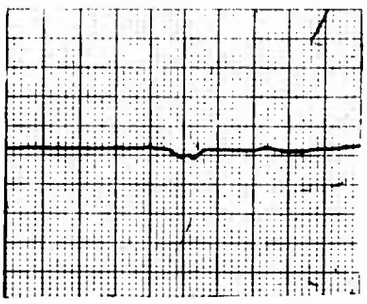

800,000 Bending Cycles

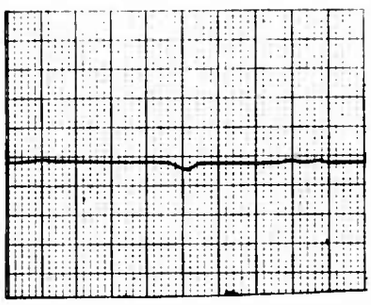

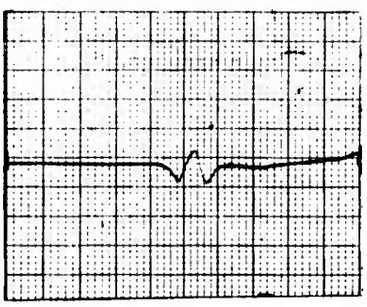

900,000

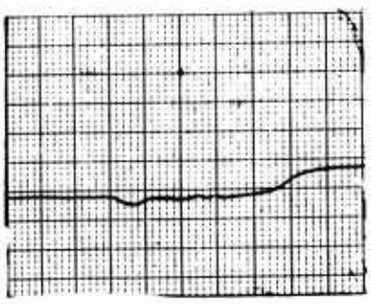

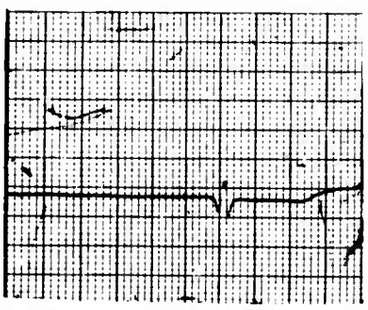

915,000

Figure 27. (continued)

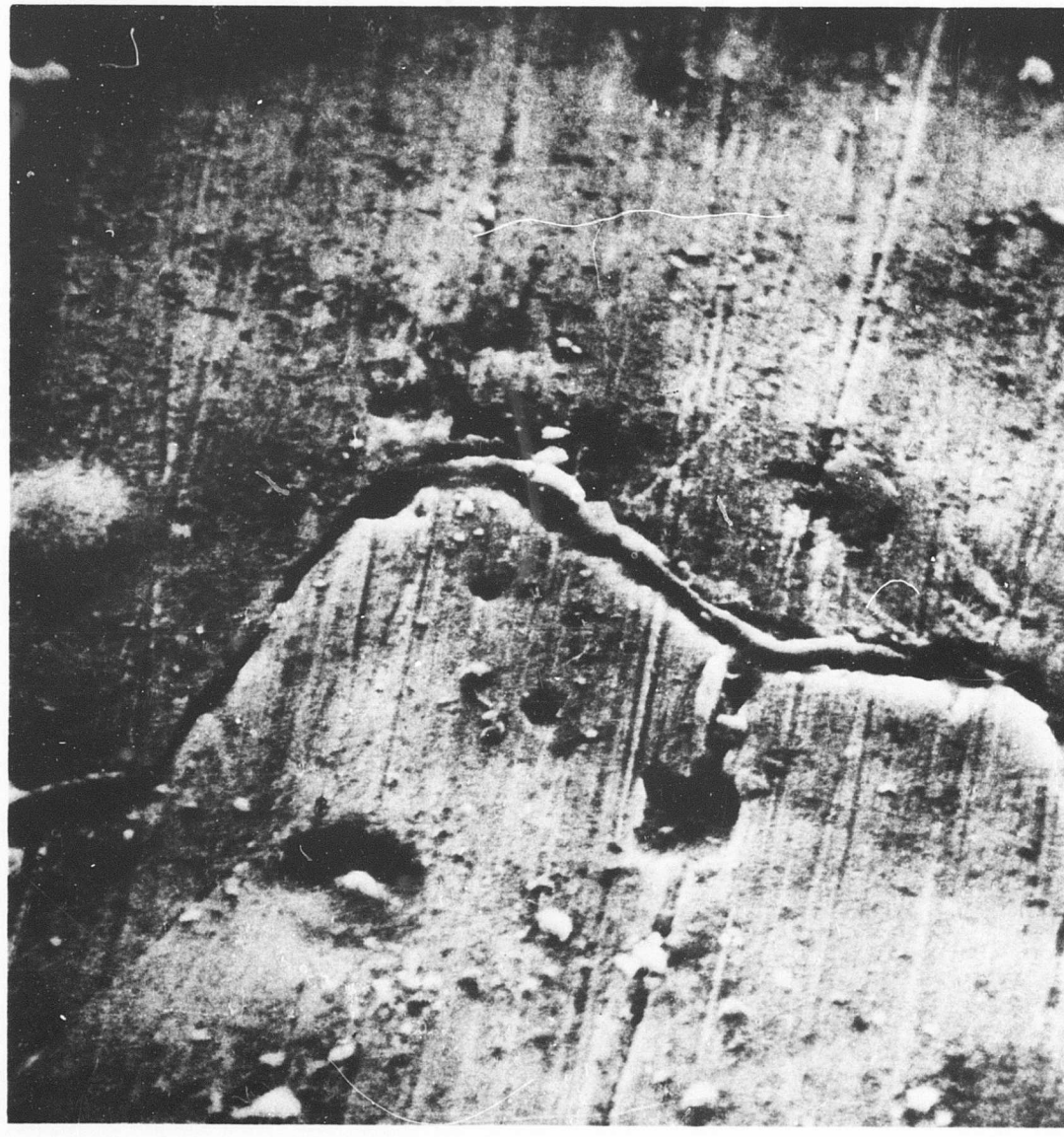

Figure 28. Aluminum Sample A5, X4000, d = 2.9 mm.

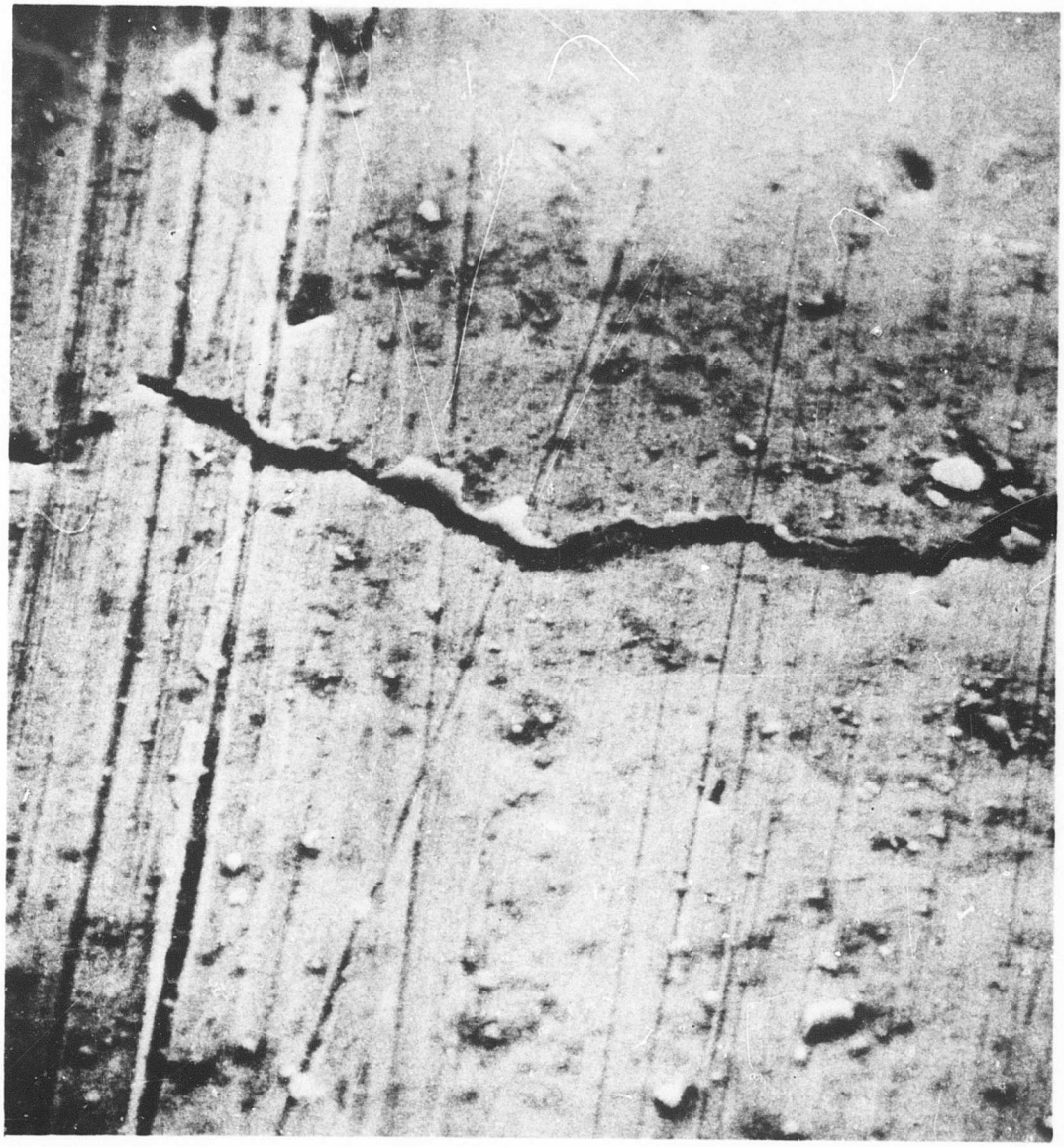

Figure 29. Aluminum Sample A5, X2200, d = 3.2 mm.

Figure 30. Aluminum Sample A5, X4000, d = 4.2 mm.

Front

Back

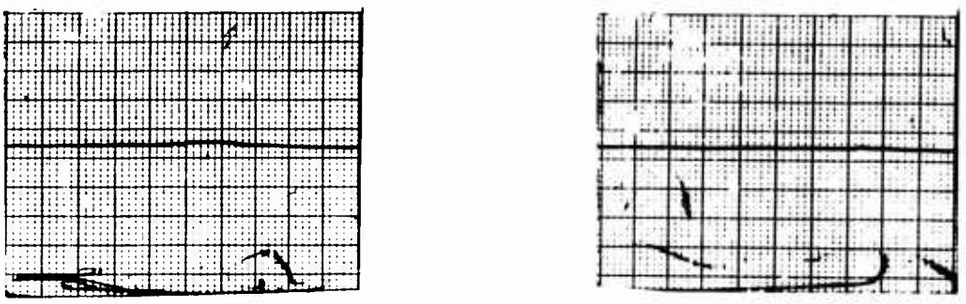

Prerun

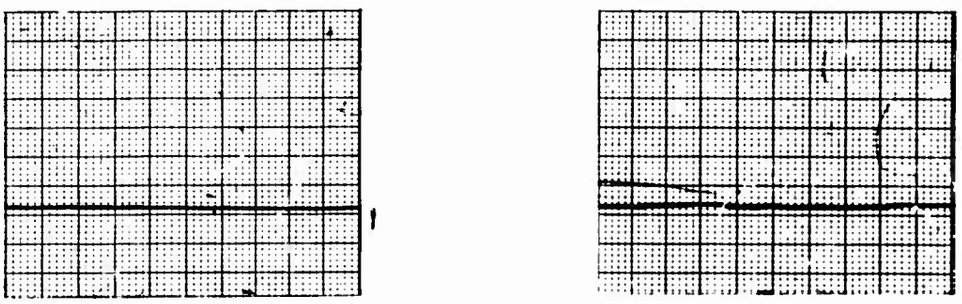

400,000 Bending Cycles

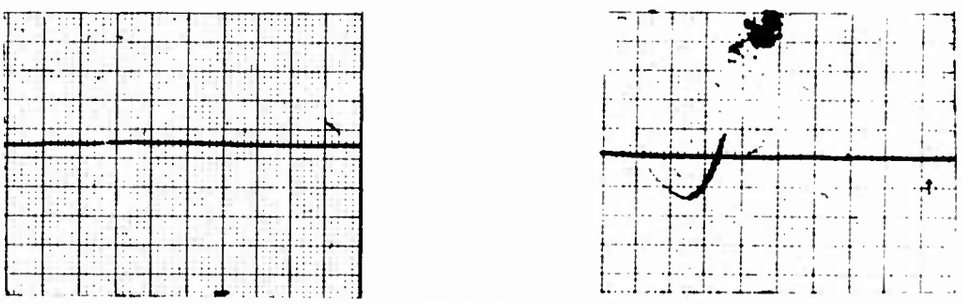

500,000

Figure 31. Aluminum Sample A11, ± .050" Deflection.

Front

Back

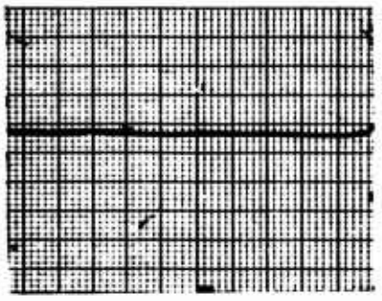

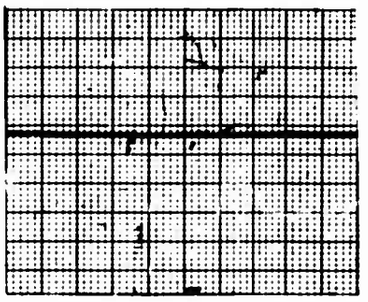

550,000 Bending Cycles

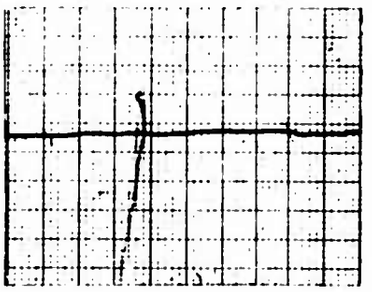

600,000

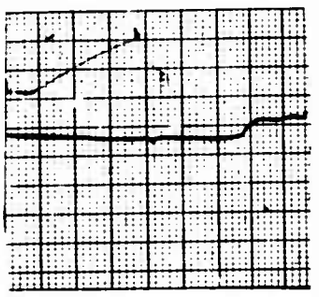

625,000

Figure 31. (continued)

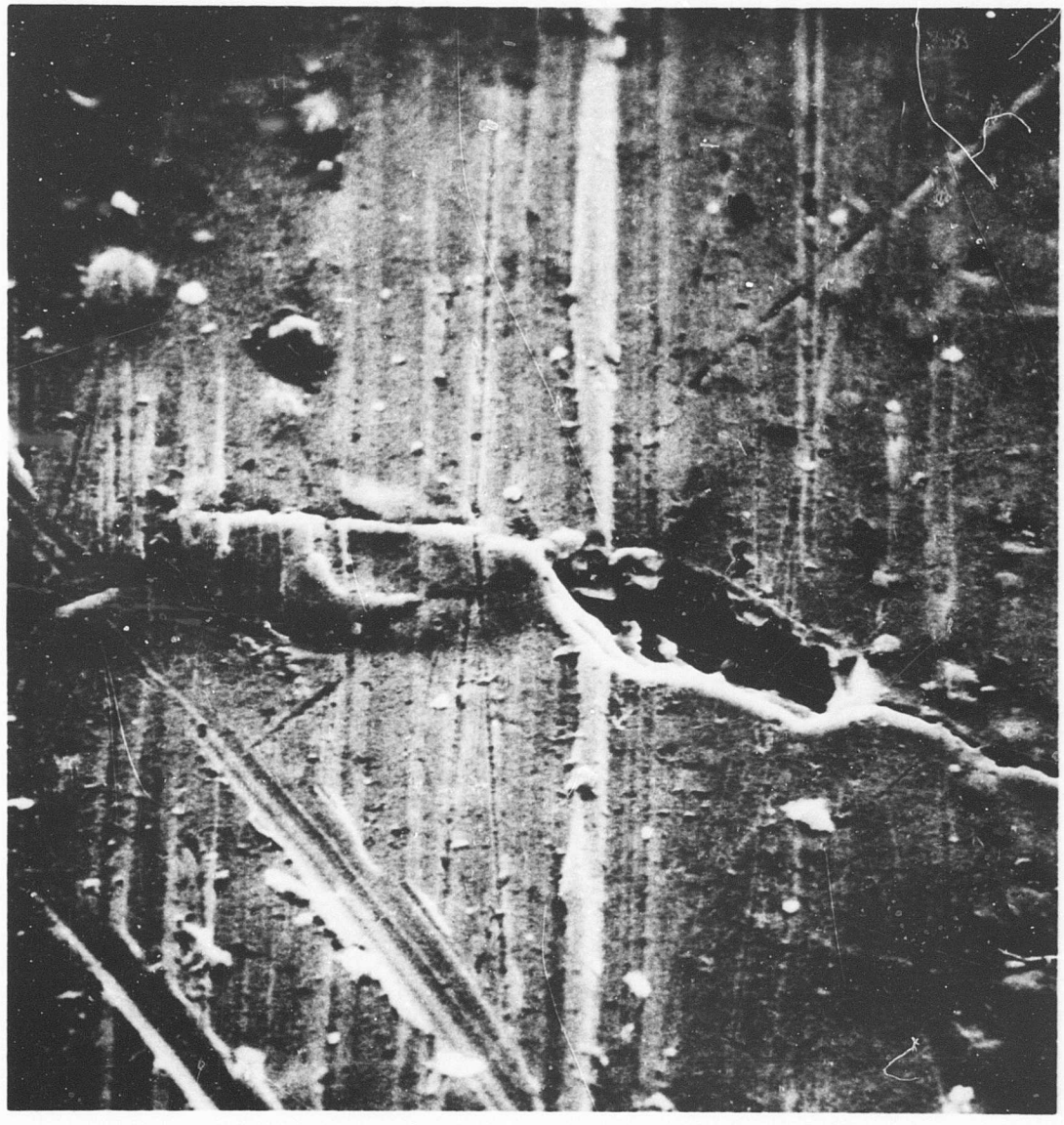

Figure 32. Aluminum Sample A11, X2200, d = 1.1 mm.

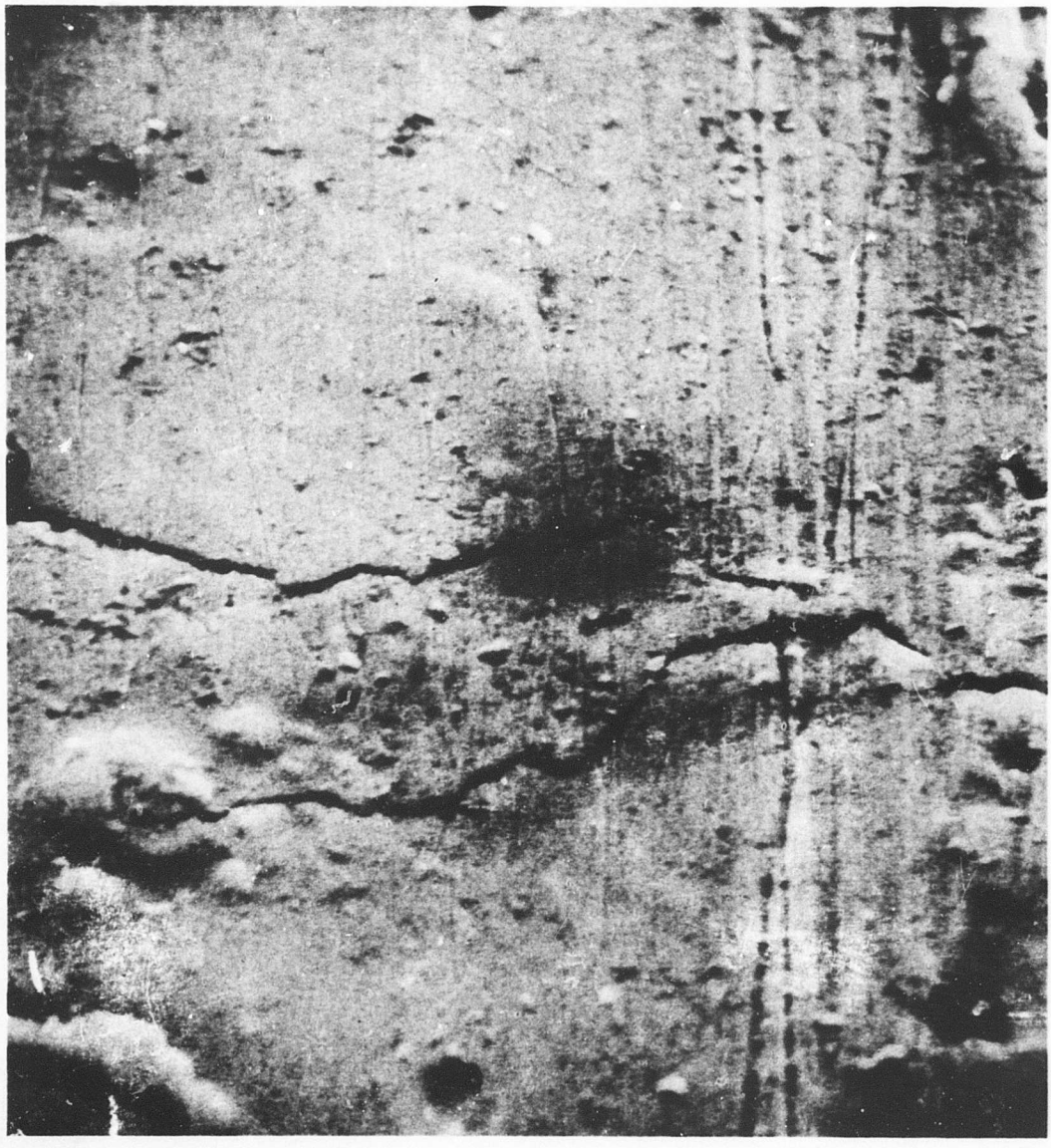

Figure 33. Aluminum Sample A11, X4000, d = 1.2 mm.

Figure 34. Aluminum Sample A11, X4000, d = 1.4 mm.

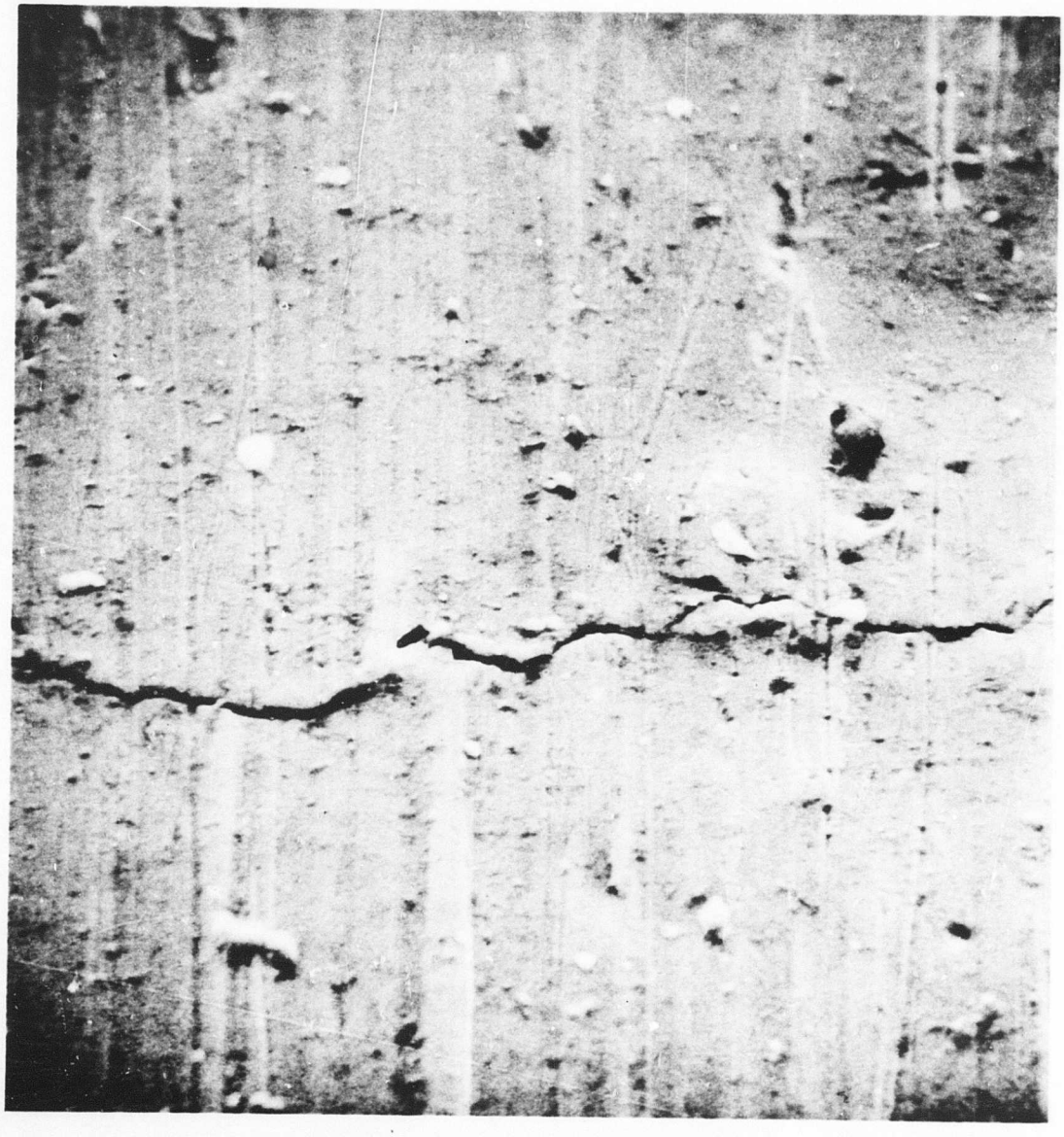

Figure 35. Aluminum Sample A11, X4000, d = 1.9 mm.

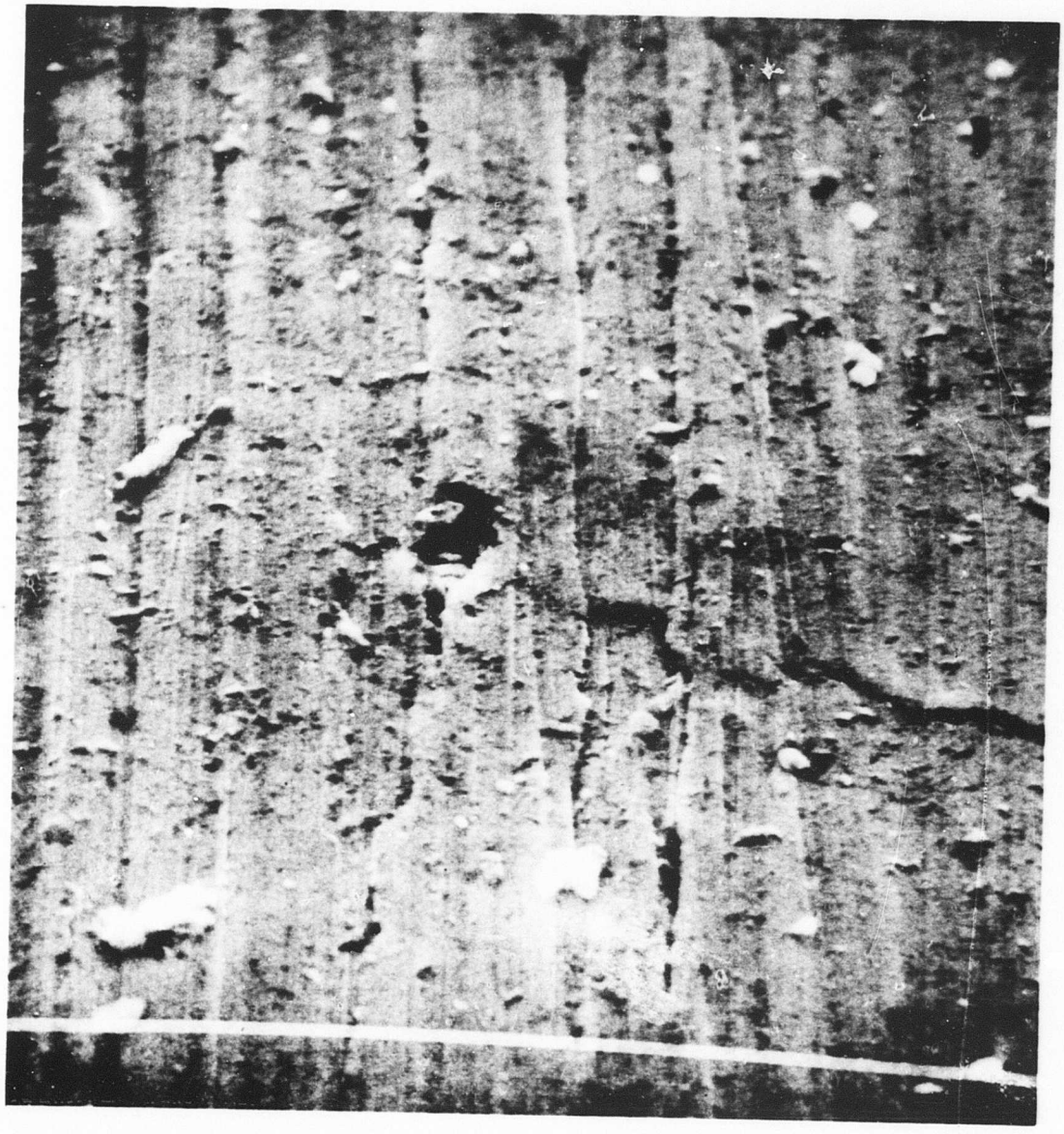

Figure 36. Aluminum Sample A11, X4000, d = 2.1 mm.

Front

Back

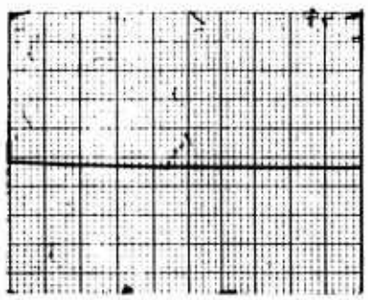

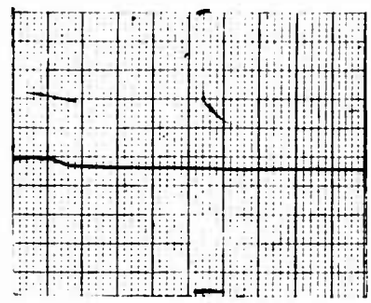

Pretest

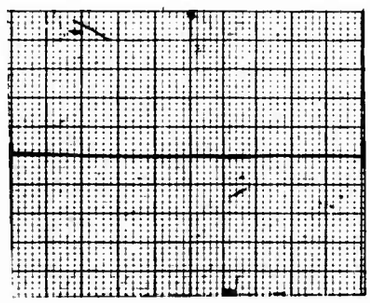

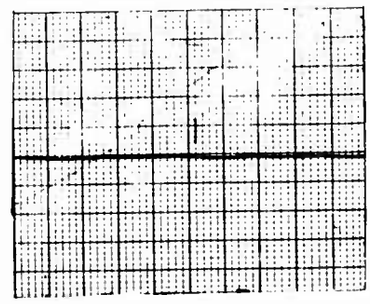

300,000 Bending Cycles

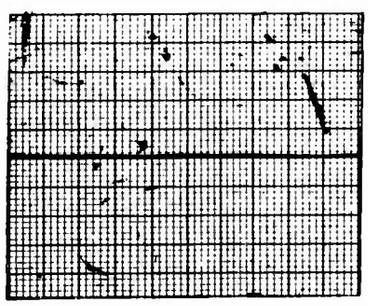

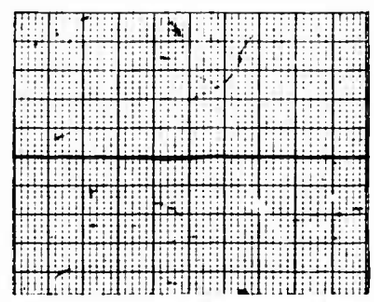

600,000

Figure 37. Inconel X Sample I7, ±.070" Deflection.

Front

Back

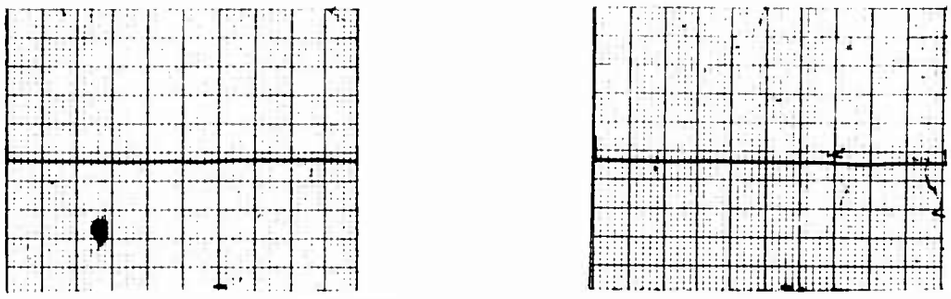

800,000 Bending Cycles

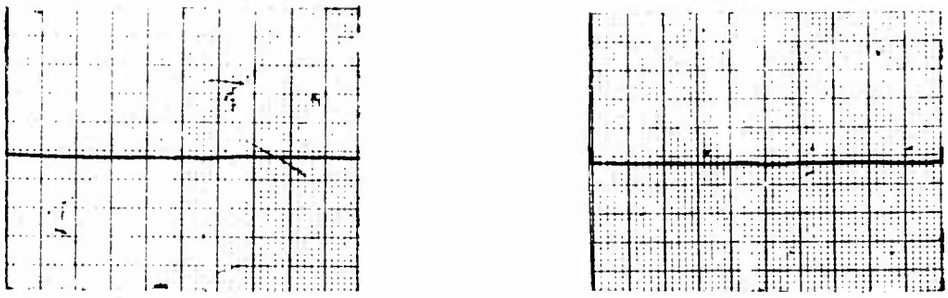

1,000,000

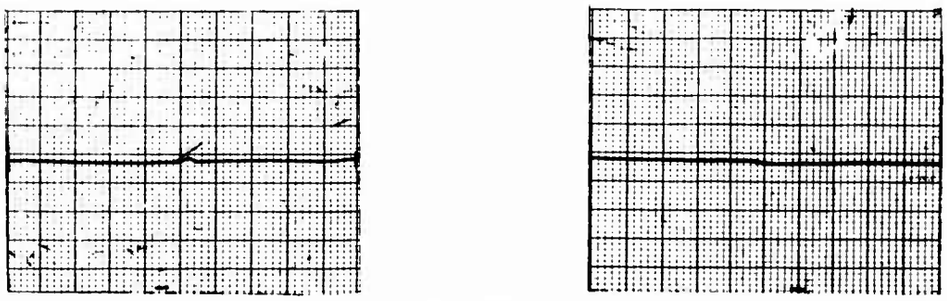

1,000,000

Figure 37. (continued)

Figure 38. Inconel Sample I7, X4000, d = .73.

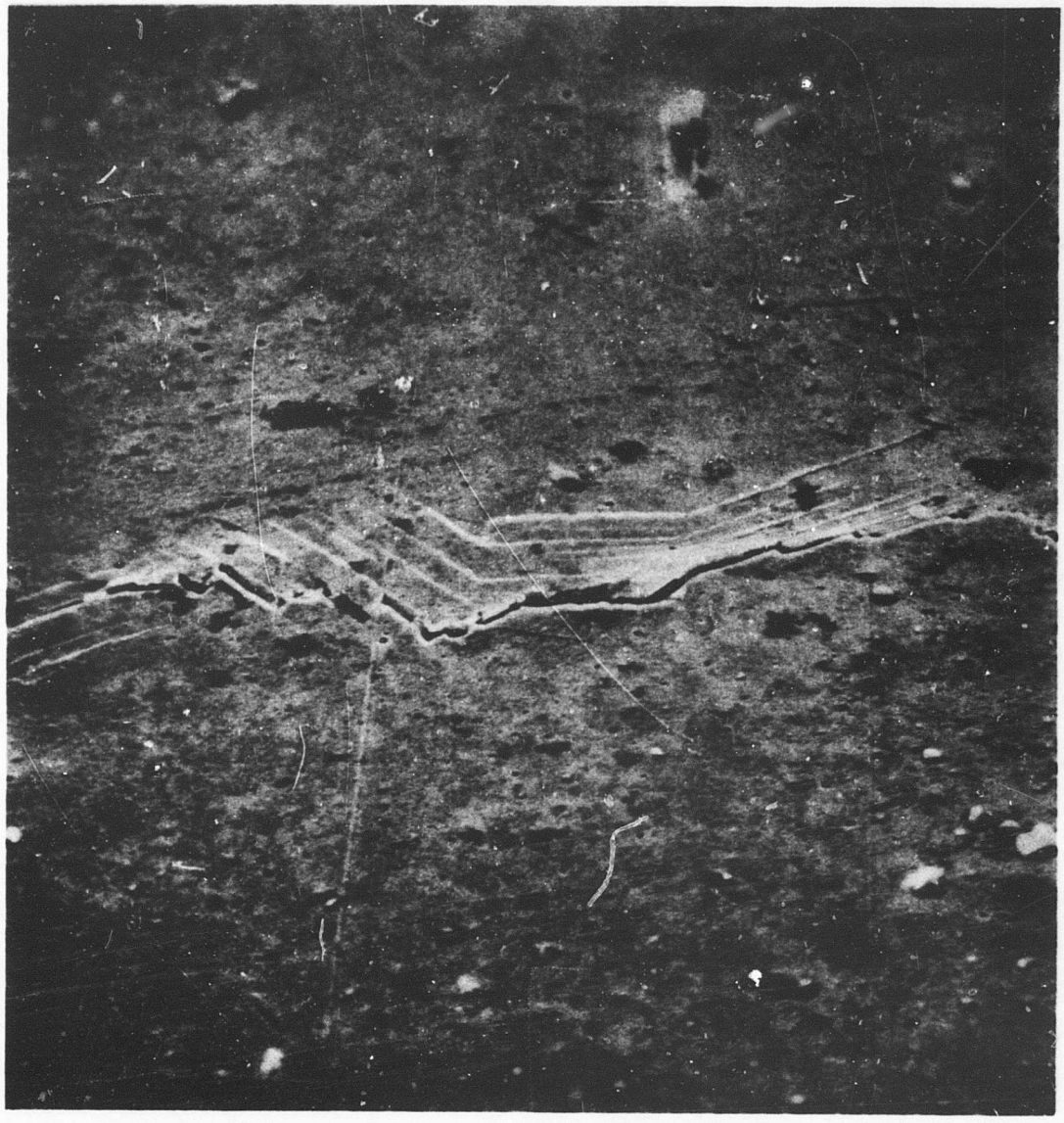

Figure 39. Inconel Sample I7, X2000, d = 1.50.

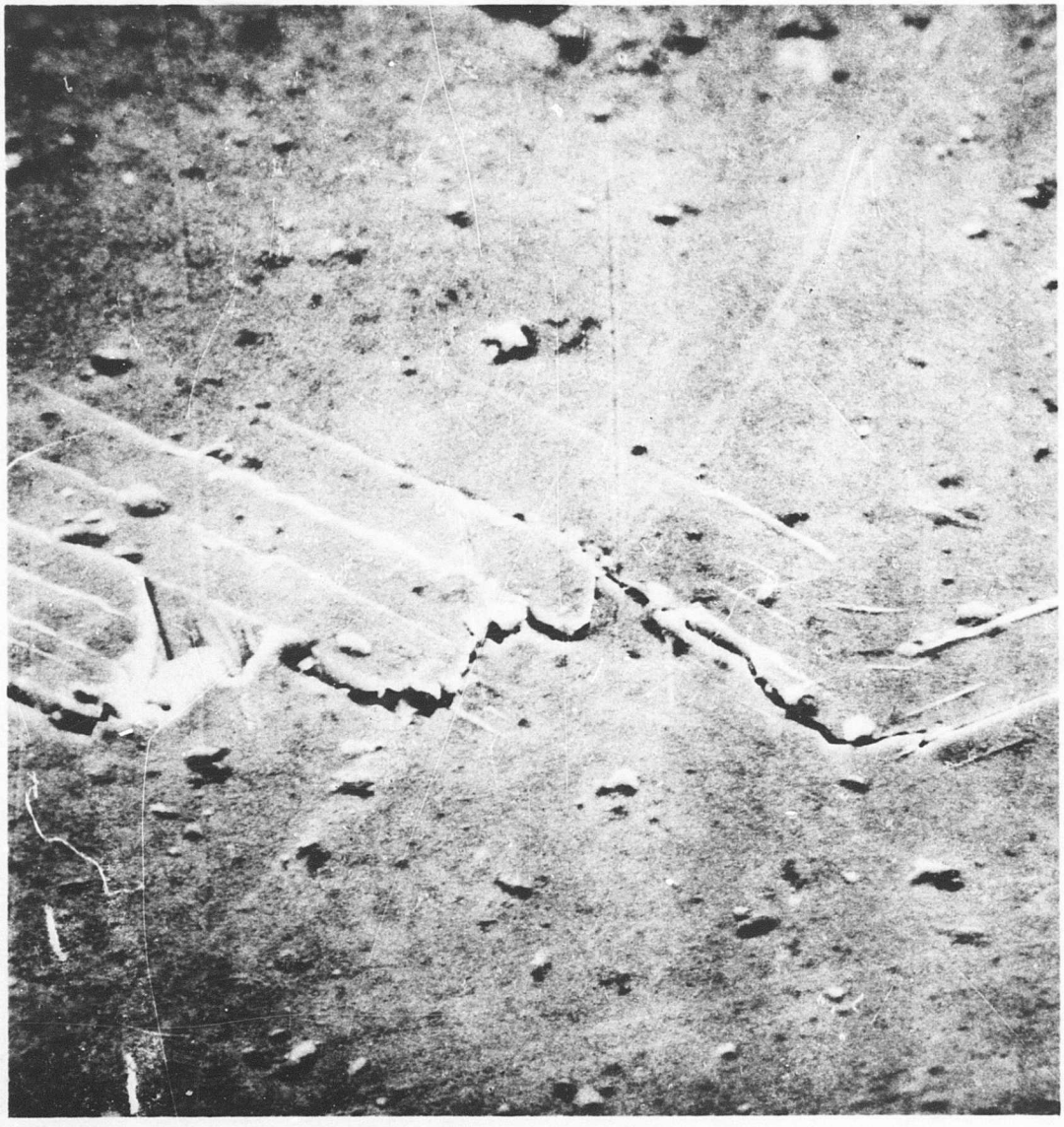

Figure 40. Inconel Sample I7, X4000, d = 2.28.

Figure 41. Inconel Sample I7, X4000, d = 2.41.

Front

Back

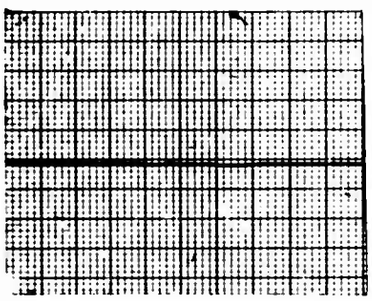

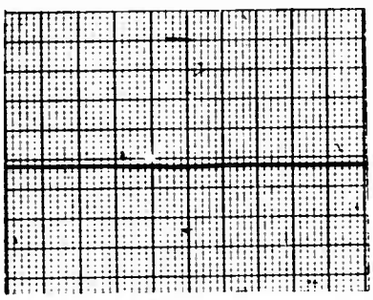

Pretest

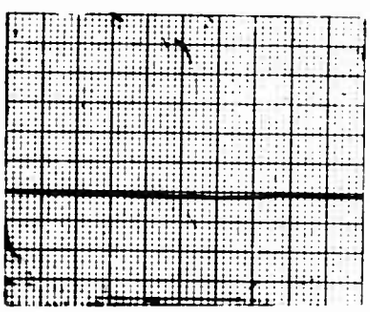

400,000 Bending Cycles

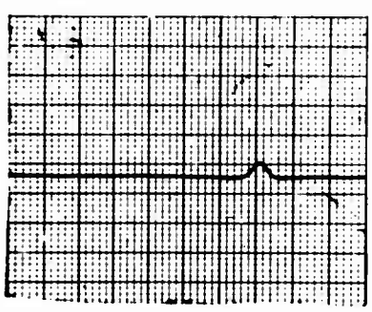

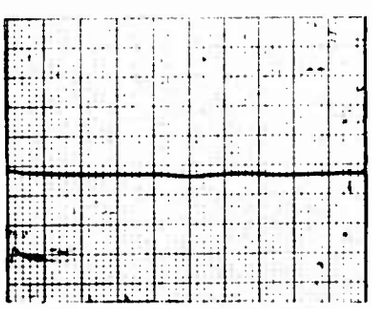

800,000

Figure 42. Inconel X Sample I10, ±.070" Deflection.

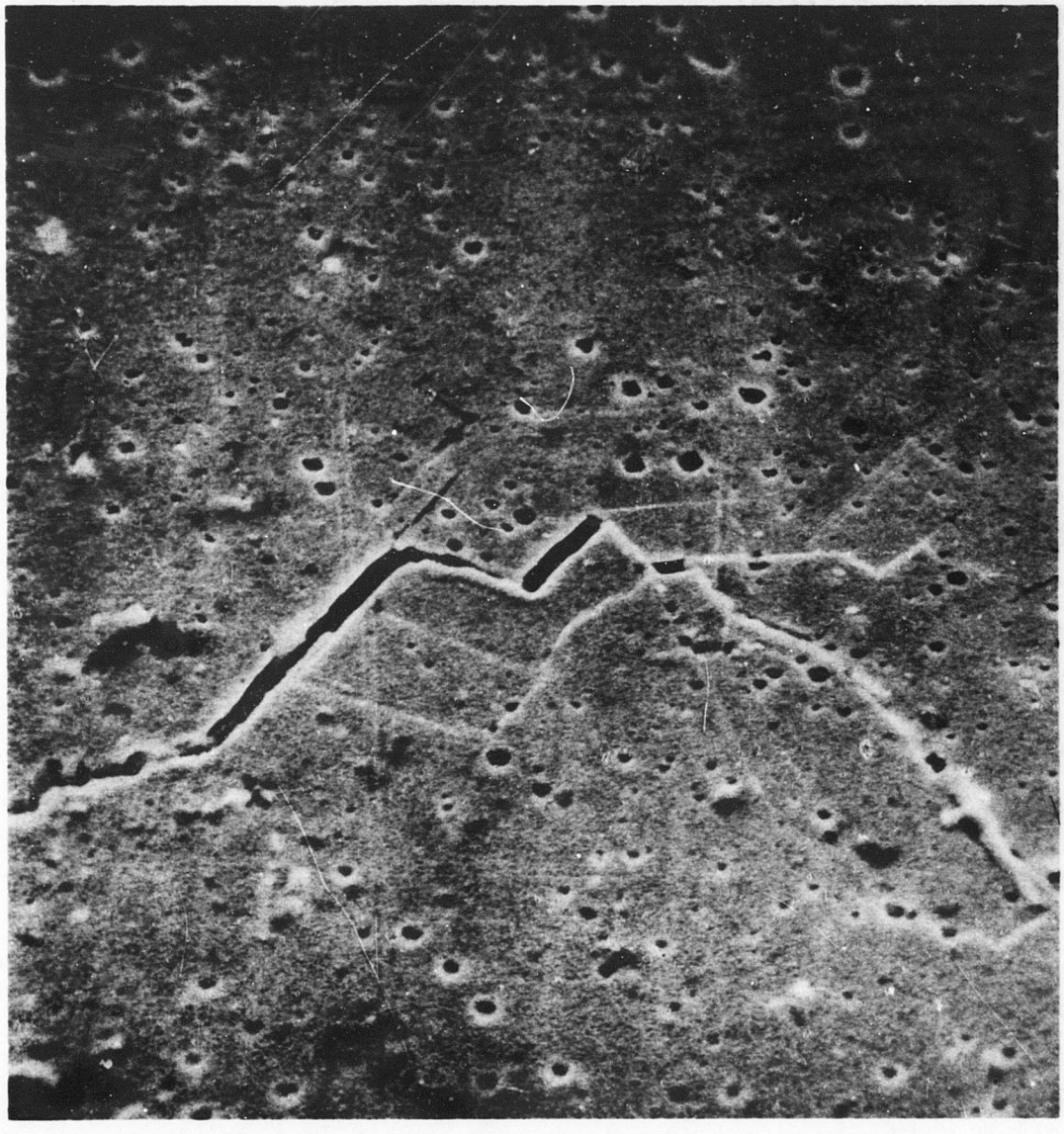

Figure 43. Inconel Sample I10, X4000, d = 1.74.

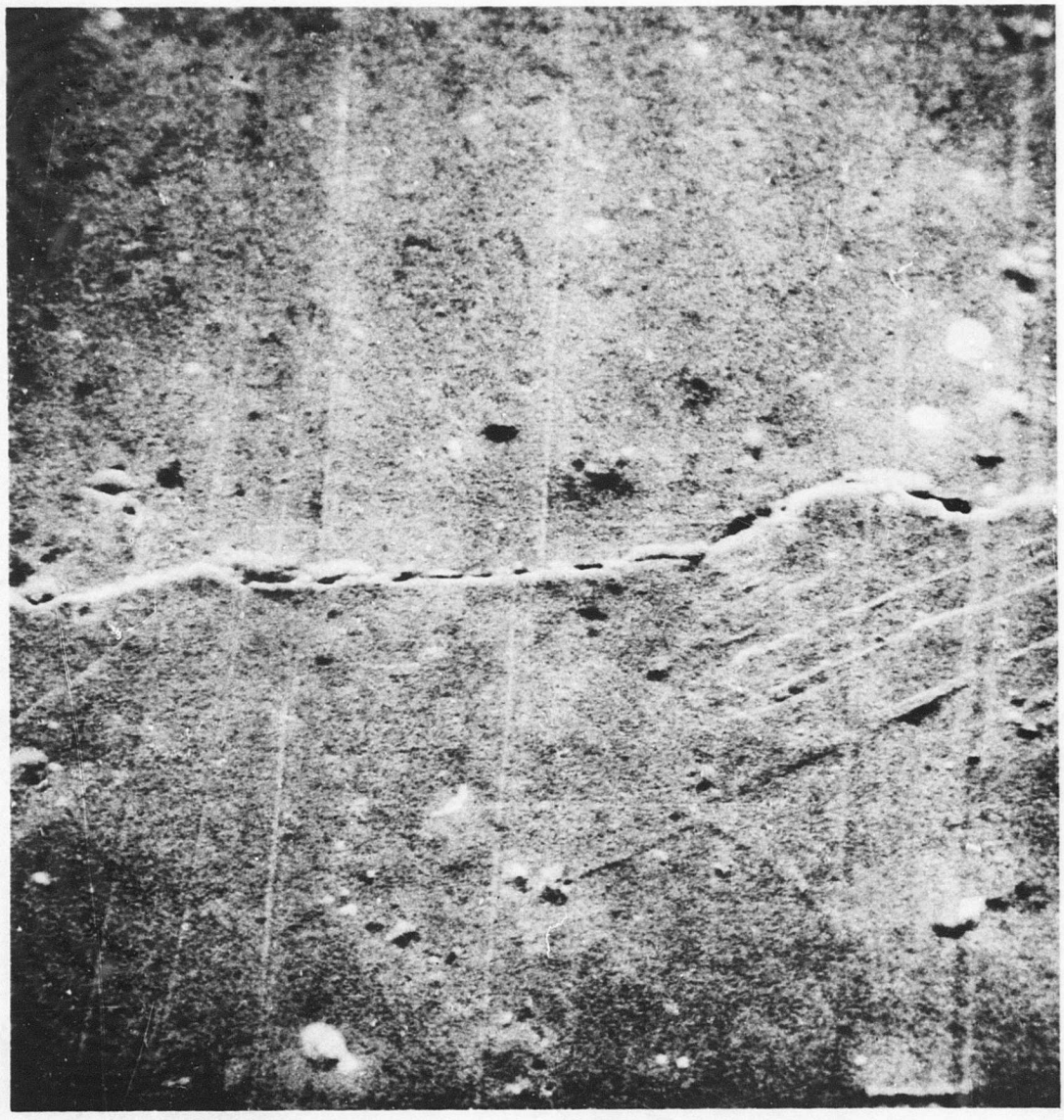

Figure 44. Inconel Sample I10, X4000, d = 2.05.

Figure 45. Inconel Sample I10, X4000, d = 2.46.

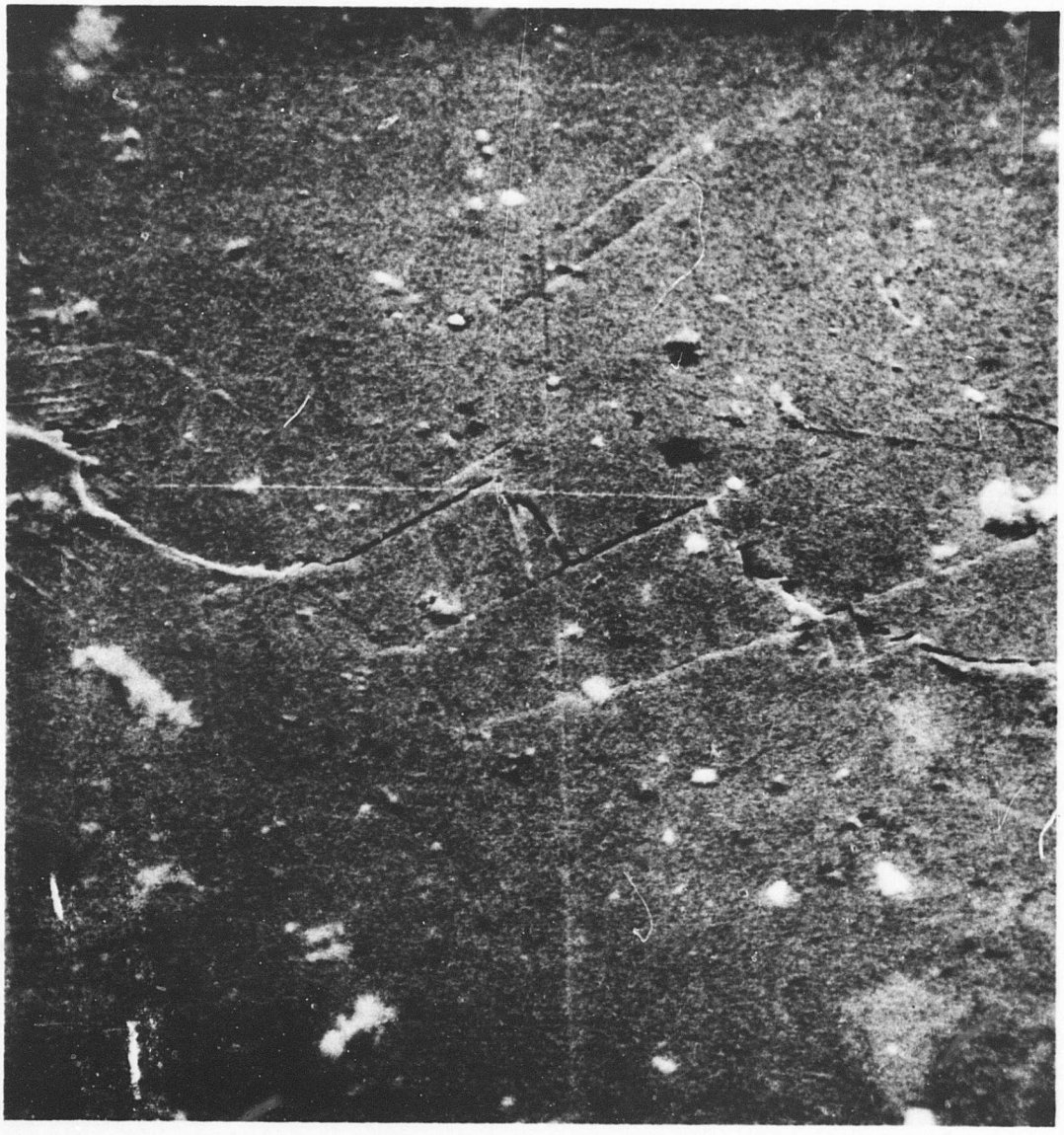

Figure 46. Inconel Sample I10, X4000, d = 3.03.

Front

Back

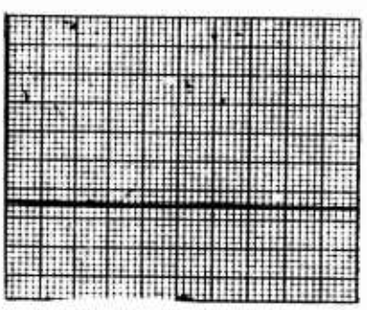

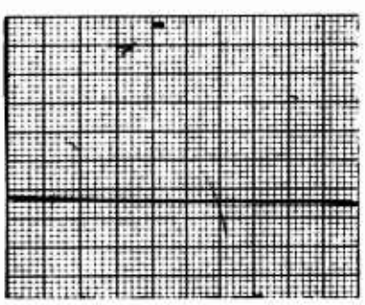

Pretest

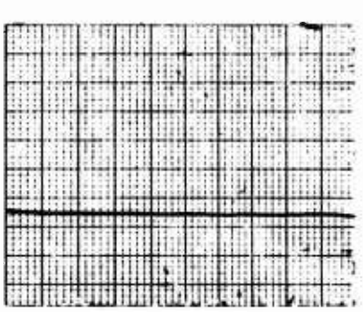

200,000 Bending Cycles

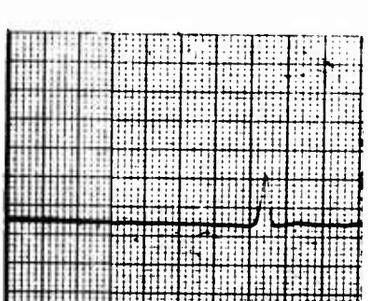

350,000

Figure 47. Steel Sample S11, ±.055" Deflection.

Figure 48. Steel Sample S11, X4000, d = 1.98.

Figure 49. Steel Sample S11, X4000, d = 2.91.

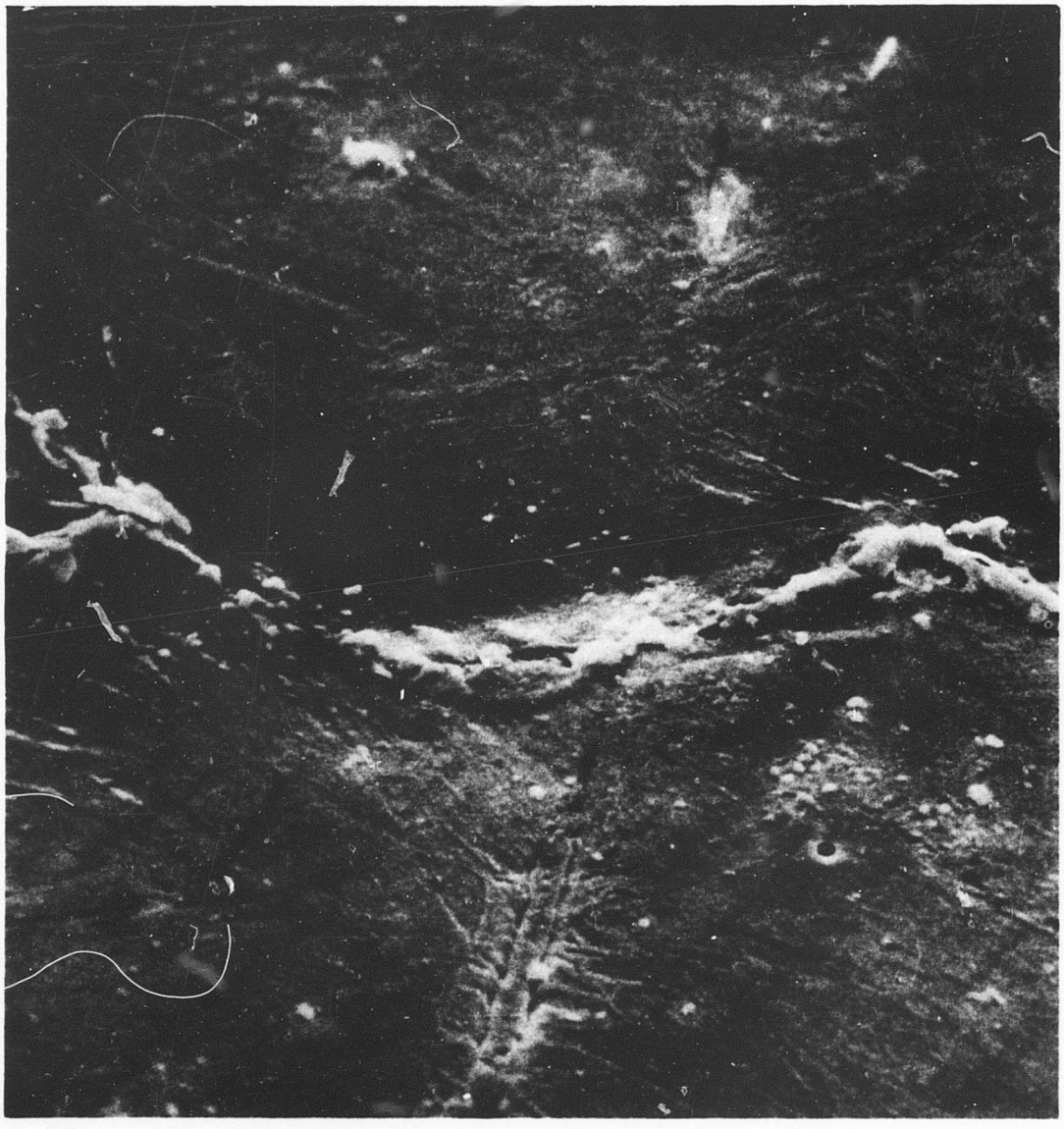

Figure 50. Steel Sample S11, X4000, d = 4.16.

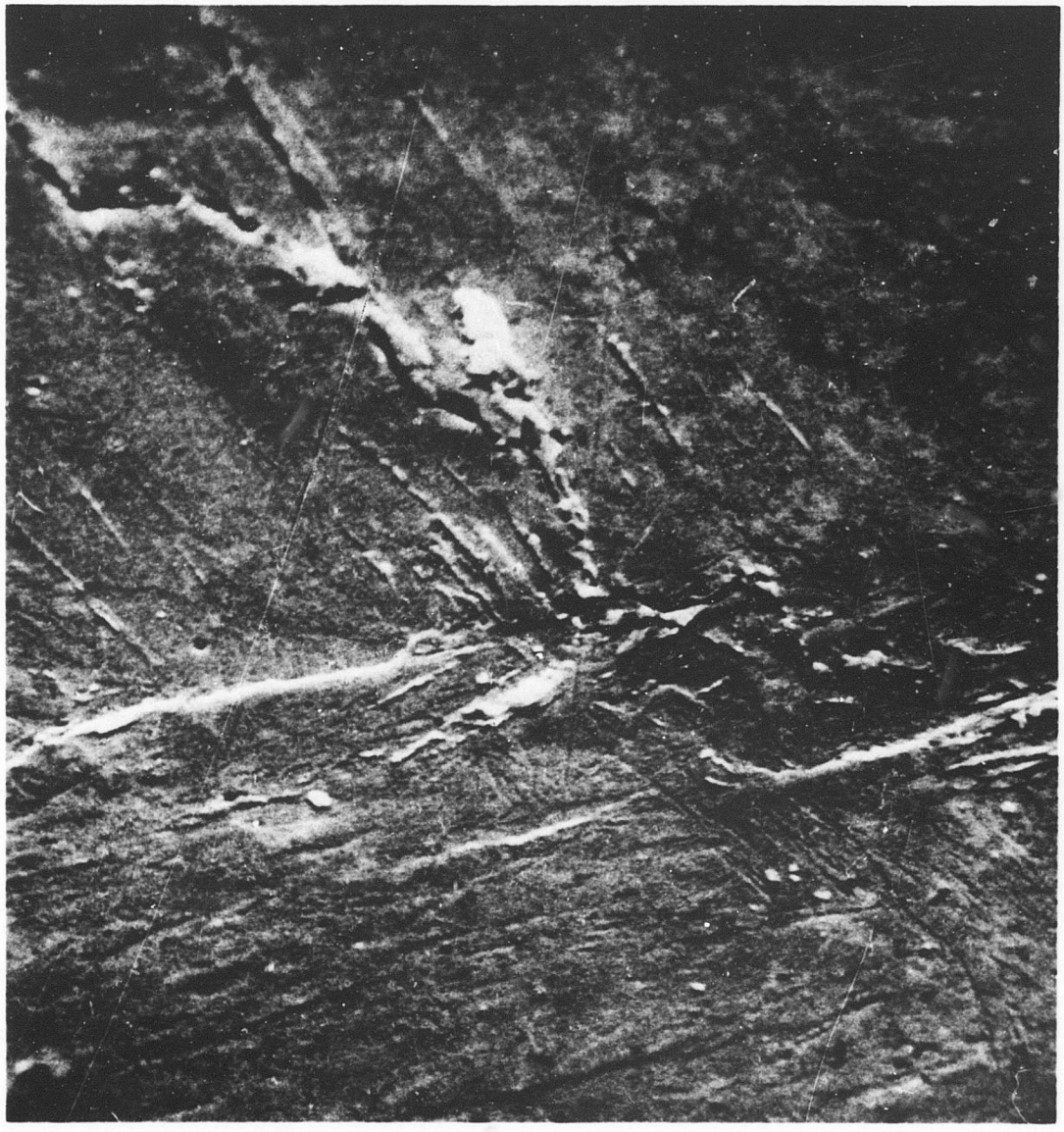

Figure 51. Steel Sample S11, X4000, d = 4.95.

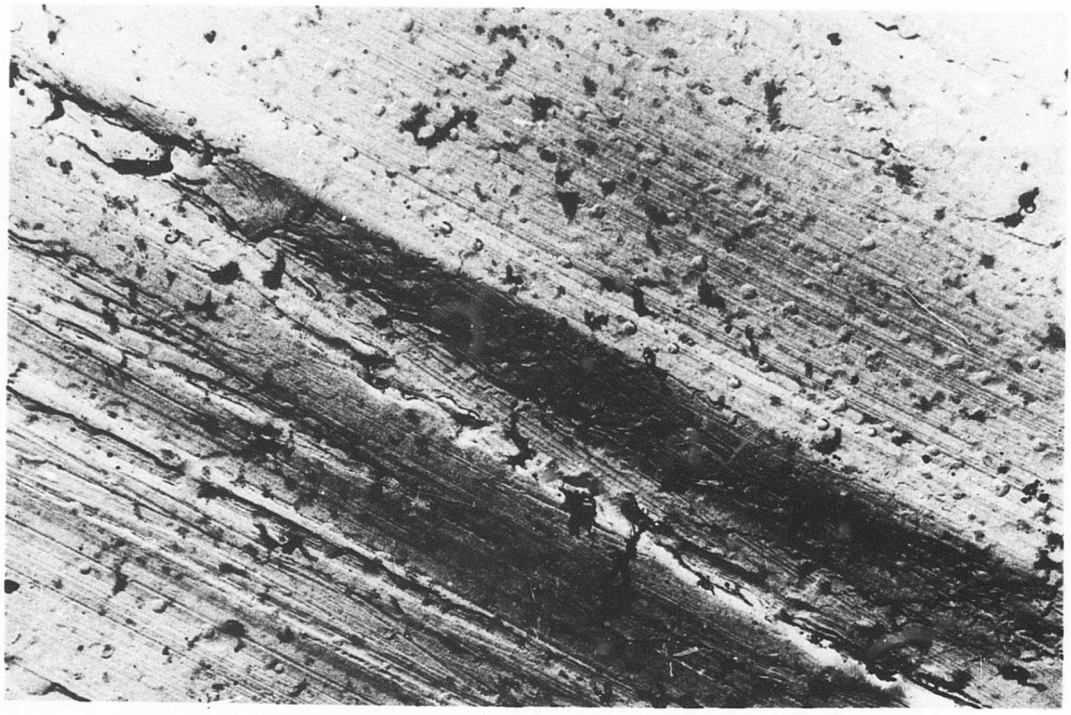

Figure 52. Surface of Sample A1 (Note Slip), X7500.

Figure 53. Surface of Sample A12, Slip in Vicinity of Crack, X9000.

Figure 54. Opposite Surface of A12, No Clear Evidence of Slip, X9000.

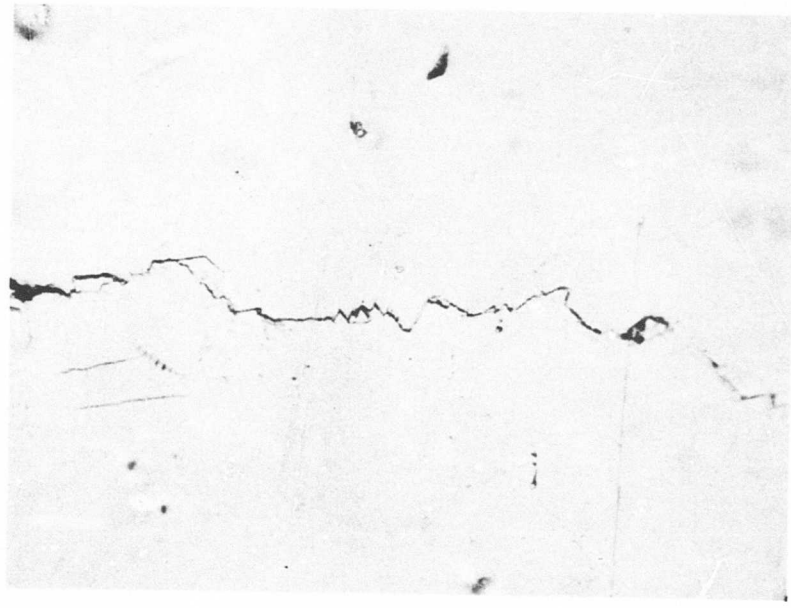

Figure 55. Overview of Crack on Surface of Inconel Sample I2, Clear Presence of Slip.

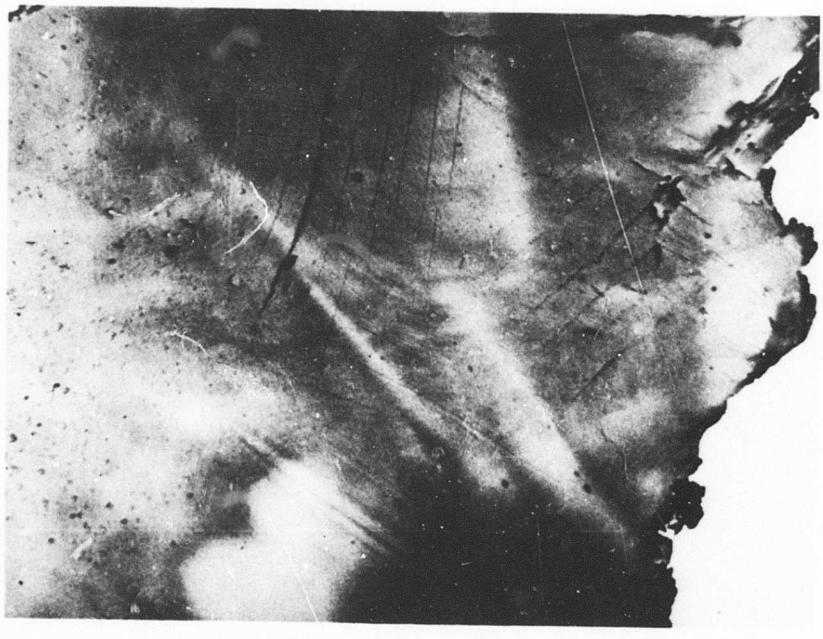

Figure 56. Sample I2, Crack Edge at Right, Slip Clearly Visible at Top Center, X3800.

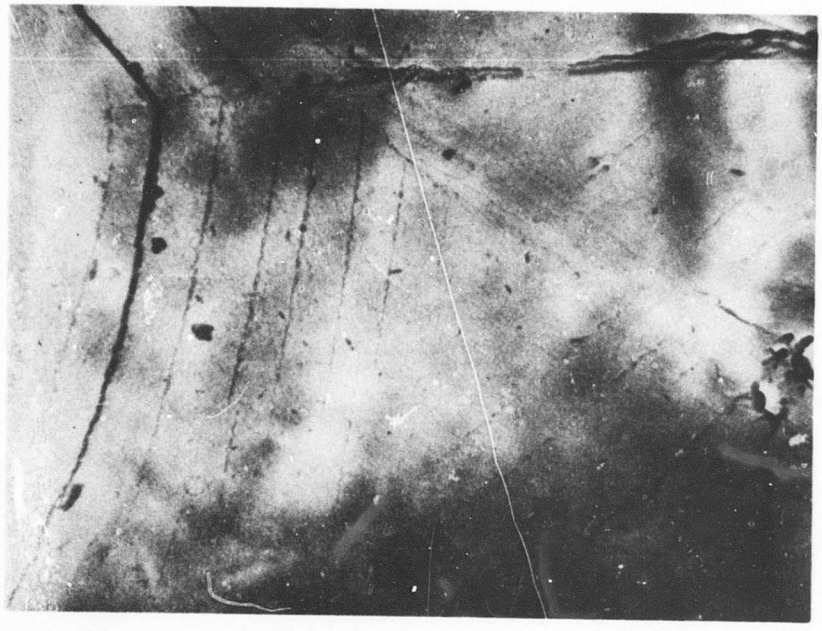

Figure 57. Sample I2, Crack Edge at Right, Slip Clearly Visible at Top Center, X9000.

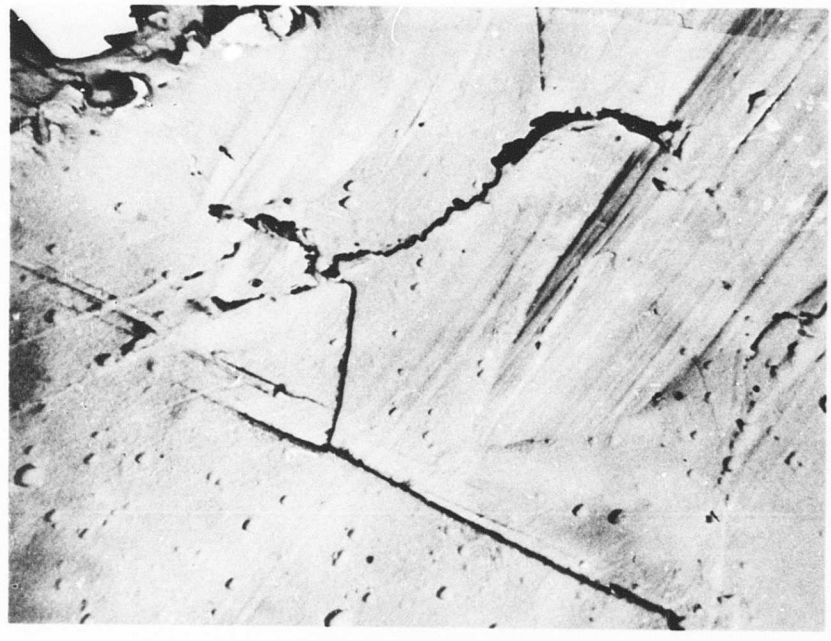

Figure 58. Sample I2, Primary Crack at Upper Left, Secondary Crack at Center, X9000.

Figure 59. Sample I2, Tip of Primary Crack, No Damage Beyond Tip, X9000.

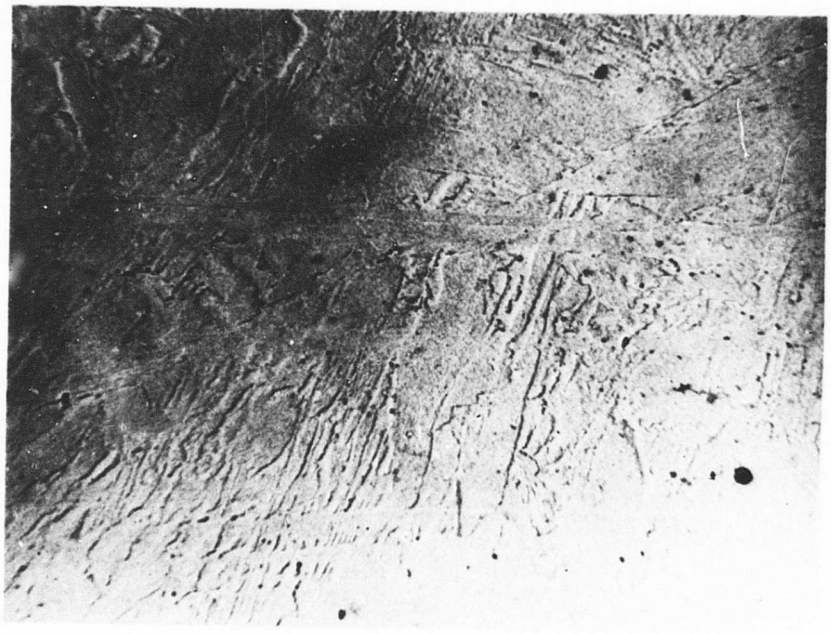

Figure 60. Surface of Steel Sample 1, Immediate Vicinity of Crack, Martensite-Like Structure, No Slip Evident, X3000.

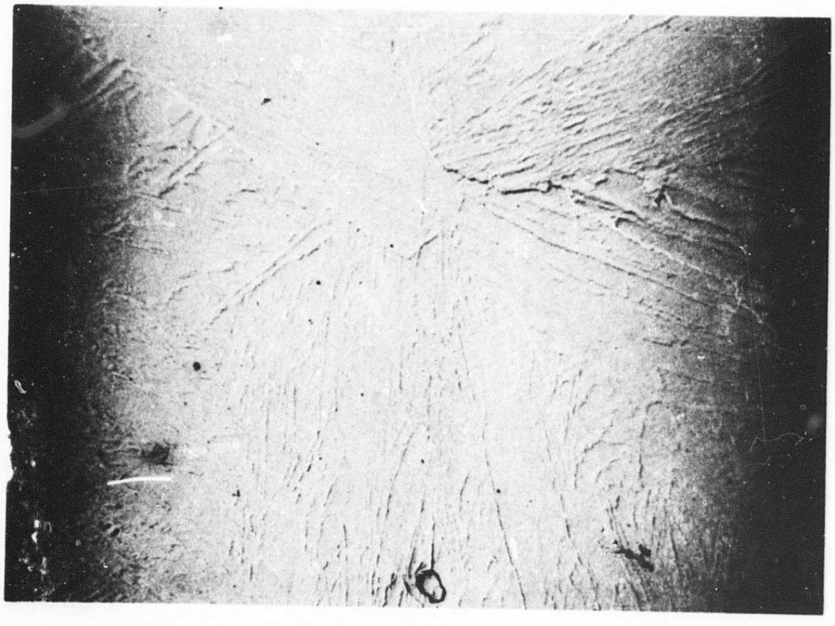

Figure 61. Surface of Steel Sample 2, Immediate Vicinity of Crack, Martensite-Like Structure, No Slip Evident, X3000.

Figure 62. Sample S1, Edge of Crack at Top, No Slip Evident (Characteristic Observation for Steel Samples), X9000.

Figure 63. Sample S1, Tip of Primary Crack, No Evidence of Other Material Damage, X9000.

BLANK PAGE

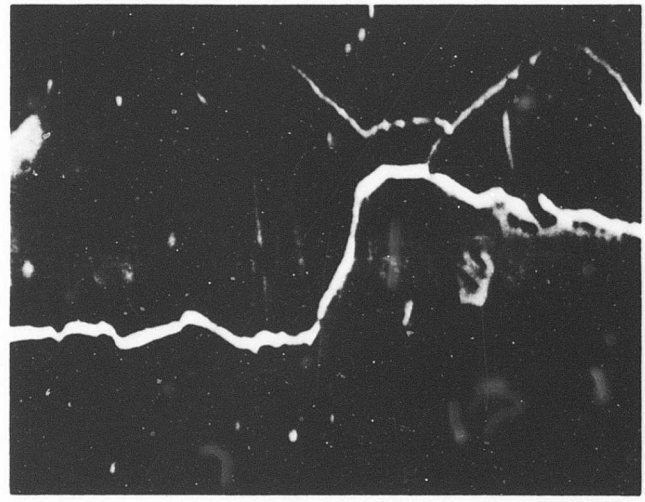

(d) Specimen Current Image of Crack in Aluminum, Site D

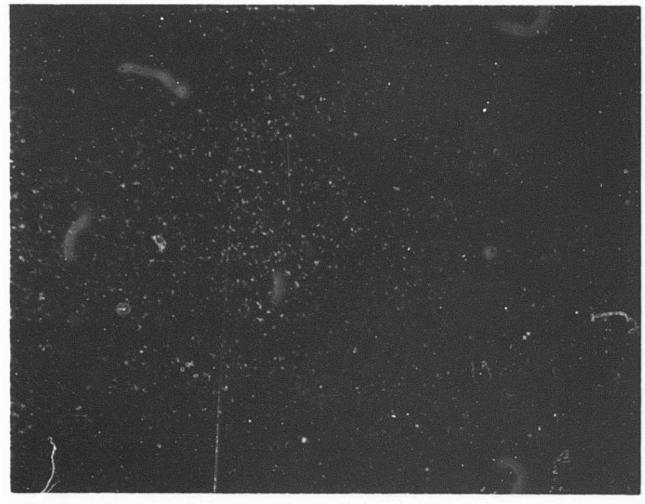

(e) Crack in Aluminum, Site D, Al K_{α} Line, 200K Counts

Figure 64. (continued)

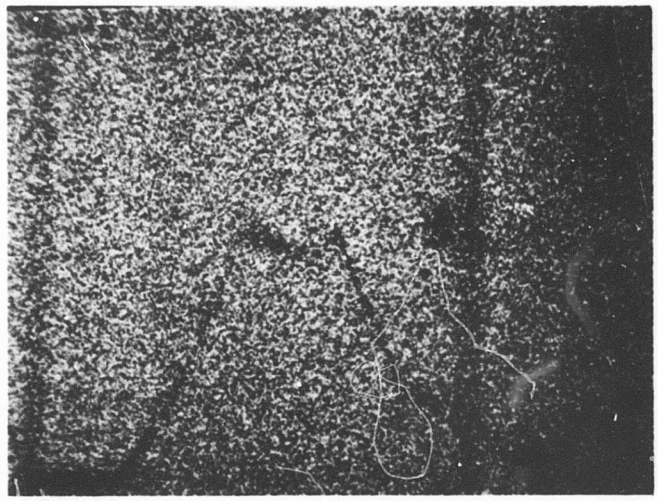

(f) Crack in Aluminum, Site E, Al K_{α} Line, 400K Counts.

Figure 64. (continued)

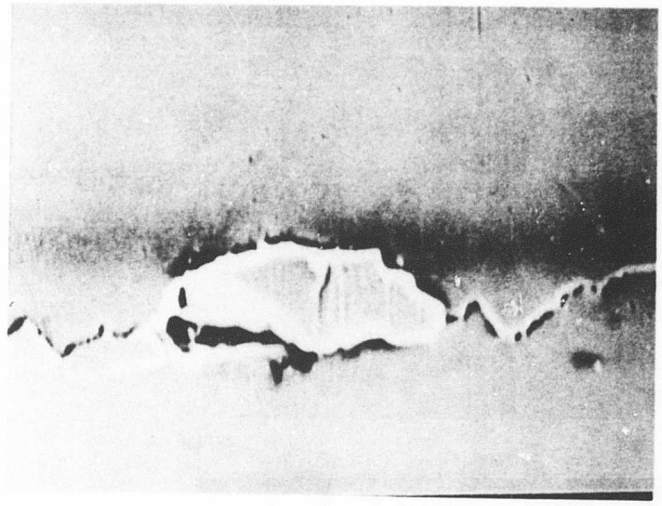

(a) Specimen Current (Neg.) Image of Crack in Inconel, Site C.

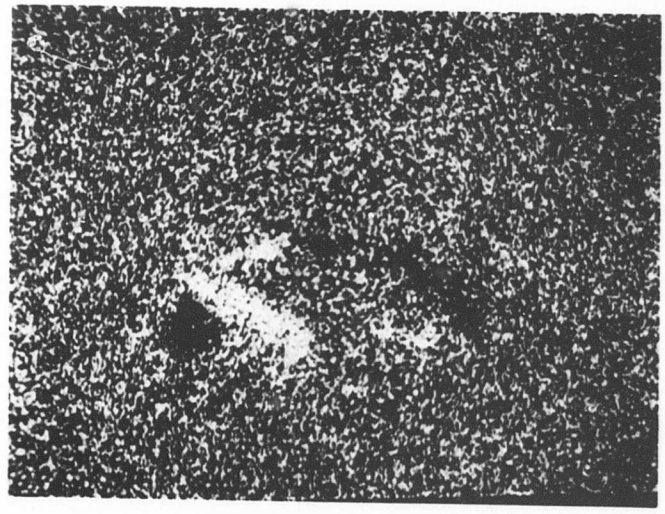

(b) Crack in Inconel, Site C, OK_{α} Line, 40K Counts (Apparent Concentrations of Oxygen Are Probably Artifacts Due to the Fact That Grain Was Elevated and Its Left End Faced the Spectrometer).

Figure 65. Microprobe Images of Inconel Samples.

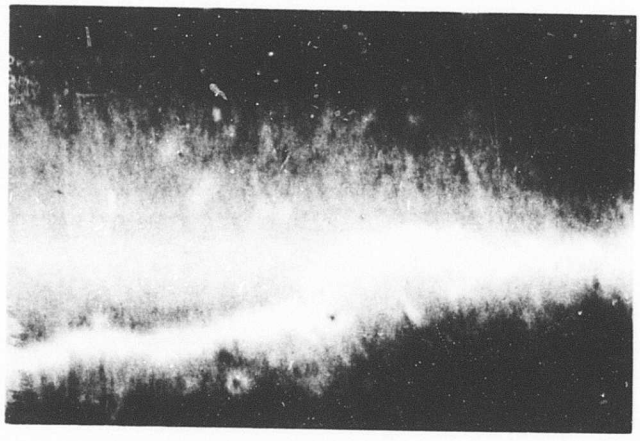

(a) Specimen Current Image of Crack in Steel, Site A.

(b) Crack in Steel, Site A, OK_{α} Image, 15K Counts.

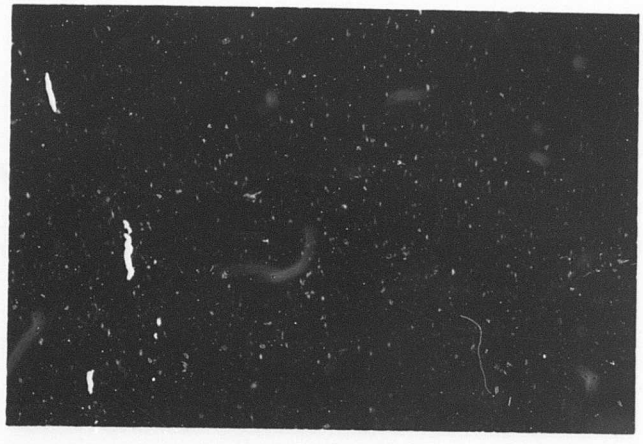

(c) Crack in Steel, Site A, Spectrometer Set on Background Near OK_{α} Line, 15K Counts.

Figure 66. Microprobe Images of Steel Samples.

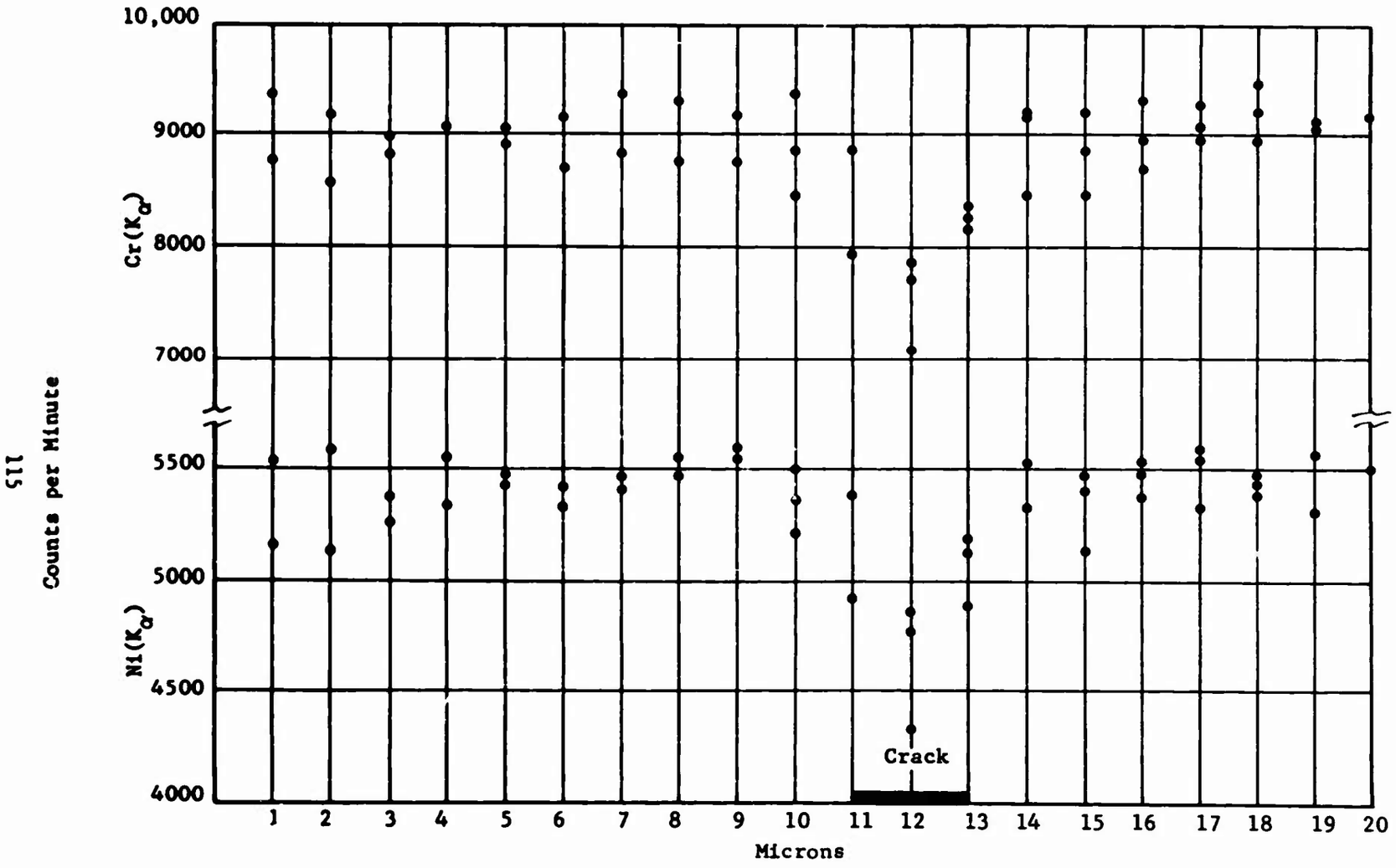

Figure 67. Step Scan of Crack on Inconel Sample Chromium and Nickel Dip at Crack.

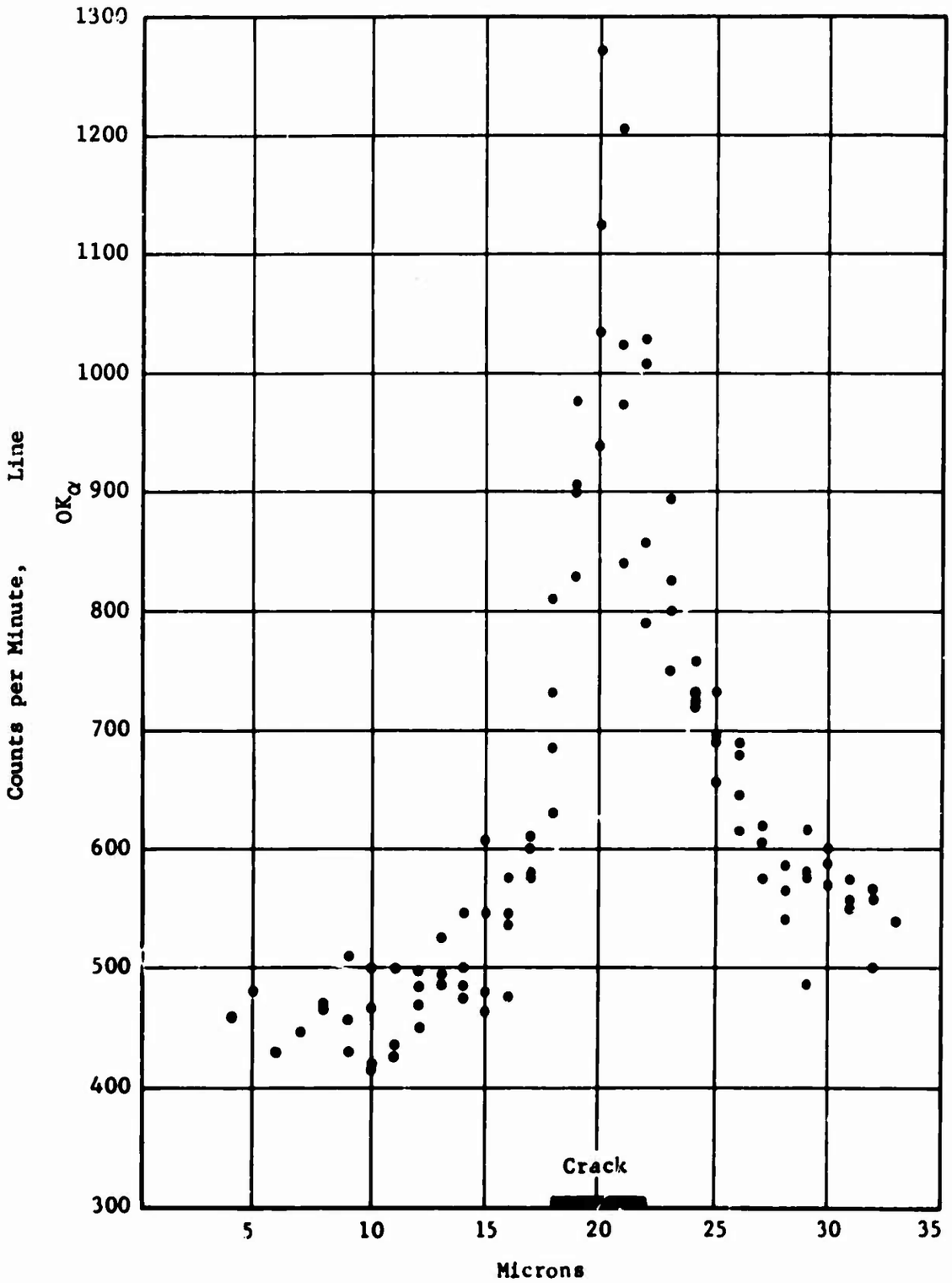

Figure 68. Step Scan of Crack on Steel Sample, Oxygen Peak at Crack.

Unclassified
Security Classification

DOCUMENT CONTROL DATA - R & D

(Security classification of title, body of abstract and indexing annotation must be entered when the overall report is classified)

1. ORIGINATING ACTIVITY (Corporate author)
Mechanical Technology Incorporated
968 Albany Shaker Road
Latham, New York

2a. REPORT SECURITY CLASSIFICATION
Unclassified

2b. GROUP

3. REPORT TITLE
INVESTIGATION TO DETERMINE THE FEASIBILITY OF DETECTING IMPENDING METAL FATIGUE FAILURE THROUGH USE OF AN INDUCTIVE SENSING DEVICE

4. DESCRIPTIVE NOTES (Type of report and inclusive dates)
Final Technical Report

5. AUTHOR(S) (First name, middle initial, last name)
George G. Moross

6. REPORT DATE	7a. TOTAL NO. OF PAGES	7b. NO OF REFS
February 1970	126	

8a. CONTRACT OR GRANT NO.	9a. ORIGINATOR'S REPORT NUMBER(S)
DAAJ02-68-C-0005	USAAVLABS Technical Report 69-97
b. PROJECT NO. Task 1F162203A43405	
c.	9b. OTHER REPORT NO(S) (Any other numbers that may be assigned this report) MTI-69-TR-47
d.	

10. DISTRIBUTION STATEMENT
This document is subject to special export controls, and each transmittal to foreign governments or foreign nationals may be made only with prior approval of U. S. Army Aviation Materiel Laboratories, Fort Eustis, Virginia 23604.

11. SUPPLEMENTARY NOTES

12. SPONSORING MILITARY ACTIVITY
U.S. Army Aviation Materiel Laboratories
Fort Eustis, Virginia

13. ABSTRACT

This program is concerned with the evaluation and development of a sensing system to detect surface and near-surface flaws in material, specifically to detect early fatigue damage. This system shows great promise in that a signal is detected at a significant time before failure, and the amplitude of the signal increases with further damage. Samples have been fatigue-cycled up to 5 x 10^6 cycles, and signals have been observed as early as 38% of fatigue life, average results showing signals between 70-80%. These studies have been performed using aluminum, steel, and Inconel, and the results show essentially the same sensitivity of these materials. Intensive metallographic and microanalytic studies have been performed in order to define the particular phenomenon responsible for the signal. Micro-cracks have definitely proved to be responsible for the signal, and thus the sensitivity of the system has been evaluated.

DD FORM 1473 REPLACES DD FORM 1473, 1 JAN 64, WHICH IS OBSOLETE FOR ARMY USE.

Unclassified
Security Classification

Security Classification

14 KEY WORDS	LINK A		LINK B		LINK C	
	ROLE	WT	ROLE	WT	ROLE	WT
Metal Fatigue Detection Inductive Detection System						

Security Classification